A SYPHON TUNNEL FOR STUDIES OF CONTROL GATES — KAPUR

A SYPHON TUNNEL FOR STUDIES OF CONTROL GATES

by

A.D. Kapur

A thesis submitted to the Faculty of Graduate Studies and Research in partial fulfilment of the requirements for the degree of Master of Engineering

Department of Mechanical Engineering
McGill University
Montreal

November 1964

SUMMARY

The design, construction and operation of a syphon tunnel meant for studies of water flow around control gates (with and without air addition) have been described. The control gates studied are of the type commonly known as 'vertical leaf gates' as shown in Figure 3.a.

The standard methods for estimating the piping losses have been used to calculate the rate of flow of water through the tunnel for the cases in which no external air is admitted into the separation eddy. The static pressures inside the test section have been calculated on the basis of the hydraulic energy balance. The analysis has been developed for any pressure level within the test section, and includes both ventilated and non-ventilated eddies.

Tables are given to compare the theoretical and experimental values of the static pressures at a selected section upstream of the gate, at the vena contracta, and at a section just beyond the point of reattachment. The tabulated values refer to all the cases of flow studied.

The performance characteristics of the syphon tunnel have been worked out for the case when there is no ventilation and no gate in the test section and the absolute pressure in the test section is desired to be zero. Comparison has also been made between the theoretical and experimental values of the cavitation parameter for various cases. The approximate value of the ventilation factor (air-water ratio) that allows continuous operation of the tunnel has been estimated.

A model of the geometry of the separation eddy has been suggested. To evaluate the pressure variation along the length of the eddy, an expression for the pressure recovery index has been derived. Values of this index based on the geometry of the model have been compared with the experimental results and the limitations of the model have been pointed out.

The eddy lengths derived from experimental results have been compared with those of the previous investigators and with the results obtained from submerged jets in an open channel.

It has been found that the length of the separation eddy increases with the increase in the ventilation factor. The theoretically predicted values of the overall pressure recover index have been comfirmed numerically by the experimental results for a wide range of solidity ratios and ventilation factors. Both these values suggest that with an increase in the ventilation factor there is a decrease in the said index and that this decrease is more pronounced when the solidity ratio is reduced.

ACKNOWLEDGEMENTS

The author is very much indebted to Dr. A.J. Reynolds for his guidance, advice and help during the investigation of this project and preparation of this thesis.

The author gratefully acknowledges the help given to him in the construction of the syphon tunnel and during the experiments by the technical staff of the Departments of Mechanical and Civil Engineering.

The author wishes to express his sincere thanks to the Canadian Commonwealth Scholarship Committee for financial support.

CONTENTS

<u>CONTENTS</u> (continued)

NOTATION

A_b	Area of blockage due to the butterfly valve
A_g	Area of opening at the control gate
A_p	Area (inner) of the circular section pipe line
A_s	Area (inner) of the aluminum square channel
A_t	Area of cross-section of the test section
A_x	Area of flow at any station x in the test section given by $d(d - h_x)$
C_c	Coefficient of contraction
C_{px}	Pressure recovery index defined by Equation (13a)
C_{p2}	Overall pressure recovery index defined by Equation (15a)
d	Size of the square test section
d_c	Mean depth of water in the open channel (article 6.h.2)
E'	Elevation (as given in Figure 7)
f	Coefficient of friction in the conduit
F_1, F_2, F_3	Functional representations
g	Acceleration due to gravity
h	Height of the control gate
h_c	Depth of immersion of sluice gate (sketch d)
h_{vc}	Distance between vena contracta section and the floor of the test section (Figure 7)
h_x	Height of the separation eddy at any section x (Figure 7)
$\bar{h}$	Mean depth of water in the supply reservoir (Mean of the depths before and after each test run)
H	Driving head (Figure 7)

H_{atmos}	Atmospheric head
H_0	Value of H as defined by Equation (22)
H'_f	Head loss due to friction
H'	Head loss contributed by factors other than friction
H'_A, H'_B, etc.	Values of H' at respective sections (Figure 7)
K_1	Loss factor associated with orifice plates (Appendix I-B)
K_2	Non-dimensional ratio given by Equation (24d)
L	Length of the pipe line
m	Hydraulic mean depth
$+m'$, $-m'$	Strengths of a source and a sink respectively
p_c	Critical pressure. Equation (16a)
p_e, p_i	External and internal pressures of a gas bubble, respectively
p_0, p_1, p_x, p_2	Absolute static pressures at respective sections (sketches a, b)
p_{0s}, p_{1s}, p_{2s}	Static suction pressures corresponding to the respective absolute pressures p_0, p_1 and p_2
p_S	Pressure used in calibration curves of the rotameter (14.7 psia)
Q_{a2}	Rate of volume flow of air at pressure p_2 and temperature T_w $\left(Q_{a2} = \frac{p_S Q_S}{T_S} \cdot \frac{T_w}{p_2}\right)$
Q_S	Rate of volume flow of air read directly from calibration curves of the rotameter
Q_w	Rate of volume flow of water
Q_{mx}, Q_{m2}	Rate of volume flow of air-water mixture at sections (x) and (2) respectively

Q_{w0}	Value of Q_w as defined by Equation (22)
r_2	Ventilation factor $\left(= \frac{Q_{a2}}{Q_w} \right)$
R_0	Radius of a spherical gas bubble
s	Half the distance between a source and a sink
T_S	Absolute temperature used in calibration curves of the rotameter
T_w	Absolute temperature of water in the supply reservoir
U	Uniform velocity of flow as defined by Equations (24a,b,c)
V	The velocity of flow at any section
V_E, V_F, V_J, etc.	Values of mean velocity at respective sections (Figure 7)
V_{mx}	The velocity of flow of the air-water mixture at a section (x) considering the hatched portion in sketch (a) as the effective area of flow
V_p	Mean velocity of flow in the circular pipe
V_s	Mean velocity of flow in aluminum square channel
V_t	Mean velocity of flow in the test section
V_{vc}	Mean velocity of flow through vena contracta in the test section
x,y	Coordinates as shown in sketch (a)
x_r	Value of x at the point of reattachment
X_r	Horizontal distance of the reattachment point from upstream face of the gate (Figure 9)
σ_c	Cavitation parameter. Equation (16b)
σ_s	Surface tension of water
ρ_{mx}, ρ_{mr}, ρ_{m2}	Densities of the air-water mixture at sections (x), (r) and (2) respectively. (Sketch a)

ρ_S	Density of air at pressure p_S and temperature T_S
ρ_w	Density of water

1. INTRODUCTION

Owing to simplicity of design, economy of construction, and ease of maintenance, leaf gates are very widely employed for flow regulation of large conduits. Such gates are of simple rectangular shape mounted either vertically or in an inclined position spanning the corresponding rectangular or square cross-section of the conduit.

In high-head installations, the high efflux velocities generated at partial openings of such a gate result in a problem which can be divided into two equally important and distinct parts:

(1) Reduction in pressure along the bottom of the gate.

(2) More severe reduction in pressure downstream of the gate, followed by a recovery in pressure further ahead.

The first part, i.e., pressure reduction along the bottom of the gate imposes a hydrodynamic load called hydraulic downpull acting in the plane of the gate. Extensive experimental and theoretical studies have been conducted to deal with this aspect; see, for example, Naudascher et al.[1] and the bibliography mentioned in Appendix II-A of this reference.

In the present case, it is proposed to study the second part of the problem, the understanding of which is of utmost importance for the following reasons:

a) Reduction in pressure downstream of the gate establishes a pressure differential between the two sides giving a net hydrostatic force on the gate. This force called hydraulic sidepull is a major factor in the design of such gates.

b) If the reduction in pressure is sufficient to cause gaseous and/or vaporous cavitation, as is usually the case in high head installations, a large number of cavities are formed. Vibration of the conduit and pitting of the conduit material is caused by fluctuations in pressure which occur when the cavities collapse in the pressure recovery zone.

The report presented herewith is a synthesis of two different projects: one concerns the design, construction, and operation of a water tunnel and suitable measuring equipment; the other describes the tunnel performance and certain analytical and experimental investigations connected with the study proposed above.

For reasons to be cited later, the decision was made to construct a syphon tunnel for the study of flow past the control gates positioned on the test section floor. Most of the material used in this construction was aluminum for its lightness and resistance to corrosion; but the parts (bends and turning vanes) that required a lot of welding were made of mild steel, because compared to aluminum, mild steel is much easier to weld. These parts were then galvanized to avoid rust formation.

For design of the gates and conduits, it is essential to know the fluctuating forces acting on them. This is possible only if evaluation of the fluctuating pressures can be made. The problem is very complex because the flow downstream of the gate is an extremely complicated one. As a first step towards the solution it is proposed to idealize the situation by making a number of assumptions (given in article 4) to investigate the pressure distribution, cavitation parameter and lengths of the separation eddy (defined ahead), and also to study their dependence on the external air addition.

Imagine a jet issuing from the gate opening. After leaving the opening, the jet would be very fast (Reynolds number of the order of 10^5 in the present case) and a short distance downstream (approximately after the vena contracta section) the region of high shear would become unstable and the turbulent flow would develop rapidly. The fluid between the jet and the floor of the test section downstream of the gate would be quickly entrained, establishing a back flow. This backflow would be drawn from underside of the jet further downstream and as this is done the jet would be drawn downwards. This process would continue and the flow would reattach to the floor enclosing an eddying or recirculating region. This region is commonly termed as a separation bubble or a cavity. In the present case where flow of water or of air-water mixture takes place, it would be more appropriate to call this region a 'separation eddy' to distinguish it from a true cavity in water or from a separation bubble usually associated with the air flow.

The present work is mainly concerned with flows completely confined in the closed test section and the work somewhat allied to this has been reported by Förthmann(2) and Arie and Rouse(3).

Förthmann(2) studied the flow in a 'partially expanding jet'* of air for a high solidity ratio of 0.833, the solidity ratio being

---

* The term 'partially expanding jet' as used in reference (2), which is a translation of Förthmann's original paper, implies that the expansion of the jet issuing from the opening is partial because it is restricted by the fourth or closing wall of the test section. This term may not be confused with that used commonly for compressible flow.

defined as a ratio between the area of blockage due to the gate and the area of the test section in which the gate is fixed. His measurements included the total head and static pressures at a number of streamwise sections permitting the determination of velocity distribution in the channel. Graphical integration of the individual velocity profiles then gave the volume of flow for each. The points of equal flow volume were then connected, resulting in a flow pattern which gave the point of re-attachment. However, no analytical approach was suggested to compute either the pressure distribution or the length of the eddy.

Arie and Rouse(3) dealt with two-dimensional flow over a normal wall in a wind tunnel, using a tail plate at the mid-height of the downstream face of the wall. The tail plate was used to arrest the free oscillations of the flow which would otherwise occur in the wake behind the wall, if the latter is isolated. The results reported mainly concern low solidity ratios of 0.083 to 0.167. Because of the complexity of the situation, no direct approach was found to predict the profile of the separation 'bubble'. The authors derived it through measurements of the velocity across and along the test section. They found the profile to approximate roughly to part of an ellipse, though for the sake of easier mathematical representation of the stream function they matched the profile to a Rankine oval of comparable dimensions.

Savage(4) suggested a theoretical approach to determine the geometry of the steady 'separation bubbles' behind bluff bodies in the case of flows with free streamlines. This approach is considered to be inapplicable to the present case (discussed in article 5), because in a completely confined situation the fluid mechanical aspects of the flow around bluff bodies (e.g. control gates) are quite different from those of the flow with free streamlines. The approach adopted in the present work for devising a model of the eddy geometry involves the use of experimentally determined eddy lengths.

The present study will be helpful in giving some insight into the general pattern of flow around the control gates, and in computing the mean hydraulic sidepull acting on them. Also, it will give an estimate of the eddy lengths and consequently the conduit lengths which would be subjected to the fluctuating forces and hence would need special strengthening. For the purpose of designing the gates and conduits, the present results must be supplemented by the results of the investigation of the fluctuating pressures behind the gate.

In actual installations a change in the gate opening may be made by movement of the gate while the water continues to flow through the conduit. During the process of this change, the flow characteristics must be affected by the rate at which the gate is moved. However, in the present case the changes in the opening were brought about by fitting in gate models of different heights after emptying the tunnel. The results of the present work would, therefore, be applicable only in a situation where the gate opening is fixed or the gate movement is very slow. In other words, to apply the present results, the flow would have to be assumed as quasi-steady.

2. APPARATUS AND INSTRUMENTATION

2.a General Remarks

The decision to design and construct a syphon tunnel was made on the basis of the following ideas.

2.a.1 Purpose

It was proposed to investigate mainly the static pressure distribution along the length of separation eddy formed behind the leaf gates in a closed conduit and also to study the effect of controlled ventilation of the eddy on this distribution. The major requirement to pursue this study was a suitable water tunnel, equipped with devices to measure the static pressures and the volume flows of air and water.

2.a.2 Water Tunnel Circuits

The investigation could be carried on by making use of a water tunnel with either a closed or open circuit. In the former case the same sample of water is used over and over again, whereas in the latter there is a continuous supply of fresh water. In hydroelectric projects, river, canal and conduit flows where the leaf gates find their use, continuous supply of fresh water is maintained and the air supplied to the eddy behind the gate is carried away continuously. To simulate this situation more closely, the open circuit seemed preferable.

Another reason for rejecting the closed circuit was that the external air supplied to ventilate the separation eddy would accumulate and change the density after each cycle of flow. To overcome this difficulty, a suitable dearation system would be needed. The other factors against the adoption of the closed circuit were its higher constructional and installation costs.

An open circuit was thus chosen, though this did entail the disadvantage of wasting water during experimental runs. However, the actual cost of water wasted by using an open circuit worked out to be a small fraction of the cost of the dearation system needed for the closed circuit.

2.a.3 Reasons for Adoption of the Syphon Tunnel

There would be three alternatives for producing flow with an open circuit. One would be to instal a suction pump and its driving unit to suck the flow from the main supply reservoir, another would be to devise a system of pumping the flow at super atmospheric pressures and the last would be to dispense with any such installation and make use of the syphon phenomenon. The last alternative was chosen for the following reasons:

(1) Cost Consideration

The cost of construction, installation and maintenance of a tunnel provided with a suction pump, a driving unit and a speed control unit would be far higher than that of a syphon tunnel. Also,no vital function of the experimental investigation proposed would be sacrificed by choosing the latter kind of tunnel, assuming the availability of enough driving head and a discharge sump that would take the tunnel flow during the period of a test run without being flooded.

(2) Readily Available Facilities

The facilities available in the laboratory were ideally suited to the last alternative. An adequate water supply reservoir was situated on the ground floor and a draining sump in the basement at a suitable distance from the tank. Thus, a driving head ranging from about 18.5 feet to 20 feet was readily available for the purpose.

An opening in the ground floor required for the installation of a large cavitation tunnel was so placed that the discharge leg of the syphon tunnel could pass vertically to reach close to the drain sump.

(3) Academic Aspect

It was proposed to note carefully the constructional and operational difficulties in such a tunnel and to try to find remedial measures for improvement. Satisfactory progress in this would be encouraging, for it would establish a method of performing certain flow studies in situations where expense is a major consideration.

2.a.4 Disadvantages of the Syphon Tunnel

(1) Control

The tunnel was designed for manual control only. On certain occasions the help of a second person was obligatory in closing and opening of the outlet.

(2) Operating Handicaps

The sump could not, in some cases, carry the full discharge of the tunnel for the periods required to let the mercury columns of the manometer stabilize. This difficulty was circumvented through the use of a squashing device to build up the mercury columns in two or more runs.

Maximum driving head was limited to 20 feet only, which in turn limited the magnitudes of flow velocities and negative pressures. Indirectly it also restricted the amount of air addition to a certain limit beyond which the flow would break down.

2.b Design and Construction of the Syphon Tunnel

Overall dimensions of the tunnel are given in article 2.b.5. Figure 1 gives an idea of the proportions of the tunnel and its general arrangement. Figure 2 shows the actual relative placement of the test section, mercury manometer board and rotameter, etc.

2.b.1 Test Section

The requirements for the test section were as follows:

(1) To have clear and transparent side panels so that visual observations and photography of the flow were possible.

(2) Test section was to operate always at sub-atmospheric pressures so that the outside air had a tendency to force its way into it. Any such leaks would modify the flow

pattern in an uncontrolled fashion, distorting the pressure measurements and the visual or photographic observations. Hence, the test section was to be made as air-tight as possible.

(3) To be able to withstand 15 psi differential pressure plus possible pounding of cavity collapse.

(4) Assembling and disassembling of the test section to be easy to facilitate general clean up and also to help in case some static pressure holes got clogged with dirt particles deposited from water and made it necessary to take the test section apart.

(5) Insertion and securing of the gate models in the test section to be performed easily.

(6) Length of the test section downstream of the gate to be larger than the maximum expected distance of reattachment by a sufficient margin.

Body of the Test Section

Figure 5 shows the 4 ft long test section with nominal cross-section of 3 in. x 3 in. (actual 3.06 in. x 3.06 in.). This size was chosen as an optimum, keeping in mind the ease in flow observations and in securing the test models. Floor and roof were made from 3 in. x 1-1/2 in. x 1/4 in. aluminum channel. The type of aluminum selected satisfied the requirements of weldability and excellent resistance to corrosion. The side panels were made from 6 in. wide and 1/2 in. thick clear and transparent plexiglas sheets.

The commonly employed method of securing aluminum channel and plexiglas sheets is to bolt them together. There were certain valid objections to this method. Owing to the large number of holes the plexiglas would be weakened; assembling and disassembling would become laborious. Moreover, the points of tightening being fixed would pose a serious problem when leaks appeared between the fully tightened bolts. To avoid all this, it was decided to use "C" clamps instead of bolts as shown in Figure 5. They provided easy manoeuverability in the shifting of clamping points to get the best sealing effect after each operation of disassembly and re-assembly.

Steel strips about 1 in. wide and 1/16 in. thick were screwed down lengthwise to the outer edges of plexiglas sheets so that the "C" clamps bore on the steel strips rather than directly on the plexiglas.

Steel strips were useful in two ways:

(1) Tightening load at the catch points was more uniformly distributed lengthwise and to some extent breadthwise also.

(2) Plexiglas sheets were protected from undesirable denting and scratching.

Flanges of the Test Section

The upstream and downstream flanges of the test section were made identical. Figure 3.b shows the arrangement of the flange assembly. The flange was composed of six detachable pieces, that is, two plexiglas sheet ends, two aluminum channel ends, and two 2 in. x 2 in. steel angles. Each end of the aluminum channel was fitted with a 1.75 in. x 2.5 in. x 0.75 in. aluminum block welded at the inner side to provide a flat face for the flange.

As the flanges were composed of many detachable pieces they provided the most vulnerable spots for leakage. Considerable difficulty was experienced in the beginning in sealing the leaks at the entrance and exit of the test section. It was first thought that the test section be assembled and the faces of the flanges be milled. This was not pursued as this would be neither an easy nor a satisfactory solution; because, in spite of this the faces would not be flat easily during any subsequent reassemblies of the test section due to the working clearance between the holes and the bolts. Thus, the idea of milling was dropped in favour of the following simple and inexpensive method. The faces of both the flanges were treated with a thin layer of epoxy glue and made roughly flat. After the epoxy glue had dried, the faces were rubbed with a fine grained sandpaper disc to achieve the desired surface. This had, of course,to be done each time the test section was assembled.

Thus, the leaks were virtually eliminated from the flanges. However, if a small leak did appear, it was easily sealed off with plasticine.

Static Pressure Holes

A total of 36 holes were provided, 22 on the floor and 14 in the ceiling of the test section. Owing to eddy formations around and inside the static pressure holes, the measured values of the static pressure get distorted. The distortion becomes smaller with decreasing hole diameter. A usually recommended size for the hole diameter is about 0.5 mm. In the present work, the hole size used was 1/64 in.

(0.4 mm approx.).

Fixing of the Gate Models

Each time a gate model was to be replaced by another, the upstream flange of the test section was disconnected from the flange of the aluminum square channel. Since there was sliding clearance between the gate and the test section, the gate was inserted from the opening in the flange and pushed forward to the correct position. Its base was then screwed on to the floor of the test section by means of three steel screws inserted from outside. Figure 3.a gives proportions of the gates. Five different gates with heights 1.0, 1.5, 2.0, 2.5 and 2.73 in. were used, one by one. The term 'gate opening' was defined as the difference between the test section width and the gate height. Thus the actual gate openings were 2.06, 1.56, 1.06, 0.56, and 0.33 in. correspondingly. For the sake of convenience these openings are referred to in the following text by their nominal values as 2, 1-1/2, 1, 1/2, and 1/4 in. respectively.

2.b.2 Turning Vanes

To minimize the losses due to separation and secondary motion arising at the right-angled bends and to obtain uniform standard flow, the turning vanes were provided at both upstream and downstream bends.

Selection of the Type

The vane design was based on the experimental investigation of Klein, Tupper and Green[5]. The curves in Figure 4.a as reproduced from this reference show the results obtained by them. The term 'resistance' used here is defined as the ratio of the pressure drop at the vanes to the upstream impact pressure and the terms gap and chord are as shown in Figure 4.b. The curves indicate the following performance characteristics:

Vane	Minimum Resistance	(Gap:Chord)
A	20%	0.30
B	21%	0.41
C	23%	0.39

Comparing the vanes A and B, it was found that if we adopted A, we would require larger number of vanes whereas reduction in resistance would be insignificant. A larger number of vanes in our case would not only add to constriction, but also would present difficulty in welding, as the space was very much limited.

On comparison between vanes B and C, we could at once conclude that the vanes B were preferable as fewer were required and were much easier to construct. At the same time they gave a minimum resistance, which was less than that of C. Thus, it was decided to adopt the design of vanes B. Four vanes were fixed in each of the two bends used.

Special Welding Technique

Normally welding of the vanes is carried out as shown in the top two sketches of Figure 4.c. Weld material is deposited on the inside and/or outside of the arc either continuously or intermittently along the boundary.

This method of fixing vanes to the body of the bend is simple and quick, but this affects adversely the very purpose of stabilizing the flow, especially in cases like this where spacing between vanes is quite small. A constriction is formed at the welded ends of vanes distorting the flow.

To overcome this difficulty, a special welding technique was adopted as illustrated in the two bottom sketches of Figure 4.c. Countersunk holes were drilled at suitable intervals in the side plates along curves that corresponded to the vane profile. Weld material was deposited from outside. These welding spots met the vane edge, but did not project much into the flow path, rendering the flow path comparatively smoother. Thus, the welding technique chosen may be considered as an improvement over the conventional one.

The vanes and the bends were made out of 1/16 in. and 1/8 in. thick steel sheets respectively. Figure 4.d gives a view of the vanes and the bend.

2.b.3 Transitions

In an effort to retain as much as possible an identical pattern of flow from the supply reservoir to the test model, it was thought advisable to use a square tube of the same inside dimensions as that of the test section. The actual size of the test section was 3.06 in. x 3.06 in. No square tube was available to conform to this size exactly, the nearest size available being 2.76 in. x 2.76 in. inside measurements (3 in. x 3 in. outside measurements).

Thus it was necessary to provide a transition upstream of the test section. For the same reason, a transition was also necessary downstream of the test section.

Upstream Transition

The aluminum tube described above was split at the corners for a length of 6 in. The freed sides were then pried apart suitably and corner-gaps filled with weld-material. This gave a change of cross-section from 2.76 in. x 2.76 in. to 3.06 in. x 3.06 in., in a length of 6 in., that is, a slope of 1:40, which may be regarded as gentle enough to leave the flow undisturbed.

Any irregularities appearing on the inside due to welding were carefully chipped off and the surface made smooth.

Downstream Transition

This transition was made integral with the downstream bend fitted with vanes. 1/8 in. thick steel sheet was used for the purpose. The cross-sectional change from 2.76 in. x 2.76 in. to 3.06 in. x 3.06 in. was brought about in a length of 2 ft., giving a slope of 1:160. The transition was galvanized along with the bend.

2.b.4 Inlet and Outlet Controls

Priming was necessary before the tunnel could be started. For priming of the tunnel, the inlet and outlet were to be blocked. For this an inlet blockage and an arrangement for opening and closing of outlet were provided.

Inlet Blockage

This consisted of a steel plate faced with rubber and fitted with two threaded brass rods which in turn were connected to two springs of 15 pounds per inch stiffness. The free ends of the springs were then joined to the handles as shown in Figure 1. The plate rested against the inlet opening firmly held by the springs in tension.

Outlet Closing and Opening Arrangement

A 4 in. Victaulic butterfly valve was fixed to the outlet in the basement. The handle of the valve was connected to two separate cords which passed around the suitably placed and rigidly supported pulleys. The free ends of the cords were located on the ground floor, so that the opening and closing operations could be performed conveniently from there. Figure 1 illustrates the closing and opening arrangement.

2.b.5 Specification of the Tunnel

Designation	SYPHON TUNNEL
Nominal Size	3 in. x 3 in.
Vertical length of the entry leg	6.5 ft
Length of the horizontal portion	13.0 ft
Vertical length of the discharge leg	24.5 ft
Maximum driving head	20 ft
Maximum discharge	1.27 cusecs (Theoretical) 1.23 cusecs (Experimental)

Cavitation Number* $\begin{cases} 2.57 \text{ (Theoretical)} \\ 2.66 \text{ (Experimental)} \end{cases}$

Ventilation factor r_2 0.2
(for continuous operation of the syphon tunnel as discussed later)

2.c Measuring Equipment

2.c.1 Volume Flow of Water

This was measured by a direct method. A piezometer tube showed the level of water in the supply tank against a scale in the background. The readings could be taken with an accuracy up to 1/40th of an inch. The fall in level of water in the tank (size 60 ft x 3 ft x 3 ft) gave the total volume of flow in a certain interval of time.

2.c.2 Volume Flow of Air

A rotameter consisting of a 150 mm scale, a plain taper tube and a spherical float was used for measuring the volume flow of air. Calibration curves supplied by the manufacturers gave the relation between level of the float and the rate of volume flow of air at specified standard conditions of pressure and temperature. Air was supplied from the atmosphere through the rotameter to a point located

---

* The values given here refer to the case in which no gate or orifice plate is used and the temperature of water is 75°F.

on the centre-line of the test section floor and at a distance of 1-5/8 in. downstream of the gate. The quantity of air could be varied by means of a built-in needle valve. The carrying base was provided with a spirit level and levelling screws to help place the rotameter properly. Maximum capacity of the rotameter was 125 cu.ft./hour at the standard conditions (T_S, p_S).

2.c.3 Measurement of Velocity of Water

The turning vanes in the upstream bend were introduced to make the velocity distribution in the flow approaching the gate as uniform as possible across the square channel. To study the success of these vanes, velocities were measured at a section 3 ft downstream of this bend. A pitot tube was traversed in the vertical plane at the lateral mid-section of the aluminum square channel. A tap for indicating static pressures was located in the side wall of the channel appropriately. The pitot tube and the static tap were connected to an inverted 'U' tube manometer. Velocity was computed from the differential head indicated.

2.c.4 Measurement of Static Pressures

(i) Multiple-tube Mercury Manometer

It was required to measure static pressures at a large number of points. A multiple-tube mercury manometer was constructed. There were in all 20 glass tubes, each of 32 inch length and 4 mm inside diameter. The manometer board was a sheet of clear and transparent plexiglas measuring 36 in. x 18 in. x 3/8 in. 'V' grooves were milled lengthwise to provide proper seating for the glass tubes. Scales in inch-fractions were engraved by the side of each groove. All the tubes were connected to a common stainless steel reservoir filled with mercury. One of the tubes was always open to atmosphere to serve as a reference.

It was convenient to take photographs of each set of readings on the manometer and interpret them later. For this, the manometer was lighted sufficiently from the back. To diffuse the light on the back uniformly, the plexiglas sheet was backed by a sheet of ground glass.

A Dexion frame was constructed to which were fixed all the components mentioned above. Figure 6 shows the arrangement described.

(ii) Squashing Device

It was essential to have some kind of a device that would isolate the manometer from the tunnel in the following situations:

(a) When the tunnel was being primed

(b) When it was needed to build up mercury columns in more than a single run of the tunnel (see article 2.a.4)

(c) When it was desired to freeze the readings on the manometer board for taking note of them.

Detailed description of the squashing or squeezing device used is given by Kwok[6]. This device was fixed on the top of the Dexion frame, as seen in Figure 6.

3. OPERATION OF THE TUNNEL

3.a Operational Sequence

As a first step it was imperative to make the mercury manometer ready for static pressure measurements before the tunnel was run. This was the most time-consuming job, in that any possible traces of air either entrapped in the glass tubes or in the Tygon tubes linking manometer to the static pressure taps had to be removed. There were 19 such tubes and each had to be attended to individually. A syringe was used to pump distilled water through the tubes, one by one, driving the entrapped air out to the atmosphere through the main mercury reservoir.

However, it was found later that all this procedure could be avoided prior to the next experiment if it were performed within a day or so. This was done by locking the squashing device when the tunnel was still running, there being no air in the tubes at that time. Unlocking was done during the next experiment when the tunnel was already running. It was inadvisable to keep the squashing device locked for more than a day, because the rubber tubes were likely to be deformed permanently and also because air evolved out of the stagnant water in the tubes became significant too.

The next step after making the manometer ready and locking the squashing device was closing the outlet valve and fitting the spring-supported blockage plate at the inlet. The air exit valve and the priming valve were then opened. While water from the mains filled the tunnel, air rushed out through the exit valve. When the gate opening was about 1 in. or less, the air had difficulty making its way to the exit valve. In those situations, one or two appropriate 'C' clamps were loosened to help the air out.

When priming was almost complete, the priming and air exit valves were closed, and the blockage plate at the inlet was removed. Further, to make sure that air pockets, if any were left, were virtually eliminated, the outlet was opened for a short time and then closed. The water rushing down dragged the air out along with it.

The tunnel was then ready for operation. It may be noted that when priming was not complete, the resultant volume flow in the tunnel was much reduced, and a complete break in the flow occurred as atmospheric air forced its way up from the outlet side to destroy the syphoning action.

3.b <u>Operational Limit (On Air-Supply)</u>

Controlled amounts of air were supplied to ventilate the separation eddies. It was found that steady runs of the tunnel were possible only up to a certain limit of the air supply. Beyond that limit, the volume flow of water became too low to let the tunnel run full. The flow first became unsteady and then broke as described above. Observations made in a large number of test runs indicated the operational limit of the tunnel as r_2 nearly equal to 0.2. The measured pressures given in the following pages for any case of $r_2 > 0.2$ are obtained from the highest values of suction indicated by the mercury manometer before the breakdown of the flow.

4. THEORETICAL ANALYSIS

The rate of flow of water through the tunnel has been found by using the standard methods of calculating the piping losses. An integral technique simplified by the assumption of uniform and unidirectional velocity has been adopted to find the relationship between the static pressures at various streamwise locations in the test section (articles 4.c.1 and 4.c.2).

4.a Evaluation of the Rate of Flow of Water

The following evaluation is given for the case when the separation eddy is not ventilated. In the case of a ventilated eddy the actually measured value of Q_w is kept as the known parameter. Incorporating Equation (A.4) into Equation (A.1) of Appendix I.A, substituting appropriate numerical values and using the continuity relation, we obtain the following expression (F.P.S. units) in which H is a known quantity.

$$H = [12.0 + 3.67 \left(\frac{A_t}{A_g C_c} - 1\right)^2] \, Q_w^{\,2} \tag{1}$$

This is valid when no orifice plate is inserted at position M (Figure 7). It may be generalized to the following form:

$$H = [(12.0 + K_1) + 3.67 \left(\frac{A_t}{A_g C_c} - 1\right)^2] \, Q_w^{\,2} \tag{2}$$

where K_1 is the loss factor associated with the orifice plates and is given in Appendix I.B. Numerical values of K_1 are:

$K_1 = 0$	Full-Open Case
$= 17.4$	Half-Open Case
$= 158.7$	Quarter-Open Case.

The above terms may be defined as follows:

'Full-Open' case	When the flow passage at M (Figure 7) is fully open, i.e. the case in which no orifice plate is used.
'Half-Open' case	When an orifice plate having a nominal area of flow equal to one-half of the area A_s is inserted at M.
'Quarter-Open' case	When an orifice plate having a nominal area of flow equal to one-quarter of the area A_s is inserted at M.

4.b <u>Evaluation of p_0</u>

p_0 is the static pressure at the section (0) shown in Figure 7. An equation of the hydraulic energy balance may be stated as follows:

$$H_{atmos} = E' + \frac{V_t^{\,2}}{2g} + \frac{p_0}{\rho_w g} + \Sigma H' \text{ (section A to 0)}$$

$$+ \Sigma H_f' \text{ (section A to 0)}$$

Substituting for the above $\Sigma H'$ and $\Sigma H_f'$ appropriately from Appendix I.A and inserting numerical values, we obtain

$$p_0 = \rho_w\, g\, [H_{atmos} - E' - 7.66\, Q_w^{\,2}] \qquad \text{(F.P.S. units)}$$

where H_{atmos} is 33.76 ft of water or 29.79 in. of mercury.

The above equation would apply when there is no orifice plate at M (Figure 7). General form of the equation would be

$$p_0 = \rho_w\, g\, [33.76 - E' - (7.66 + K_1)\, Q_w^{\,2}] \qquad (3)$$

where K_1 has the same meaning as in Equation (2) and $E' = (7.5 - \overline{h})$ ft, as evident from Figure 7.

4.c Pressure Relationships

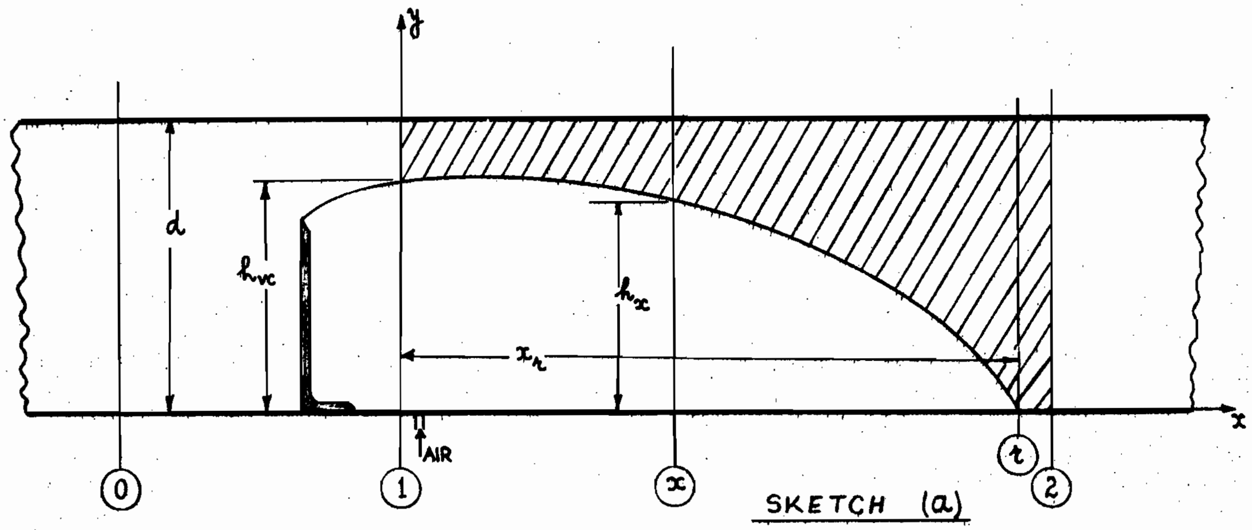

SKETCH (a)

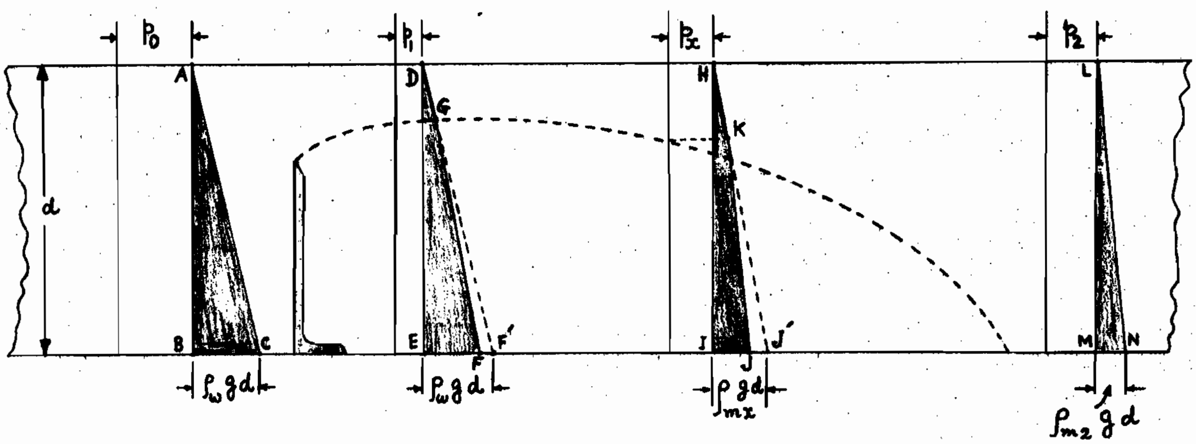

SKETCH (b)

Assumptions

1. Pressure acting across each section varies due to gravitational effect only.

2. Temperature of water T_w in the test section remains at the reservoir level.

3. The Reynolds number of the flow is very high (approximately of the

order of 10^5), so that shearing forces at the wall may be neglected. Also, the effect of the boundary layer development is assumed to be negligible.

4. Air on entry into the test section is swept downstream instantaneously so that the density of the fluid in the hatched portion at section (1) in the sketch (a) is unaffected. Thereafter, the downstream variation of density of the air-water mixture is assumed to be linear up to section (r), i.e. the density changes linearly in the hatched portion from ρ_w at section (1) to ρ_{mr} at section (r). After section (r) the density is assumed to remain constant at the latter value.

5. The water is already saturated with air and other gases at its temperature T_w, so that the air drawn in from outside into the separation eddy retains its identity in the air-water mixture rather than being absorbed.

6. $\int_0^A V^2 dA = \frac{Q^2}{A}$ where V is the velocity, A is the corresponding area of flow and Q is the rate of volume flow. Note that the net flux of air-water mixture through any vertical section of the separation eddy is assumed to be negligible.

7. The effect of surface tension on the pressures is assumed negligible (Appendix II.A).

<u>Sketch (b)</u>

Pressure varies across any section due to gravity. At the section (0) the variation is uniform as the density of the flow is the same across the section; but from the gate up to the section (r) the density is different at the inside and outside of the ventilated eddy and hence the variation is non-uniform. For example, at the section (1) the density outside the eddy is ρ_w, whereas inside it is less due to the addition of air. Thus, the pressure at the floor of the test section may be $(p_1 + EF)$ instead of $(p_1 + EF')$. Similar argument may be applied to the other sections along the length of the eddy.

4.c.1 <u>Relation between p_0 and p_1</u>

Momentum balance at sections (0) and (1) may be established as follows (see sketch a):

$$\left[\int_0^{A_t} p\, dA + \rho_w \int_0^{A_t} V^2 dA\right]_{\text{section (0)}} = \left[\int_0^{A_t} p\, dA + \rho_w \int_0^{A_g C_c} V^2 dA + H'_G \rho_w g A_t\right]_{\text{section (1)}}$$

Evaluating $\int p\, dA$ from sketch (b) and applying assumption (6), we get

$$p_0 A_t + (\text{Area ABC}) \times d + \rho_w \frac{Q_w^2}{A_t} = p_1 A_t + (\text{Area DEFG}) \times d + \rho_w \frac{Q_w^2}{A_g C_c} + H'_G \rho_w g A_t$$

or

$$(p_0 - p_1) = (\text{Area DEFG} - \text{Area ABC}) \times \frac{1}{d} + \rho_w \frac{Q_w^2}{A_t A_g C_c} - \rho_w \frac{Q_w^2}{A_t^2} + H'_G \rho_w g$$

where

$$H'_G = \frac{Q_w^2}{2g}\left[\frac{1}{A_g C_c} - \frac{1}{A_t}\right]^2$$

The pressure term (area DEFG - area ABC) x $\frac{1}{d}$ is negligible as shown in Appendix II.B. Applying the equation of continuity, the above expression may be simplified to the following:

$$(p_0 - p_1) = \frac{\rho_w Q_w^2}{2}\left[\left(\frac{1}{A_g C_c}\right)^2 - \left(\frac{1}{A_t}\right)^2\right] \qquad (4)$$

4.c.2 Relation between p_1 and p_x

An equation similar to the one in the previous article may be written for the sections (1) and (x) with reference to sketch (a).

$$\left[\int_0^{A_t} p\, dA + \rho_w \int_0^{A_g C_c} V^2\, dA\right]_{\text{section (1)}}$$

$$= \left[\int_0^{A_t} p\, dA + \rho_{mx} \int_0^{A_x} V_{mx}^2\, dA\right]_{\text{section (x)}} \qquad 0 < x \leqslant x_r \qquad (5a)$$

This may be simplified to the form given below by applying assumption (6) and evaluating $\int p\, dA$ from sketch (b).

$$p_1 A_t + (\text{area DEFG}) \times d + \frac{\rho_w Q_w^2}{A_g C_c} = p_x A_t + \text{area (HIJK)} \times d + \frac{\rho_{mx} Q_{mx}^2}{A_x}$$

or

$$(p_x - p_1) = (\text{area DEFG} - \text{area HIJK}) \times \frac{1}{d} + \frac{\rho_w Q_w^2}{A_t}\left[\frac{1}{A_g C_c} - \frac{\rho_{mx} Q_{mx}}{\rho_w Q_w^2} \cdot \frac{Q_{mx}}{A_x}\right]$$

$$0 < x \leqslant x_r \qquad (5b)$$

Now

$$\rho_{mx}Q_{mx} = \rho_w Q_w + \rho_S Q_S \qquad x > 0$$

or

$$\rho_{mx}Q_{mx} \doteq \rho_w Q_w \qquad x > 0 \qquad (6)$$

This simplification is justified because the mass of air drawn into the eddy is a very small fraction of the mass of water, although the volume is appreciable. The pressure term (area DEFG - area HIJK) x $\frac{1}{d}$ may be neglected as small, as illustrated numerically in Appendix II.B. Thus Equation (5b) may be changed to the following form:

$$(p_x - p_1) = \frac{\rho_w Q_w^{\ 2}}{A_t}\left(\frac{1}{A_g C_c} - \frac{Q_{mx}}{Q_w A_x}\right) \qquad 0 < x \leqslant x_r \qquad (7)$$

Assumption (4) regarding linear density variation may be interpreted mathematically as

$$\rho_{mx} = \rho_w - (\rho_w - \rho_{mr})\frac{x}{x_r}, \qquad 0 < x \leqslant x_r \qquad (8)$$

Applying Equation (6) at section (2) we get

$$\rho_{m2}Q_{m2} \doteq \rho_w Q_w$$

where

$$Q_{m2} = Q_w + Q_{a2}$$

so that

$$\rho_{m2} = \frac{\rho_w Q_w}{(Q_w + Q_{a2})} \qquad (8a)$$

But $\rho_{m2} = \rho_{mr}$ (assumption 4)

Therefore

$$\rho_{mx} = \rho_w \left[1 - \frac{r_2 \frac{x}{x_r}}{(1 + r_2)} \right] \qquad 0 < x \leqslant x_r \qquad (9)$$

where

$$r_2 = \frac{Q_{a2}}{Q_w}$$

Combining Equations (6) and (9), we deduce

$$\frac{Q_{mx}}{Q_w} = \frac{(1 + r_2)}{(1 + r_2 - r_2 \frac{x}{x_r})} \qquad 0 < x \leqslant x_r \qquad (10)$$

Inserting this relation in Equation (7) we may write finally

$$(p_x - p_1) = \frac{\rho_w Q_w^{\ 2}}{A_t} \left[\frac{1}{A_g C_c} - \frac{(1 + r_2)}{A_x(1 + r_2 - r_2 \frac{x}{x_r})} \right], 0 < x \leqslant x_r \qquad (11a)$$

When no air is introduced, $r_2 = 0$, Equation (11a) is reduced to

$$(p_x - p_1) = \frac{\rho_w Q_w^{\ 2}}{A_t} \left[\frac{1}{A_g C_c} - \frac{1}{A_x} \right], \qquad 0 < x \leqslant x_r \qquad (11b)$$

4.c.3 <u>Relation between p_1 and p_2</u>

By virtue of the assumption (4) the density of the air-water mixture is a discontinuous function at the point of reattachment, because the value of the term ($\frac{x}{x_r}$) in the above equations being unity at $x = x_r$ remains unity for $x > x_r$. Therefore, at the section (2) the Equation (11a) may be modified as follows:

$$(p_2 - p_1) = \frac{\rho_w Q_w^2}{A_t} \left[\frac{1}{A_g C_c} - \frac{(1 + r_2)}{A_t} \right] \tag{12a}$$

When no air is introduced, $r_2 = 0$ and Equation (12a) changes to the following

$$(p_2 - p_1) = \frac{\rho_w Q_w^2}{A_t} \left[\frac{1}{A_g C_c} - \frac{1}{A_t} \right] \tag{12b}$$

4.d <u>Pressure Recovery Index</u>

(i) $\underline{C_{px}}$

This is an index of the recovery of pressure along the length of the separation eddy after the flow has passed the vena contracta. By definition

$$C_{px} = \frac{(p_x - p_1)}{\frac{1}{2} \rho_w V_{vc}^2} \qquad 0 < x \leqslant x_r \tag{13a}$$

or

$$C_{px} = \frac{2(p_x - p_1)(A_g C_c)^2}{\rho_w Q_w^2} \qquad 0 < x \leqslant x_r \tag{13b}$$

Combining Equations (11a) and (13b), we obtain

$$C_{px} = \frac{2(A_g C_c)^2}{A_t} \left[\frac{1}{A_g C_c} - \frac{(1 + r_2)}{A_x(1 + r_2 - r_2 \frac{x}{x_r})} \right], \; 0 < x \leqslant x_r \tag{14a}$$

For $r_2 = 0$

$$C_{px} = \frac{2(A_g C_c)^2}{A_t} \left[\frac{1}{A_g C_c} - \frac{1}{A_x} \right], \qquad 0 < x \leqslant x_r \tag{14b}$$

(ii) $\underline{C_{p2}}$

This is an overall pressure recovery index representing the total amount of pressure recovered from section (1) to section (2) (see sketch a). By definition,

$$C_{p2} = \frac{(p_2 - p_1)}{\frac{1}{2}\,\rho_w V_{vc}^{\;2}} \tag{15a}$$

By the same argument as given in article 4.c.3, the term $\left(\frac{x}{x_r}\right)$ in Equation (14a) is unity beyond the point of reattachment. Thus, at section (2) this equation may be modified as below:

$$C_{p2} = \frac{2(A_g C_c)^2}{A_t} \left[\frac{1}{A_g C_c} - \frac{(1 + r_2)}{A_t} \right] \tag{15b}$$

When no air is added, $r_2 = 0$, hence

$$C_{p2} = \frac{2(A_g C_c)^2}{A_t} \left[\frac{1}{A_g C_c} - \frac{1}{A_t} \right] \tag{15c}$$

4.e <u>Cavitation Parameter</u>

In its well known form the cavitation parameter is defined as

$$\sigma_c = \frac{p - p_c}{\frac{1}{2}\rho V^2} \tag{16a}$$

where σ_c = cavitation parameter

p_c = critical pressure generally taken equal to the water vapour pressure

p = static pressure at a point

V = velocity of flow at that point

ρ = mass density of the fluid.

In our case, the cavitation parameter may be taken as

$$\sigma_c = \frac{p_1 - p_c}{\frac{1}{2}\rho_w V_{vc}^{\ 2}} \qquad (16b)$$

Since changes in the values of E' and H, in our case, are too small to affect the cavitation parameter, we may write the following functional relationships for any fixed value of K_1.

$$(p_1 - p_c) \sim (h,\ d,\ T_w,\ Q_{a2},\ V_{vc},\ \rho_w).$$

Changes in temperature T_w affect p_c. A proper value of p_c at known T_w should take care of the temperature effect. The value of p_c at any temperature may be found from standard tables or curves. In a non-dimensional form we may state the above relation as follows:

$$\frac{p_1 - p_c}{\frac{1}{2}\rho_w V_{vc}^{\ 2}} = F_1 \left[\frac{h}{d},\ \frac{Q_{a2}}{V_{vc}(d-h)\ d} \right]$$

In other words

$$\sigma_c = F_2\left(\frac{h}{d},\ \frac{Q_{a2}}{Q_w} \right) \qquad \text{where } Q_w \propto V_{vc}\ (d-h)\ d$$

$$= F_2\left(\frac{h}{d},\ r_2 \right) \qquad (17)$$

Theoretical values of Q_w and p_1, as derived from Equations (2), (3), and (4) where $r_2 = 0$, make it possible to plot values of σ_c against $\frac{h}{d}$ for the known orifice plate openings. Figure 34 compares such values with those found from experiments.

Similarly, Figure 35 shows the comparison between the theoretical and experimental values of σ_c against r_2 when $\frac{h}{d}$ is fixed.

4.f Performance Characteristics of the Syphon Tunnel

General

Equations (2) and (3) indicate the possibility of constructing a similar syphon tunnel or of modifying the present one to obtain desired values of Q_w or p_0 (hence p_1 and p_2) through manipulation of H, E', K_1 and $A_g C_c$.

For a similar syphon tunnel there will be changes only in the constants of these equations, depending mainly upon the internal dimensions of the tunnel. These changes can easily be arrived at following the procedure detailed in Appendix 1.A and I.B.

The performance characteristics described as follows relate specifically to a syphon tunnel free of control gate and having internal dimensions equal to those of the present one, when the variation limits as noted below are allowed in the values of H and E', putting theoretically no restriction on the values of K_1.

Justifications for the Analysis Used

For a given position of water supply level, a change in driving head H necessitates a corresponding change in the length of the discharge leg; whereas, a change in elevation E' brings about equal changes in the lengths of both the entry and discharge legs of the syphon tunnel.

To obtain pure cavitation (vaporous type) in the test section, pressure must be equal to or less than the vapour pressure which may be of the order of $\frac{1}{4}$ psia or so, depending upon the temperature of water. In the extreme case it may be equal to zero psia. So let us consider an ideal situation when a zero value for the pressure in the test section is aimed at. For a real value of Q_w, E' is always less than 33.76 ft or H_{atmos}. In practice it may be only about 25 feet or even less. The value of H, however, can be made as much as needed by lengthening the discharge leg vertically, though this is also severely limited in the case of an experimental set-up in a laboratory.

The lengths of the vertical entry and discharge legs of the present tunnel are 6.5 ft and 24.5 ft respectively and the governing equations are (2) and (3). If we assign arbitrarily high values of 30 ft and 80 ft respectively to the lengths of the vertical entry and discharge legs, the new governing equations would be

$$H = [\,(13.89 + K_1) + 3.67\,\left(\frac{A_t}{A_g C_c} - 1\right)^2]\,Q_w^{\,2} \tag{18}$$

and

$$P_0 = \rho_w g\,[33.76 - E' - (8.86 + K_1)\,Q_w^{\,2}] \tag{19}$$

Comparing the new Equations (18) and (19) with the old ones (2) and (3), we find that the extent of modification, though not negligible, is definitely small in the context of drastic changes introduced in the lengths of the legs. The gap between the new equations and the old ones would be much narrower for moderate values of these lengths. This is so because the dominating factors contributing to the loss of head are bends, entrance and exit and the abrupt changes in cross-sections, etc., rather than friction in the pipe.

This justifies the sufficiency of Equations (2) and (3) in discussing the performance characteristics, provided moderate values of the lengths of the legs are used.

The Analysis

In the absence of a control gate Equation (2) reduces to

$$Q_w^{\,2} = \frac{H}{(12.0 + K_1)} \tag{20}$$

For $p_0 = 0$, Equation (3) becomes

$$Q_{w_o}^{\,2} = \frac{(33.76 - E')}{(7.66 + K_1)} \tag{21}$$

and Equation (20) changes to

$$Q_{w_o}^{\,2} = \frac{H_0}{(12.0 + K_1)} \tag{22}$$

where Q_{w_o} and H_0 are the respective values of Q_w and H when $p_0 = 0$.

Relating Equations (21) and (22) we obtain

$$H_0 = (33.76 - E')\,\frac{12 + K_1}{7.66 + K_1} \tag{23}$$

The performance characteristics are given in the form of curves, relating parameters K_1, Q_w, Q_{w_o}, H, H_0, and E', where loss coefficient K_1 is a function of the orifice plate design. Figures 10 to 13 show curves deduced from Equations (20) to (23). These curves are helpful in the tunnel design, in that one can read off directly the value of any one parameter when the others are known.

Possible Modification (in the Present Tunnel)

It is not easily possible in our Hydraulics Laboratory to increase the driving head appreciably. However, to get to the case of pure cavitation in the present tunnel, we have to depend on the changes being made in E' and K_1. But, we have already used quarter-open orifice plate with the factor K_1 nearly equal to 160. There is not much point in increasing K_1 any further, because it will reduce the rate of discharge considerably and make the flow susceptible to break-down in the same way as described in article 3.a. It is therefore suggested that a change be made in the elevation E'. The existing value of E' is about 5 ft. It is evident from Figure 13 that for the maximum driving head of 20 ft (as in our case) and K_1 approximately equal to 50, an elevation E' of nearly 15 ft is sufficient to give us the zero absolute pressure. Thus, we would have to raise our horizontal portion of the tunnel by about 10 ft, making corresponding changes in the entry and discharge legs and the working platform.

Role of Factor K_1

K_1 is the loss factor associated with the orifice plates that were inserted at section M (Figure 7). The orifice plates were used to vary the flow rate and to obtain a considerable pressure drop before the flow reached the test model. This drop was helpful to induce cavitation and to draw air in for ventilating the separation eddy.

In the beginning an attempt to reduce the flow rate was made by inserting various orifice plates at a section just upstream of the Victaulic valve K (Figure 7). This method was found much less effective than the use of orifice plates at the section M. This simply gave a greater loss of kinetic head at the outlet decreasing the flow rate to some extent, but increased the pressure in the test section which was not desired.

5. GEOMETRY OF THE SEPARATION EDDY

The geometry of the separation eddies formed in several different situations has been of interest to various investigators. It has been studied by Bourque and Newman[7], Sawyer[8], Wyganski[9] and others, in connection with the reattachment of two-dimensional incompressible jets to adjacent surfaces. In all these cases the basic assumptions were the same, i.e. uniformity of pressure inside and outside the eddy and description of the the velocity profile of the jet similar to that of a free jet, with the centre-line of the jet a circular arc. The assumption of the uniformity of pressure inside the bubble is somewhat doubtful as the experimental results show that the pressure varies significantly in almost all the cases studied.

However, in the present case the pressure is assumed to vary along the length of the eddy; as confirmed by the measured velocity distribution of Förthmann[2] in a partially expanding jet†, there is no similarity in velocity profiles; and finally the geometry of the eddy denies conformability to any single shape. Though there are some helpful factors, e.g. the continuity relation and the assumption of the pressure remaining constant across any vertical plane in the test section*, yet the problem remains complicated. The complexity

---

† see footnote on page 3

* Note that the assumption (1) in article 4.c allows the effect of gravity on the pressure across a vertical plane, but it is shown in Appendix II.B that this effect is negligible, so that ultimately it amounts to saying that the pressure remains constant across any vertical plane in the test section.

of the problem is confirmed by Arie and Rouse[3] who, while studying the two-dimensional flow over a normal wall, approached the geometry of the separation eddy with knowledge of the experimental results a priori.

A theoretical approach has been suggested by Savage[4] for determining the geometry of the steady 'separation bubbles' behind bluff bodies in the case of flows with free streamlines. Implicit in this approach are a number of basic assumptions including the similarity of velocity profiles downstream of the bluff body and taking of the static pressure at reattachment equal to that of the free streamline. It has already been pointed out that this assumption about velocity profiles cannot be made in the present situation. Also, since the flow studied is completely confined, the assumption about the static pressure at reattachment being equal to that of the free streamline is not relevant. Thus, the above approach is considered as unadaptable to the present case.

As a result of several attempts, it has been found that any single model based on an elliptical form, circular arc, a sloping straight line etc. or combinations of these does not simulate the eddy geometry for all the cases of flow studied presently.

A Model of the Eddy Geometry

A model that does give fairly satisfactory results for solidity ratios $\gg 0.8$ nearly is described as follows:

It is assumed that the vena contracta is about one gate opening downstream of the gate and that from the vena contracta up to the point of reattachment the eddy profile is simulated by a quarter of

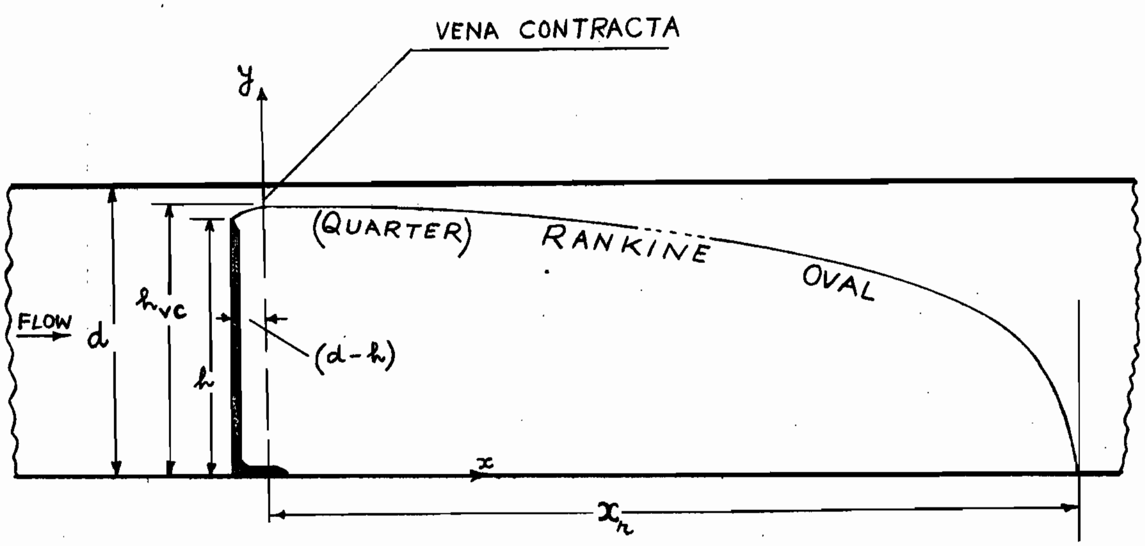

SKETCH (C)

a Rankine oval shown in the above sketch.

The Rankine oval is a stagnation streamline generated by lining a source and a sink with a uniform flow. If U is the velocity of uniform stream, source of strength +m' and sink of strength -m' are situated 2s apart, x_r is the semi-major axis and h_{vc} is the semi-minor axis of the oval, then following reference (10) we may write

$$\frac{h_{vc}}{s} = \cot \frac{\pi U h_{vc}}{m'} \tag{24a}$$

$$\frac{x_r^2}{s^2} = 1 + \frac{m'}{\pi U s} \tag{24b}$$

and

$$x^2 + y^2 - s^2 = 2ys \cot \frac{2\pi U}{m'} y \tag{24c}$$

Let us put

$$K_2 = \frac{s}{h_{vc}} \tag{24d}$$

With simple manipulation Equations (24a) and (24b) yield

$$\tan^{-1} K_2 = \frac{K_2}{\left(\frac{x_r}{h_{vc}}\right)^2 - K_2^{\,2}} \tag{25}$$

Substituting this in Equation (24c) we get

$$x^2 = 2\, h_{vc}\, K_2\, y \cot\left(\frac{2 \tan^{-1} K_2}{h_{vc}}\; y\right) + K_2^{\,2} h_{vc}^2 - y^2 \tag{26}$$

h_{vc} can be derived for a given value of h; x_r is determined experimentally as illustrated in Figure 9 for a typical case; so that K_2 is given by Equation (25). Now Equation (26) can be solved to get the complete geometry of the oval.

Pressure Distribution From the Model

Pressure distribution in the form of pressure recovery index, C_{px}, can now be found from Equation (14a) at any station x along the length of the eddy. Plots of this are shown for solidity ratios 0.892 and 0.817 in Figures 15 to 24. Limitation about the application of the model is clearly stated in article 6.d.

6. EXPERIMENTAL RESULTS AND DISCUSSION

6.a Flow Pictures

Pictures of the flow with and without ventilation of the eddies are given in Figure 8 for a few typical cases with a nominal gate opening of 1/2 in. (or $\frac{h}{d} = 0.817$). The pictures were taken with an exposure of 1/1000 sec. in each case. They are arranged from the top of the page (Figure 8) in increasing order of the ventilation factor.

Picture 8.a is given in respect of a non-ventilated eddy for which the absolute pressure at the vena contracta in the test section was only 5.09 in. of mercury. At that low pressure the diffusion of the dissolved gases (gaseous cavitation) resulted in the generation of gas bubbles behind the gate. These bubbles appear as black specks in the picture.

Pictures 8.b, 8.c, and 8.d refer to the ventilated eddies. The former two pictures represent the eddies with ventilation factors (r_2) less than 0.2, whereas the last represents an eddy with the factor greater than 0.2. As pointed out earlier, 0.2 was the approximate limiting value of the ventilation factor above which the continuous operation of the syphon tunnel was not possible. Thus, in the last case when r_2 was equal to 0.305 the flow through the test section seemed to be continuous only for a short period (about 15 seconds) after which it broke down. Picture 8.d shows the flow at the time of such a breakdown

6.b Tabulated Comparison Between Analytic and Measured Pressures

The comparison is reported in direct tabular form to give a clear idea of the behaviour of the pressures when the ventilation factor r_2, and orifice plate opening, and solidity ratio (h/d) are varied.

It may be stressed here again that in the case of ventilated eddies the operation of the tunnel was continuous only up to a value of r_2 nearly equalling 0.2. For $r_2 > 0.2$, the results given for pressures simply refer to the highest values of suction reached before the breakdown of the flow.

(i) Static pressure p_0 and hence p_{0s} were found analytically from Equation (3) for each case. Corresponding experimental values of p_{0s} were determined at a distance 1 ft downstream of the entrance of the test section.

(ii) Theoretical values of p_{1s} were determined from Equation (4), whereas the experimental values were determined at the vena contracta section (assumed to occur at a distance equal to one gate-opening from the gate edge) from the mean experimental curves whose qualitative picture is as shown in Figure 9.

(iii) Theoretical values of p_{2s} were found from Equation (12a). It is seen from the typical experimental curve in Figure 9 that beyond a certain section (reattachment section) downstream of the gate, the pressures become sensibly constant. For all the cases the experimental values of p_{2s} were determined from such curves.

6.c Upstream Velocity Profiles

The inverted 'U' tube manometer was used to find the velocities of flow at a section 3 ft ahead from the upstream bend. Plots of these velocities are given in Figure 14. It is found from these plots that the vanes were partially successful in achieving the object of making the velocity distribution across the channel fairly uniform.

6.d Pressure Recovery Index

Pressure distributions along the length of both the types of eddy (ventilated and non-ventilated) are presented in the form of pressure recovery index C_{px} against a non-dimensional ratio (x/h).

The curves based on the Rankine oval geometry of the eddy (Equation 26) were computed for all the cases of flow studied. Agreement between the curves thus computed and the experimental values was just satisfactory only for the cases of h/d equal to 0.892 and 0.817 [Figures 15 to 24].

It is seen from Figures 25 and 26 (for $\frac{h}{d} = 0.653$) that the divergence between these curves and the experimental points is quite large. The divergence remains large for $\frac{h}{d}$ equal to 0.49 and 0.327. The reason for this divergence may be given as follows: The geometry of the Rankine oval is fixed uniquely by the lengths of the eddy which are determined experimentally. The experimental results show these lengths to be such that the ratio of the minor to the major axis of the oval is considerably reduced when the solidity ratio is made less. Thus, it is expected that for lower solidity ratios the profile given by quarter-oval shall be flatter for larger portions of the eddy lengths. For these portions, in other words, the model would predict a much slower change in the effective area of flow (shown hatched in sketch a) and consequently in the velocity or in the static pressure. This fact is not borne out by the actual measurements and gives rise to the divergence mentioned above.

The model postulated in reference (3) is meant for very low solidity ratios ($\frac{h}{d} \leqslant 0.17$) only. It is part of a half Rankine oval and is quite different from the model given here. In that model the length between source and sink is arbitrarily varied to match the resulting stagnation streamline with the experimentally determined shape of the cavity.

Figures 27 to 32 give only the mean experimental curves relating C_{px} with x/h. In some of the curves for C_{px} versus x/h we find that C_{px} goes negative. This only implies that in such cases the absolute pressure is not a minimum at the assumed vena contracta section but at some section further downstream. This situation seems to arise mainly because of the ventilation. As discussed in article 6.h.3, the ventilated eddies are longer than non-ventilated ones, so that in general the effective area of flow (shown hatched in sketch a, article 4.c) changes more slowly in their case. At the same time, the volume flux passing through the ventilated eddies becomes larger due to the additional entrainment of the air supplied. All this results in increased dynamic pressure and reduced static pressure, explaining thereby the existence of negative values of the pressure recovery index C_{px}.

The experimentally determined variation of C_{p2} against r_2 is compared with the theoretical curves in Figure 33. C_{p2} decreases when r_2 increases, the decrease being more pronounced for lower solidity ratios. This can be easily predicted on examining the difference between the expressions of the Equations (15b) and (15c). It is evident from Figure 33 that almost all the experimental points tend to lie below the theoretical curves. This discrepancy can, to some extent, be explained by the facts that we have neglected friction and non-uniformity of velocity and also we have not accounted for the air or gases evolving out of water (due to gaseous cavitation). The last fact, if accounted for, would give increased air-water ratio so that the real value of r_2 would be higher and all the plotted experimental points ought to shift to the right on the same horizontal level in Figure 33 giving a better agreement with the theoretical curves.

6.e Cavitation Parameter*

The theoretical and experimental values of the cavitation parameter σ_c are given in Figure 34 for various combinations of h/d

---

* The minimum value of cavitation parameter σ_c reached in this tunnel was 0.018. This value was reached during an experiment on a venturimeter model fixed in the test section. σ_c in this case was defined as

$$\frac{p_{th} - p_c}{\frac{1}{2} \rho_w V_{th}^2}$$

where p_{th} and V_{th} represented the static pressure and velocity respectively at the throat of the venturimeter.

and orifice plate openings when $r_2 = 0$. Figure 35 gives σ_c versus r_2 for a typical case of solidity ratio $(\frac{h}{d} = 0.817)$. Figure 34 indicates in general a fall in σ_c for a rise in the solidity ratio $\frac{h}{d}$ for the same value of K_1. In other words, it broadly implies that other significant variables remaining constant, the tunnel is more susceptible to cavitation at lesser gate openings. Figure 35 shows that the increase in ventilation factor gives higher values of cavitation parameter. This is so because the flow rate of water goes down and the static pressure at the vena contracta goes up as the supply of air is increased.

6.f Overall Flow Ratio

To find the values of maximum discharge that the tunnel could carry, experiments were performed for the full, half, and quarter-open cases (for definition, see article 4.a) with no ventilation and no control gate in the test section. These values were named as $Q_{w\ max}$ correspondingly. Also, the measured values of Q_w for all possible combinations of the orifice plate openings and the five gate openings were already known. Thus, the ratio $Q_w / Q_{w\ max}$ (i.e. overall flow ratio) could be worked out for every such combination. The experimental values of this ratio have been compared in Figure 36 with the theoretical ones, the latter being found by using Equation (2). The figure indicates substantial agreement between the experimental and theoretical results.

6.g Reattachment Slope and Pressure Gradient

The quantity $\frac{h}{X_r}$, which is the slope of the line joining the top edge of the gate with the point of reattachment, may be termed as the average reattachment slope and another quantity $\frac{p_2 - p_1}{X_r} \cdot \frac{d}{\frac{1}{2} \rho_w V_{vc}^2}$ may be termed as the average non-dimensional pressure gradient. Figure 37 gives mean experimental curves relating the above two quantities for different values of K_1 when $r_2 = 0$. From these curves it is found that:

(i) In general, for any particular control gate the average reattachment slope increases with the increase in K_1. This is so because the flow approaching the gate is initially more turbulent for higher values of K_1 and therefore spreads more quickly after passing through the gate opening.

(ii) As the value of $\frac{h}{d}$ is reduced, the dependence of the average reattachment slope on the average non-dimensional pressure gradient becomes progressively less. It may, therefore, be expected that the slope (or the ratio of the height of the gate to the reattachment distance) would tend to be almost constant when $\frac{h}{d}$ is reduced below a certain value. This is in agreement with the results of Arie and Rouse[3] who, while investigating a similar case, found that the said ratio was almost constant at about 0.06 when $\frac{h}{d}$ was varied from 0.083 to 0.167.

6.h Reattachment Distances

Visual and Graphical Determination of X_r

It may be noted that it was possible, by direct visualization, to locate roughly the region of reattachment inside the test section during those experimental runs in which the ventilation factor was either zero or small (up to .07 approximately). For large ventilation factors, the clouding of the flow prevented satisfactory visualization. The reattachment regions that were thus located seemed to extend over a few inches. The distances between the gate and the middle of these visually located regions were recorded and named as X_r. On comparison, it was found that these distances matched satisfactorily (see Table II) with those determined graphically by the method illustrated in Figure 9.

On this basis it was assumed that the graphical method would give satisfactory values of X_r for higher values of r_2 also. In the absence of any better method of finding X_r experimentally, it was thought reasonable to use the graphically found values throughout.

6.h.1

With the given geometry of the syphon tunnel, it is possible to relate the quantities X_r, h, d, Q_{a2} and Q_w as follows:

$$\frac{X_r}{h} = F_1\left(\frac{h}{d}, \frac{Q_{a2}}{Q_w}\right)$$

$$= F_1\left(\frac{h}{d}, r_2\right)$$

when $r_2 = 0$, $\frac{X_r}{h} = F_2\left(\frac{h}{d}\right)$

or when $\frac{h}{d}$ is fixed, $\frac{X_r}{h} = F_3\ (r_2)$.

Experimental plots of these relations are given in Figures 38 and 39. Figure 38 shows that the mean experimental curve is in close agreement with the value determined by Förthmann[2]. The values found by Arie and Rouse[3] are given in the figure for reference.

In connection with the mean experimental curve in Figure 38 it may be pointed out that it was not possible with the present experimental set-up to extend the experimental results for $\frac{h}{d}$ greater than 0.892 or less than 0.327. The reasons are:

(1) When a gate with $\frac{h}{d} = 0.915$ ($h = 2.8$ in.) was used, the discharge was so small that air was able to push up from the outlet end and the flow broke down soon after the tunnel was started.

(2) The capacity of discharge sump was too small to allow the use of a gate of height much less than 1 in. (i.e. $\frac{h}{d} < 0.327$). For example, it was expected that the discharge sump would start overflowing in about 10 seconds, if a gate of 1/2 in. height were used. The squashing device was not considered efficient enough for building up the mercury columns for runs of such a short duration.

It is relevant to remark here that during the experimental runs without any gate, the discharge rate was very high and the sump limited the continuous run to about 8 seconds, so that the squashing device was not really useful. However, for this case, it was obvious that the pressure throughout the test section would be sensibly constant, so that it would be sufficient to determine the pressure at one or two points only. This object could be achieved by building up just two pressure columns of the mercury manometer in a number of test runs by squashing the corresponding pressure carrying rubber tubes carefully between the fingers.

6.h.2 Some Auxiliary Experiments

Experiments were conducted in an open channel fitted with an adjustable sluice gate to find the eddy lengths for comparison with those found already in the test section of the syphon tunnel.

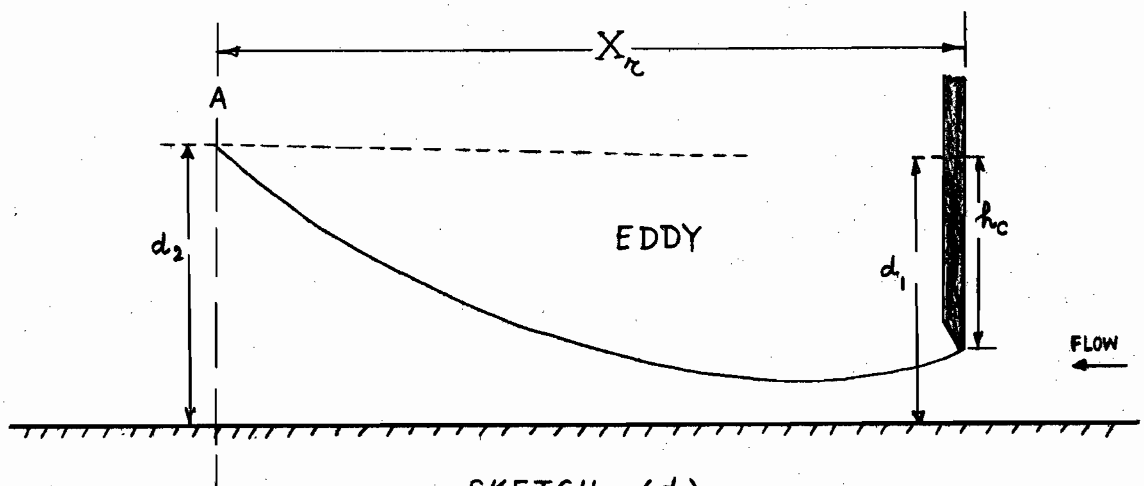

SKETCH (d)

$d_2 > d_1$

MEAN DEPTH OF WATER $d_c = \frac{d_1+d_2}{2}$

SOLIDITY RATIO $= h_c/d_c = h/d$

Width of the open channel was 12-1/4 in. Depth of water in the channel was different in the different experiments. It ranged from about 10 in. to 14 in., so that the ratio of the depth to the width lay between 0.8 to 1.1 approximately. Value of this ratio in the case of test section was fixed as 1.0. Thus, the above ratio which represented the geometry of the cross-section of the flow was roughly of the same order in both the open channel and the test section.

The section A (sketch d), where the reattachment occurred, was located simply by sprinkling small bits of paper on the surface of the water and watching their movement. It was observed that the bits dropped on the surface to the right of A moved upstream while those dropped to the left of A moved downstream. Thus, it was possible to locate the section A, because the bits dropped there got divided, some moving upstream and some downstream. It may be pointed out here that the reattachment section A could not be defined sharply. In fact, it was a reattachment region, the centre of which was located by judgement and was designated as the reattachment section A.

The gate opening and the depth of water in the channel were varied and the values of X_r determined by the method explained above. The results are reported in Figure 38. The points given by the open-channel experiment diverge considerably from the mean curve (obtained from the closed test section of the syphon tunnel) for the low solidity ratios, but they show better agreement with the curve for higher solidity ratios. For $\frac{h}{d} > 0.9$ the trend of the points from the open-channel and the trend of the mean curve are virtually the same.

The Reynolds numbers of the flow investigated both in the open channel and the test section were large enough to justify the assumption that shear stresses at the walls did not play much part to account for the divergence stated above. Numerical value of Reynolds number (based on the gate opening) in the case of the open channel was almost constant at about 20,000 for all the cases investigated, whereas in the case of the test section it varied approximately from 60,000 for $\frac{h}{d} = 0.892$ to 300,000 for $\frac{h}{d} = 0.327$.

To verify the validity of the assumption about shear stresses at the walls, experiments were conducted in the open channel with a plastic sheet floating on the surface of water. The sheet spanned the channel with some clearance on both lengthwise edges between the sheet and the vertical sides of the channel. Wrinkling of the sheet was avoided by stretching it appropriately. The length of the sheet was such that the reattachment distances were well within it. The plastic sheet would, to a large extent, simulate the fourth (enclosing) wall of the test section of the syphon tunnel as far as the wall shear stresses were concerned.

The reattachment sections in this case were located as follows. Small bits of paper were mixed with water and the mixture was fed deep into the water supply a short distance upstream of the gate. The water flowing through the gate opening carried the bits along. Movement of these bits was watched through one of the transparent sides of the channel. On observing the paths followed by the bits a region could be located roughly where a number of these bits hit the bottom of the floating plastic sheet or came very close to it and then separated into the upstream and downstream directions. The middle of this region was chosen as the reattachment section.

The results of these experiments are also plotted in Figure 38. It is observed from this figure that there is no conspicuous difference between the experimental plots for the two cases (with and without plastic sheet) of the open channel. This observation substantiates the assumptions made regarding the wall shear stresses. On this basis, it may be assumed that these stresses play no significant role in causing the apparent divergence between the results obtained from the test section and from the open channel (Figure 38).

Let us now consider the gravitational effect on the hydrostatic pressure distribution. Pressure difference between any two points lying in the same horizontal plane would not be affected by gravity in the case of flow in the test section whereas it would be affected in the open channel as follows. The floor of the open channel was almost horizontal. The depth of water in the channel was observed to increase from a section just downstream of the gate up to a section beyond the point of reattachment. Thus, owing to the gravitational effect there would be a rising pressure gradient along the flow between the two sections, which would help the jet to spread more quickly. In other words, the length of the eddy would be reduced due to the said effect. However, the actual difference in the depths between the above two sections in the present case was only about 1/2 in. at the most, whereas the mean depth of water was near about 1 ft. It appears, therefore, that the gravitational effect alone could not account for the divergence mentioned above. Further, it is not clear as to why this divergence, which is reasonably small for high solidity ratios ($\frac{h}{d} > 0.8$ say), grows considerably as the solidity ratio is reduced.

6.h.3 Effect of Ventilation

Figure 39 shows convincingly that the reattachment distance increased with r_2, being the least when r_2 was equal to zero.

As already described in the introduction, the fast moving jet issuing through the gate opening entrains the fluid from the region (A) near the gate. Loss of this fluid is replenished by the fluid from further downstream. This establishes a back flow which is drawn from

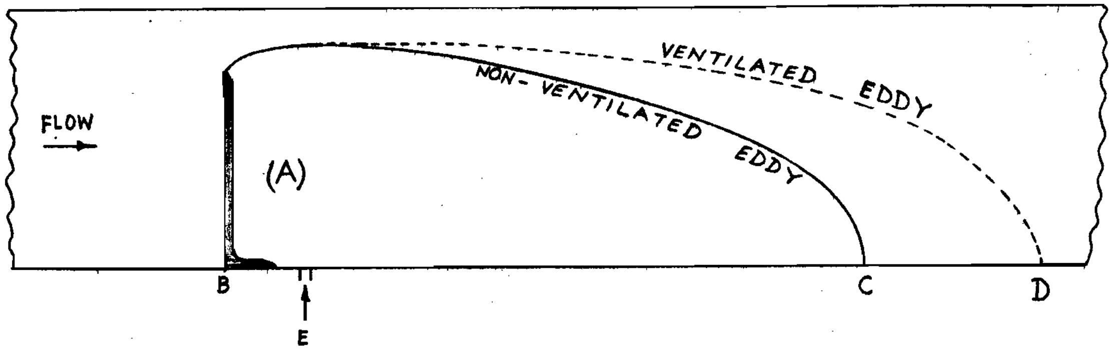

SKETCH (e)

the underside of the jet. As this is done the jet is drawn downwards. This process continues and the flow reattaches to the floor. Let us assume that the reattachment occurs at C in the case of non-ventilated eddy. Now when the eddy is ventilated, there is a source of continuous supply of air at E, shown in sketch (e). The fluid entrained by the jet from the region (A) is replenished partly by this air supply and partly by the fluid from further downstream. Thus, in the case of a ventilated eddy the tendency of the jet to bend downwards after passing the region A is less, so that the reattachment distance is longer (say BD instead of BC).

7. CONCLUSIONS

1. Though the syphon tunnel was designed and constructed primarily for the studies of control gates, it is believed to be potentially more useful. Various types of models like aerofoils, venturimeters, cylinders and spheres can also be fixed in the existing test section. In some cases, of course, it would be necessary to make some slight modification in the test section.

2. With the help of the performance characteristics derived it is possible to bring about some alterations in the existing tunnel or construct another similar tunnel so as to obtain desired values of volume flow of water, pressure level or cavitation parameter in the test section.

3. With an increase in the ventilation factor, there is a decrease in the overall pressure recovery index C_{p2}, and, as anticipated, this decrease is more pronounced when the solidity ratio is reduced. Moreover, the value of this index can be predicted quite accurately.

4. Control of the cavitation parameter in a flow similar to the one investigated can be achieved by proper ventilation of the eddy. Increase in the ventilation factor seems to increase the cavitation parameter rapidly, so that the severeness of cavitation is reduced.

5. The profiles of the separation eddies formed behind control gates in closed conduits are influenced considerably by the solidity ratio $\frac{h}{d}$, so that they are not, in general, conformable to any specific geometrical shape.

6. The length of an eddy is invariably affected by ventilation. On the basis of the present experimental data it is found that the higher the ventilation factor, the larger is the reattachment distance or the length of the eddy.

7. The present work could be usefully extended in the following areas:

a) Study of the pressure fluctuations in the flow and the pulsations of the eddy downstream of the control gate, both for ventilated and non-ventilated cases.

b) Study of the influence of the dissolved and free gas content of water on the pressure fluctuation and distribution in the case of ventilated and non-ventilated eddies.

c) Study of the pressure distribution and flow stability for:

   i. 'Bled-off eddies' where the term would signify the controlled bleeding off of water from the recirculating or dead water region behind the control gate by a suitable suction pump.

   ii. 'Water-fed eddies' where the term would apply to the feeding of the eddy by controlled amounts of water, either from an outside source or from a point at a higher pressure in the same water tunnel.

d) Reinforcement of the present study by extending the experimental work into the realm of pure cavitation and into a range of solidity ratios higher than 0.892 and lower than 0.327. These figures refer to the range covered in the present study.

APPENDIX 1

(a) Details of the Losses Through the Tunnel

Driving head H is the known parameter in this case. A hydraulic equation of head balance (when no orifice plate is inserted at section M) may be written as follows, with reference to Figure 7:

$$H = \Sigma H' + \Sigma H'_f$$

$$= H'_A + H'_B + H'_G + H'_E + H'_F + H'_J + (H'_K + H'_N) + H'_f \text{ (ABEJN)} \quad \ldots(A.1)$$

where

H'_A = Entrance loss at A = $0.5 \dfrac{V_s^2}{2g}$

H'_B = Bend loss at B = $0.21 \dfrac{V_s^2}{2g}$ .... Klein et al.[5]

H'_G = Abrupt contraction loss at G = $\dfrac{(V_{vc} - V_t)^2}{2g}$

H'_E = Bend loss at E = $0.21 \dfrac{V_s^2}{2g}$ .... Klein et al.[5]

H'_F = Expansion loss at F = $\dfrac{(V_s - V_p)^2}{2g}$

H'_J = Head loss due to 45^o bend = $K' \dfrac{V_p^2}{2g}$

where $K' = 0.9457 \sin^2\left(\frac{\theta}{2}\right) + 2.047 \sin^4\left(\frac{\theta}{2}\right)$, as given in some standard text books.

For $\theta = 45^o$, $K' = 0.182$

H'_K = head loss due to the butterfly valve at K

H'_N = Dynamic head loss at the outlet

and

$$H'_f\text{(ABEJN)} = f \left[\left(\frac{L}{m}\right)_{ABC} \frac{V_s^2}{2g} + \left(\frac{L}{m}\right)_{CD} \frac{V_t^2}{2g} + \left(\frac{L}{m}\right)_{DEF} \frac{V_s^2}{2g} + \left(\frac{L}{m}\right)_{FJN} \frac{V_p^2}{2g} \right]$$

Note that

$$\Sigma H'_f \text{ (section A to 0)} = f \left[\left(\frac{L}{m}\right)_{ABC} \frac{V_s^2}{2g} + \left(\frac{L}{m}\right)_{C \text{ to } 0} \frac{V_t^2}{2g} \right]$$

and $\Sigma H'$ (section A to 0) $= H'_A + H'_B$

<u>Equation for $(H'_K + H'_N)$</u>

For large hydraulic conduits, head loss incurred at the fully open butterfly valve has little importance; whereas in the present situation, the valve does provide a sizeable area of blockage A_b (shown shaded in the following sketch), thus prohibiting the neglect of H'_K .

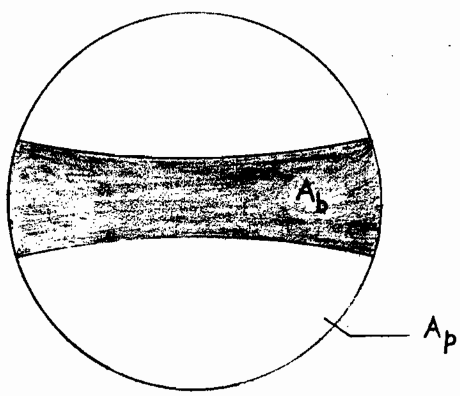

There are two ways in which $(H'_K + H'_N)$ may be evaluated:

(1) If we assume that the flow contracts at the valve and then expands to fill the pipe before the outlet, then

$$H'_K = \frac{(V'_K - V_p)^2}{2g}$$

where V'_K = velocity at the vena contracta formed downstream of the butterfly valve

$$= \frac{V_p A_p}{(A_p - A_b)C_c}$$

And $H'_N = \frac{V_p^{\ 2}}{2g}$

so that

$$(H'_K + H'_N) = \frac{(V'_K - V_p)^2}{2g} + \frac{V_p^{\ 2}}{2g} \tag{A.2}$$

(2) We may note that the distance between the outlet and the valve blockage is very short, so that the flow may issue as two separate jets on either side of the open valve.

Then

$$(H'_K + H'_N) = \frac{(V'_K - V_p)^2}{2g} + \frac{(V'_K)^2}{2g} \tag{A.3}$$

However, it was observed actually that water issued out first as two separate jets, remained so for some time and then merged to fill the outlet pipe. Hence, neither equation (A.2) nor (A.3) is truly representative.

It may, however, be pointed out that the difference in the two expressions (A.2) and (A.3) is small in the context of overall values of the losses. Either of the expressions would do approximately. Mean value of the two expressions was ultimately accepted as a compromise.

Thus

$$(H'_K + H'_N) = \frac{(V'_K - V_p)^2}{2g} + \frac{1}{2} \left[\frac{(V_p)^2 + (V'_K)^2}{2g} \right]$$

Substituting the value of V'_K and rearranging the terms we obtain

$$(H'_K + H'_N) = \frac{V_p^{\ 2}}{2g} \left[1.5 \left\{ \frac{A_p}{(A_p - A_b)C_c} \right\}^2 + 1.5 - \frac{2A_p}{(A_p - A_b)C_c} \right] \tag{A.4}$$

(B) Head Loss at Section M (Figure 7)

To vary the velocity in the tunnel and to obtain sizeable pressure drop in the flow before it reached the test model, orifice plates were inserted at the section M. The terms full-open, half-open, and quarter-open used below are defined in article 4.a. If the head loss due to an orifice plate inserted at M be worked out in the form $K_1 Q_w^{\ 2}$, we may call K_1 the 'loss factor' associated with that orifice plate.

Full-open Case

Since no orifice plate was used in this case, the flow passage at M was fully open. There was no head loss and hence $K_1 = 0$.

Half-open Case

The orifice plate used in this case consisted of 13 holes of 5/8 in. diameter each, so that the ratio of the area of each hole to the corresponding average area of supply was 1/1.91. Knowing this, the coefficient of contraction could be worked out.

Let V_{vch} = Velocity at the vena contracta of the hole

$$= \frac{Q_w}{\text{Area of the hole x coefficient of contraction}}$$

$$\text{Head loss} = \frac{(V_{vch} - V_s)^2}{2g} \quad \text{where} \quad V_s = \frac{Q_w}{A_s} \ .$$

Putting numerical values and working in F.P.S. units we get

$$\text{Head loss} = 17.4\ Q_w^{\ 2} \qquad \text{(ft of water)}$$

so that $K_1 = 17.4$

Quarter-open Case

The orifice plate used in this case had 17 holes of 3/8 in. diameter each. Proceeding in the above manner it is found that

$$\text{Head loss} = 158.7\ Q_w^{\ 2} \qquad \text{(ft of water)}$$

so that

$$K_1 = 158.7$$

APPENDIX II

(A) Surface Tension

There are two types of cavitation, vaporous and gasous, as defined by Strasberg[11]. Inception pressure for vaporous cavitation in water is either equal to or less than the corresponding vapour pressure. Gaseous cavitation, however, is a consequence of the diffusion of dissolved gases out of water at a pressure which may be higher than the vapour pressure, but must be lower than the saturation pressure for the gases dissolved in water.

During the present study, it was found from the measured mean static pressures that they were always above the corresponding water vapour pressures. Therefore, it would be safe to neglect any consideration of the vaporous cavitation. There was, of course, ample gaseous cavitation resulting in the evolution of gas bubbles. The gas bubbles are capable of retaining an internal pressure higher than the ambient external pressure due to the surface tension, obeying the following principle:

$$(p_i - p_e) = \frac{2\sigma_s}{R_o}$$

The static pressure determined experimentally ignores the existence of p_i and is, therefore, not truly representative. From a practical point of view, a correction to account for p_i is necessary only when the problem of surface tension is serious.

The size of the gas bubbles could be estimated approximately by direct observation through the transparent panels of the test section for the cases in which the value of r_2 lay between zero and 0.05 nearly. Thus, the qualitative effect of ventilation on the size of the bubbles could be roughly ascertained for this range of r_2. For higher values of r_2 the mixture of air and water became clouded and the size of bubbles could not be judged. However, the observations that were possible did give an indication that the increase in ventilation factor increased the proportion of larger sized bubbles. Although it was not possible to make any definite assertion about the size of the bubbles when the factor r_2 was increased beyond .05, it seemed plausible to assume that the above indication would hold. Further, most of the bubbles observed appeared to be about a mm or bigger in size, so that if we take σ_s = 0.005 lb/ft for ordinary water at 68°F, then $(p_i - p_e)$ would be $\leqslant$ 0.02 psi. This is very small in comparison with the value of the pressures measured. In view of this, no allowance was made to compensate for the effect of surface tension.

(B) Density-affected Pressure Terms

In articles 4.c.1 and 4.c.2 we come across the following terms:

$$(\text{area DEFG} - \text{area ABC}) \times \frac{1}{d}$$

and

$$(\text{area DEFG} - \text{area HIJK}) \times \frac{1}{d}$$

For brevity let us represent these terms by Y_1 and Y_2 respectively. These terms may be designated as density-affected pressure terms, because they represent pressure and owe their existence solely to the difference in densities of water and the air-water mixture.

It is obvious from sketch (b) in article 4.c that the area ABC is the largest and the area LMN the smallest among the shaded areas. If we represent the term (area ABC - area LMN) x $\frac{1}{d}$ by Y_3, we may say that Y_3 is greater than Y_1 or Y_2. It is possible to evaluate Y_3 numerically as follows:

$$Y_3 = (\rho_w gd \times \frac{d}{2} - \rho_{m2} gd \times \frac{d}{2}) \times \frac{1}{d}$$

$$= \frac{gd}{2} (\rho_w - \rho_{m2})$$

From Equation (8a)

$$\rho_{m2} = \frac{\rho_w}{1 + r_2} \qquad \text{where} \quad r_2 = \frac{Q_{a2}}{Q_w}$$

so that

$$Y_3 = \rho_w \frac{gd}{2} (\frac{r_2}{1 + r_2})$$

Y_3 can be evaluated from the above equation for any given value of r_2, for example,

if $r_2 = 0.2$, $Y_3 = 0.02$ in. of mercury

and if $r_2 = 0.4$, $Y_3 = 0.034$ in. of mercury.

The values of r_2 constituting the main body of the investigation are less than 0.2, which means that Y_3 in most of the cases would be less than 0.02 in. of mercury. Also Y_1 and Y_2 both are smaller than Y_3, so that their values in most of the cases studied would be much less than 0.02 in. of mercury. Hence, on examining the equations containing Y_1 and Y_2 it is possible to assume that both Y_1 and Y_2 would be negligible in comparison with the other quantities involved in those equations.

LIST OF REFERENCES

1. Naudascher, E., Kobus, H.E. and Rao, R.P.R. Hydrodynamic Analysis for High-Head Leaf Gates. Journal of the Hydraulics Division, Proceedings of the A.S.C.E., Vol. 90, No.HY 3, May 1964, Part 1, p. 155.

2. Förthmann, E. Turbulent Jet Expansion. N.A.C.A., T.M., 789 (1936).

3. Arie, M. and Rouse, H. Experiments on Two-Dimensional Flow Over a Normal Wall. Journal of Fluid Mechanics, Vol. 1, (1956).

4. Savage, S.B. An Approximate Analysis for Reattaching Turbulent Shear Layers in Two-Dimensional Incompressible Flow. Mech.Eng. Res. Lab. Report No. Ae-3, (1960). McGill University.

5. Klein, G.J., Tupper, K.F. and Green, J.J. The Design of Corners in Fluid Channels. Canadian Journal of Research, Vol. 3, (1930).

6. Kwok, C.K.C. Construction and Calibration of the McGill Supersonic Wind Tunnel. Mech.Eng.Res.Lab. T.N. 62-6 (1962) McGill University.

7. Bourque, C. and Newman, B.G. Reattachment of a Two-Dimensional Incompressible Jet to an Adjacent Flat Plate. Aero. Quart. Vol. XI, p. 201 (1960).

8. Sawyer, R.A. Two-Dimensional Reattaching Jet Flows Including the Effects of Curvature on Entrainment. Journal of Fluid Mechanics, Vol. 17 (Dec. 1963).

9. Wygnanski, I. The Reattachment of a Two-Dimensional Incompressible Jet to an Inclined Flat Surface in Parallel Streaming Flow. Mech.Eng.Res.Lab. Tech. Memo. (1964), McGill University.

10. Milne-Thomson, L.M. Theoretical Hydrodynamics. Macmillan and Co. London. (1960), p.206.

11. Strasberg, M. Undissolved Air Cavities as Cavitation Nuclei. N.P.L. Symposium on "Cavitation in Hydrodynamics" (1955).

TABLE I

TABLE OF PRESSURES

Nominal Gate Opening	Nominal Orifice Plate OPENING	Ventilation factor r_2	P_{0s} inches of Hg		P_{1s} inches of Hg		P_{2s} inches of Hg	
			Theoret.	Experim.	Theoret.	Experim.	Theoret.	Experim.
1/4 in.	Full	0.0	4.72	4.92	24.01	23.96	21.57	21.25
		0.164	4.67	4.88	20.45	19.95	18.49	18.07
$(\frac{h}{d}=0.892)$	Half	0.0	5.34	5.60	23.94	23.65	21.59	21.45
		0.166	5.28	4.76	19.18	19.15	17.45	17.55
	Quarter	0.0	7.69	7.32	23.66	23.45	21.64	21.50
		0.133	7.33	6.85	21.08	21.00	19.37	19.35
		0.260	6.06	6.11	13.43	13.40	12.54	12.75
1/2 in.	Full	0.0	5.89	5.65	25.49	25.10	21.32	20.85
		0.075	5.77	5.60	22.78	22.85	19.31	19.75
$(\frac{h}{d}=0.817)$		0.165	5.70	5.61	20.58	20.40	17.72	17.70
		0.250	5.63	5.60	16.32	14.85	13.99	13.00
	Half	0.0	6.75	7.22	25.20	24.70	21.34	21.15
		0.078	6.71	6.89	22.26	22.50	19.14	19.60
		0.167	6.60	6.53	19.32	19.35	16.69	17.00
		0.252	6.39	6.09	16.00	14.40	14.22	12.60
	Quarter	0.0	12.01	11.54	24.00	23.55	21.51	21.20
		0.070	11.25	11.23	22.45	22.30	20.28	20.15
		0.166	9.76	9.58	19.04	19.05	17.41	17.60
		0.224	8.66	8.61	14.82	14.70	13.61	13.45
1 in	Full	0.0	7.07	8.11	26.47	24.90	18.73	18.65
		0.033	6.77	8.06	23.59	23.95	17.44	18.00
$(\frac{h}{d}=0.653)$		0.152	6.45	7.77	20.88	21.15	15.85	16.10
	Half	0.0	10.79	11.99	25.77	24.80	20.02	19.95
		0.038	9.68	11.71	22.17	22.60	17.77	18.20
		0.105	9.42	10.97	21.54	20.90	16.82	17.10
	Quarter	0.0	17.92	17.56	23.28	23.50	21.30	21.00
		0.072	16.98	16.45	21.93	21.80	20.14	19.90
		0.177	14.38	13.89	18.17	18.05	16.82	16.70

TABLE I (continued)

Nominal Gate Opening	Nominal Orifice Plate OPENING	Ventilation factor r_2	p_{0s} inches of Hg		p_{1s} inches of Hg		p_{2s} inches of Hg	
			Theoret.	Experim.	Theoret.	Experim.	Theoret.	Experim.
1-1/2 in.	Half	0.0	14.87	15.45	25.17	23.80	19.82	18.80
($\frac{h}{d}$ =0.49)		0.051	13.11	14.80	21.89	21.80	17.47	17.60
		0.081	12.75	14.45	20.98	21.05	16.94	17.30
	Quarter	0.0	20.09	20.45	22.51	22.80	21.26	21.40
		0.070	19.17	18.96	21.44	21.25	20.32	20.20
		0.172	16.51	16.05	18.35	18.20	17.49	17.30
2 in.	Half	0.0	17.51	16.75	23.15	21.90	19.39	18.70
($\frac{h}{d}$ =0.327)		0.024	15.29	16.64	19.92	20.40	16.91	17.40
		0.059	14.87	16.15	19.25	19.35	16.51	17.00
	Quarter	0.0	20.81	21.35	21.85	22.10	21.16	21.30
		0.071	20.02	20.30	21.00	21.10	20.39	20.50
		0.176	17.85	17.20	18.69	18.60	18.24	18.15

TABLE II

REATTACHMENT DISTANCES

Nominal Gate Opening	Nominal Orifice Plate Opening	Ventilation factor r_2	X_r (inches) By Visualization Approx. Range	Mean	By Graphical Method (see Fig. 9)
1/4 in.	Full	0	$17\frac{1}{2}$ - $19\frac{1}{2}$	$18\frac{1}{2}$	17.90
	Half	0	16 - 18	17	17.40
	Quarter	0	$14\frac{1}{2}$ - $16\frac{1}{2}$	$15\frac{1}{2}$	16.80
1/2 in.	Full	0	$17\frac{1}{2}$ - 20	$18\frac{3}{4}$	19.80
		0.075	21 - 24	$22\frac{1}{2}$	20.40
	Half	0	$17\frac{1}{2}$ - 19	$18\frac{1}{4}$	19.00
	Quarter	0	$16\frac{1}{2}$ - $18\frac{1}{2}$	$17\frac{1}{2}$	18.40
		0.07	17 - 20	$18\frac{1}{2}$	19.80
1 in.	Full	0	20 - 22	21	21.90
		0.033	22 - 24	23	21.90
	Half	0	21 - 23	22	20.40
		0.038	$21\frac{1}{2}$ - $23\frac{1}{2}$	$22\frac{1}{2}$	21.80
	Quarter	0	19 - 21	20	20.40
		0.072	$22\frac{1}{2}$ - $24\frac{1}{2}$	$23\frac{1}{2}$	22.00
1-1/2 in.	Half	0	19 - 21	20	19.80
		0.051	$19\frac{1}{2}$ - $21\frac{1}{2}$	$20\frac{1}{2}$	21.40
	Quarter	0	$16\frac{1}{2}$ - $18\frac{1}{2}$	$17\frac{1}{2}$	18.80
		0.07	19 - 22	$20\frac{1}{2}$	21.60

TABLE II (continued)

Nominal Gate Opening	Nominal Orifice Plate Opening	Ventilation factor r_2	X_r (inches)		
			By Visualization		By Graphical Method (see Fig. 9)
			Approx.Range	Mean	
2 in.	Half	0	14 - 16	15	16.20
		0.024	$16\frac{1}{2}$ - $18\frac{1}{2}$	$17\frac{1}{2}$	16.80
		0.059	$17\frac{1}{2}$ - 19	$18\frac{1}{4}$	17.40
	Quarter	0	14 - $15\frac{1}{2}$	$14\frac{3}{4}$	15.80
		0.071	$15\frac{1}{2}$ - $17\frac{1}{2}$	$16\frac{1}{2}$	17.40

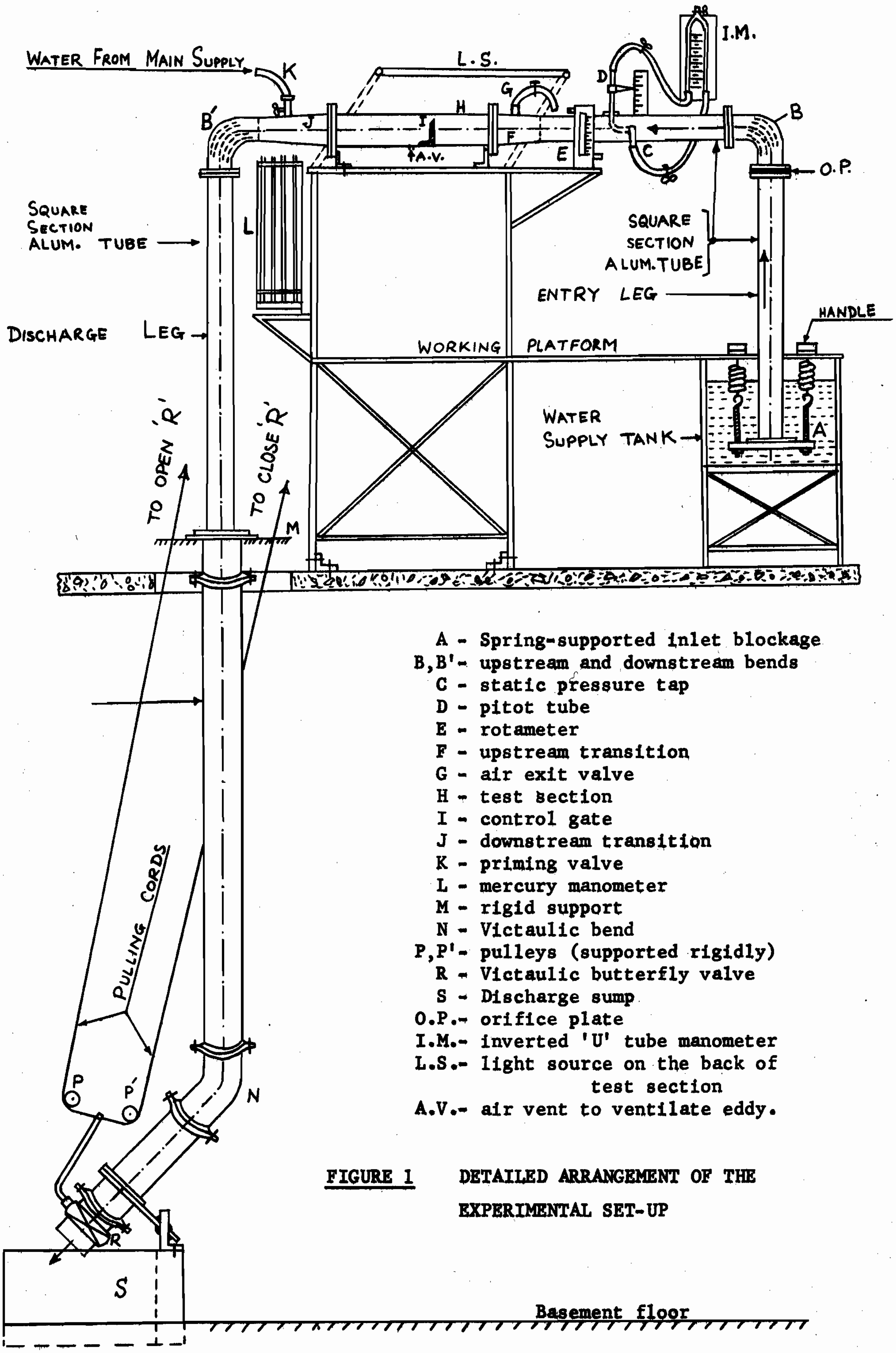

A - Spring-supported inlet blockage
B,B'- upstream and downstream bends
C - static pressure tap
D - pitot tube
E - rotameter
F - upstream transition
G - air exit valve
H - test section
I - control gate
J - downstream transition
K - priming valve
L - mercury manometer
M - rigid support
N - Victaulic bend
P,P'- pulleys (supported rigidly)
R - Victaulic butterfly valve
S - Discharge sump
O.P.- orifice plate
I.M.- inverted 'U' tube manometer
L.S.- light source on the back of test section
A.V.- air vent to ventilate eddy.

FIGURE 1 DETAILED ARRANGEMENT OF THE EXPERIMENTAL SET-UP

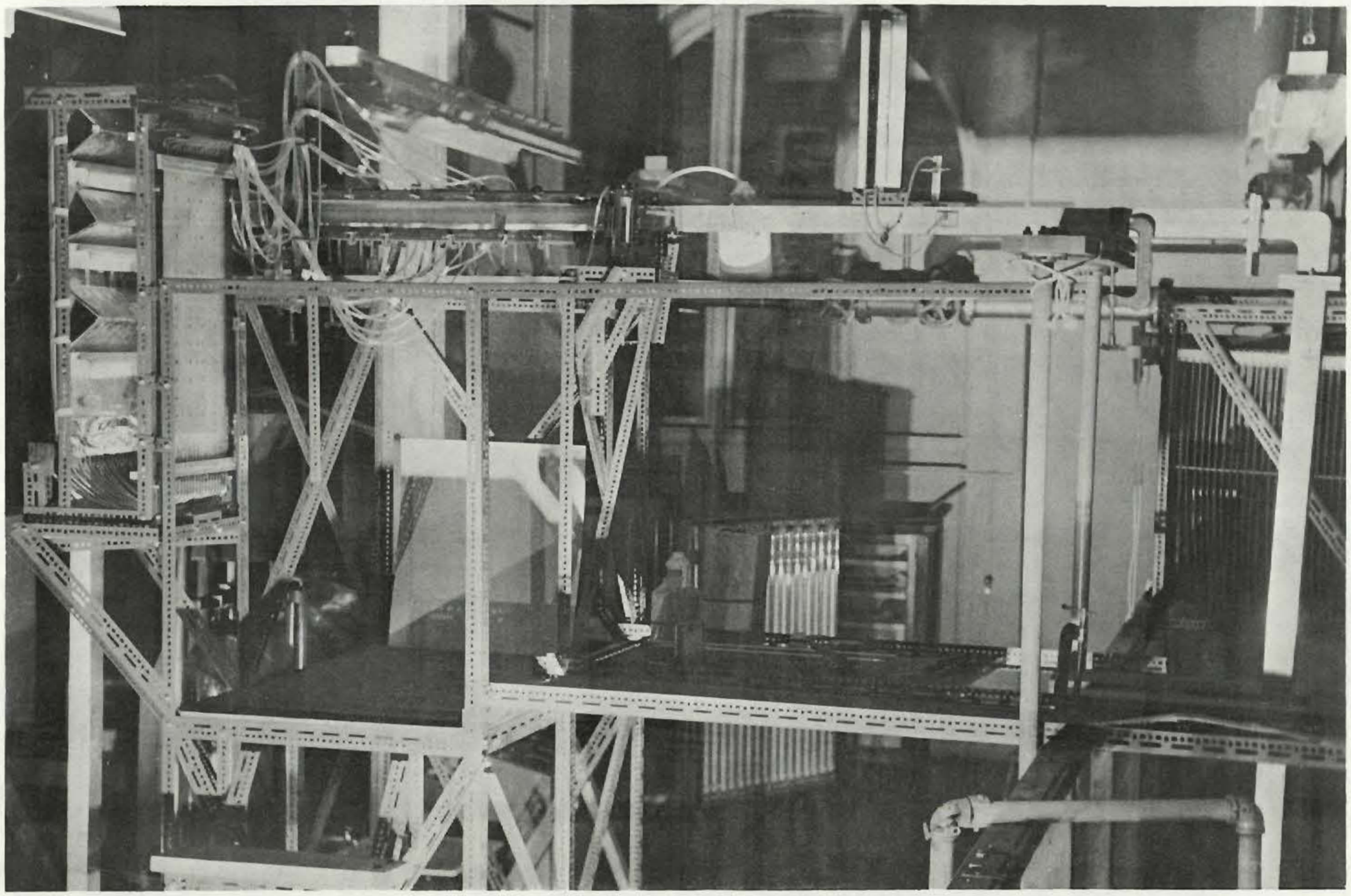

GENERAL VIEW OF THE APPARATUS

Fig. 2

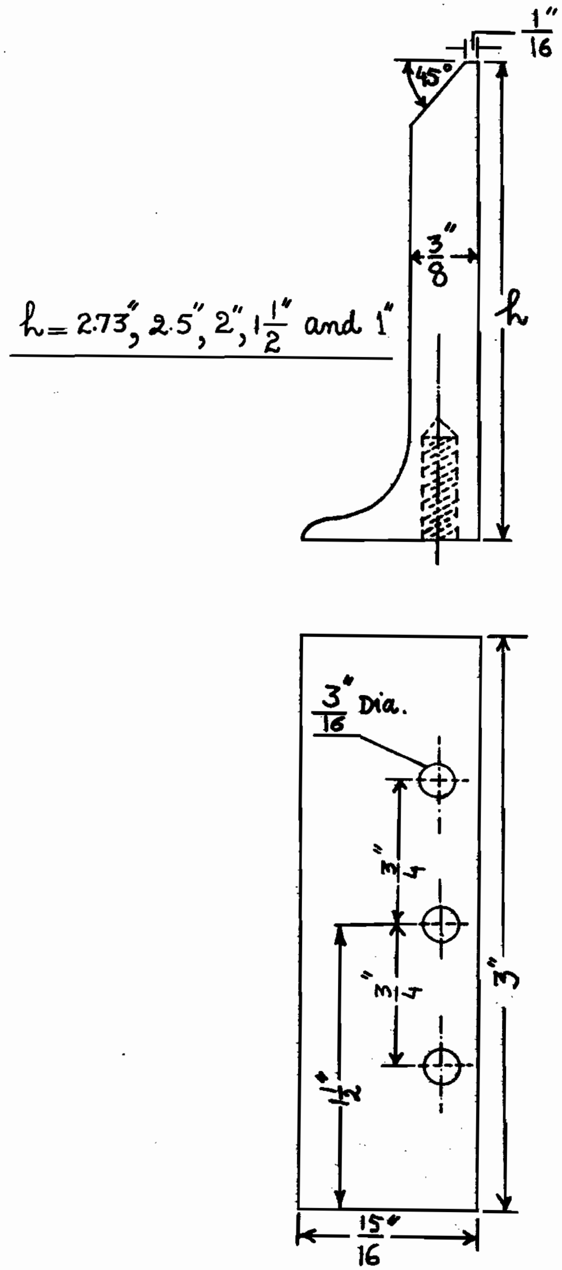

FIGURE 3.a CONTROL GATE

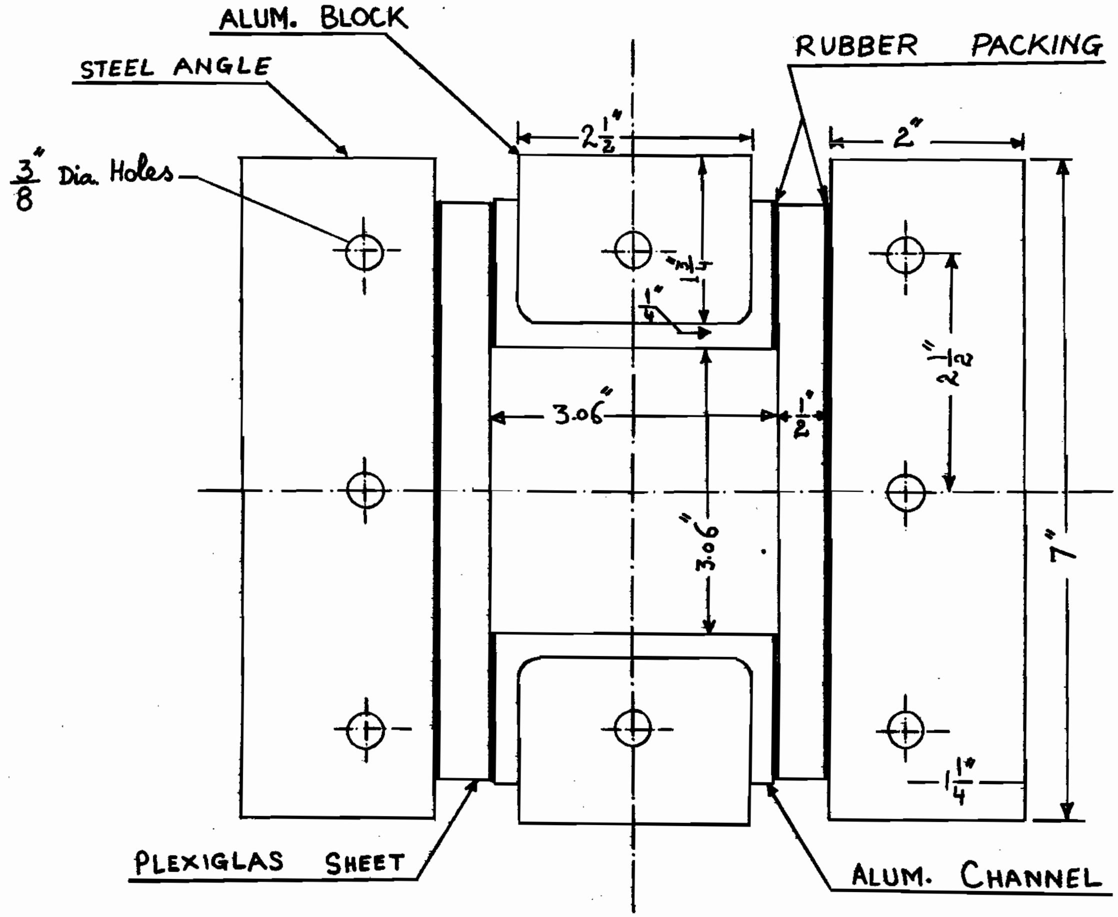

FIGURE 3.b FLANGE OF THE TEST SECTION

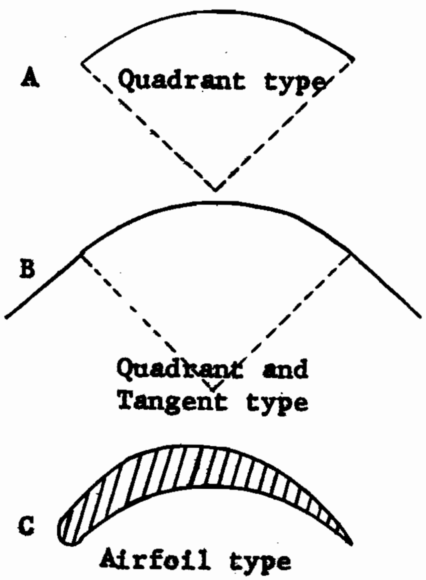

VANES

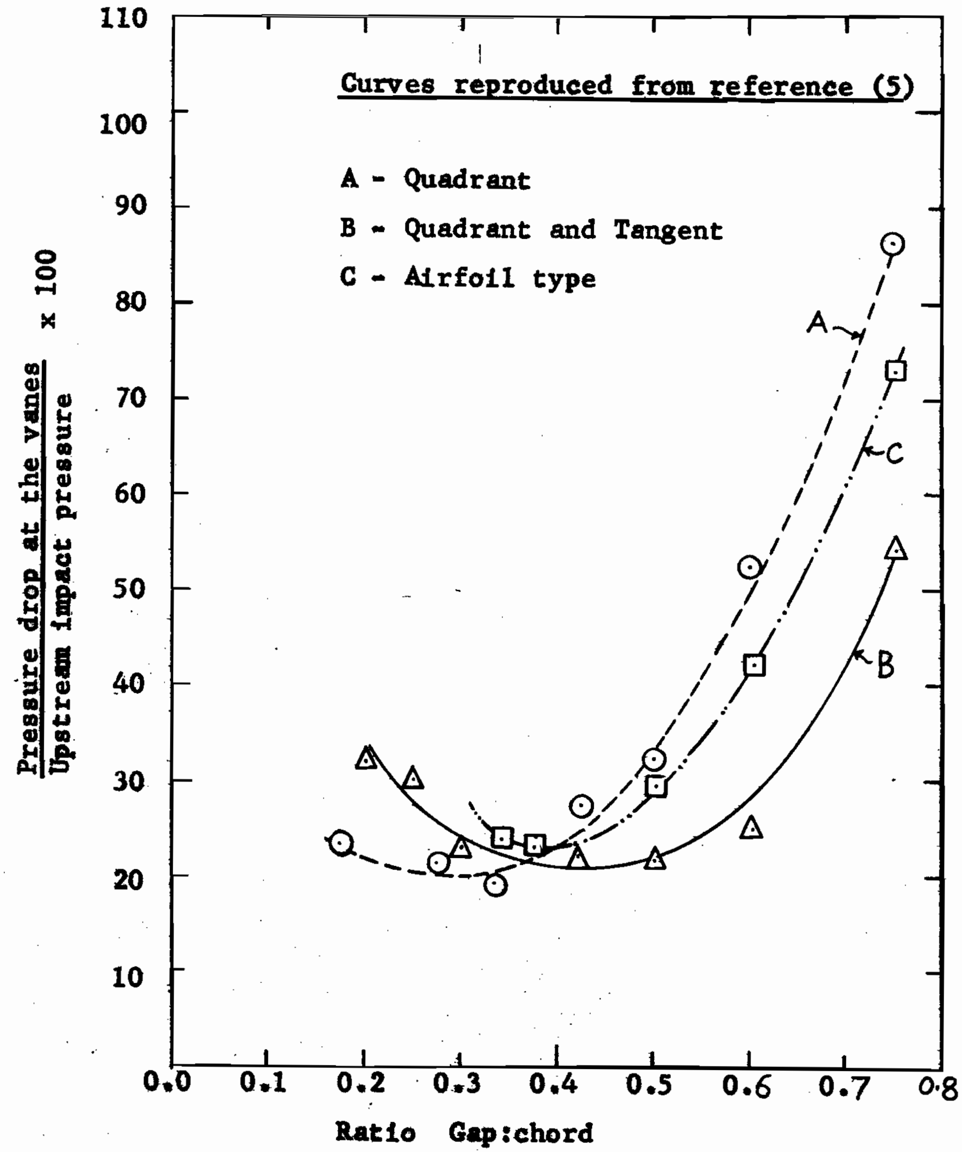

FIGURE 4.a CORNER RESISTANCE CURVES

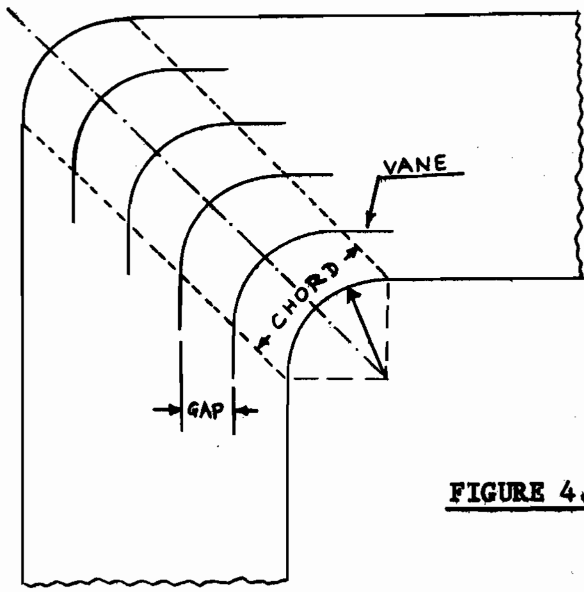

FIGURE 4.b

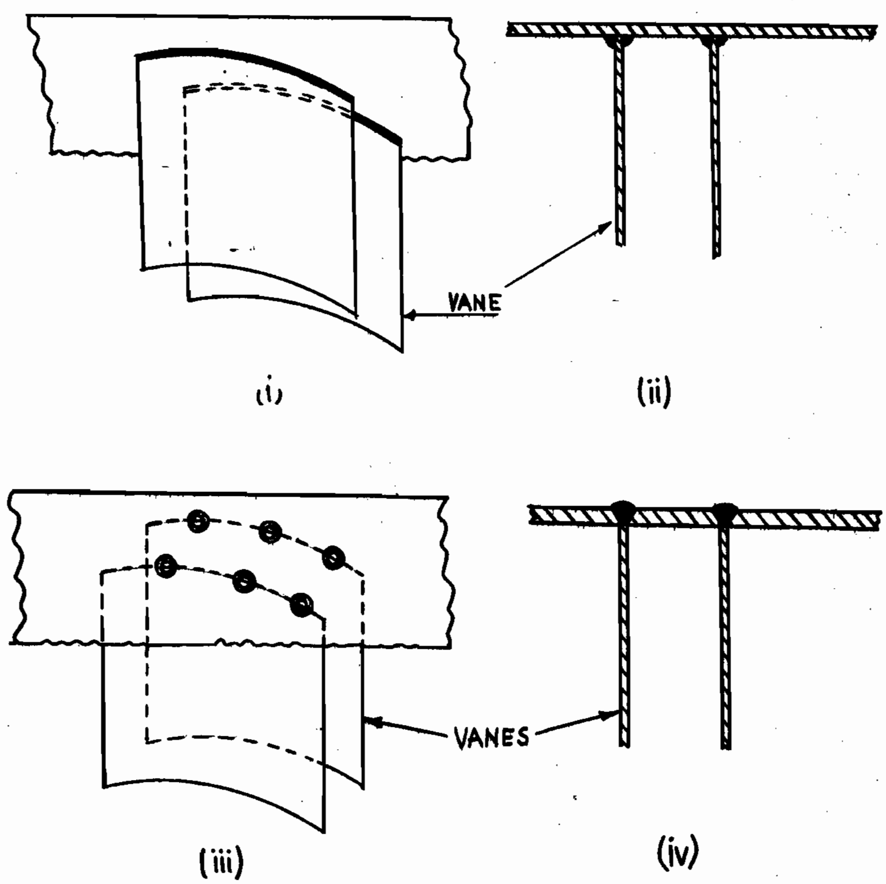

FIGURE 4.c WELDING TECHNIQUE

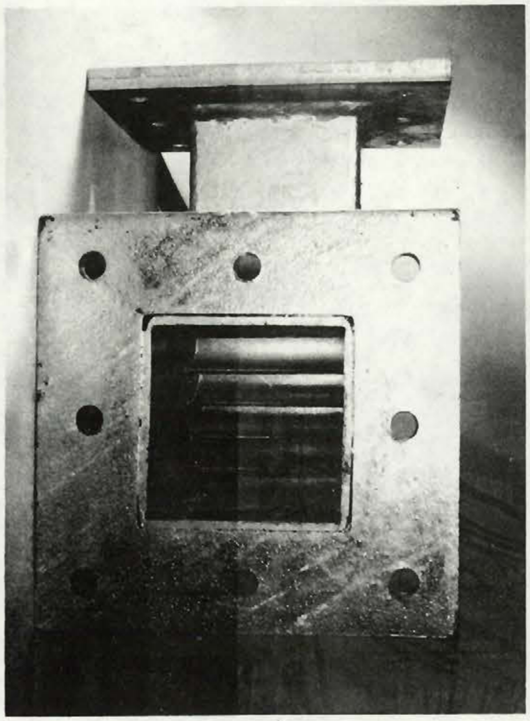

Right-angled bend with the vanes

Fig. 4.d

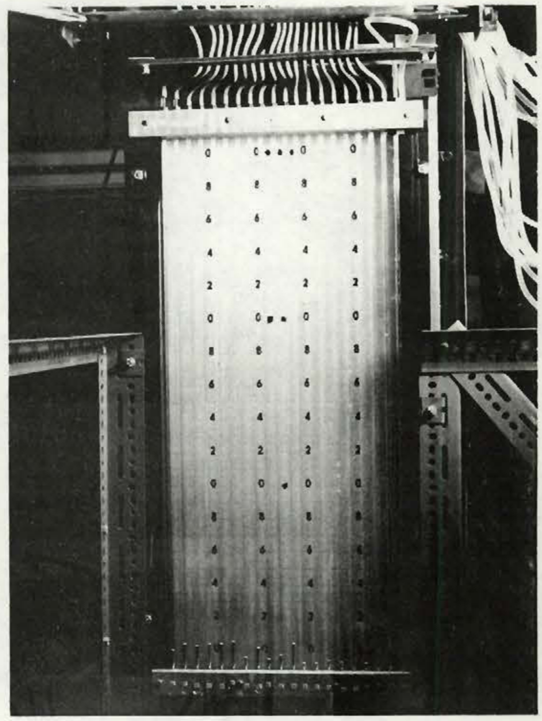

Mercury - Manometer

Fig. 6

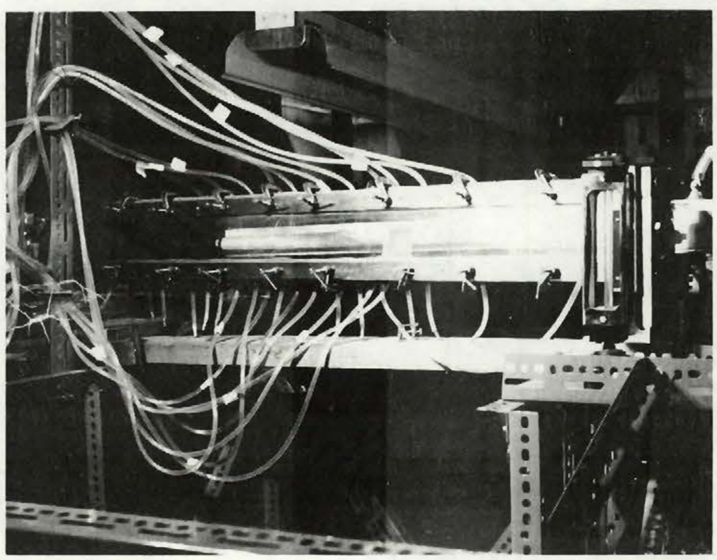

Test Section

Fig. 5

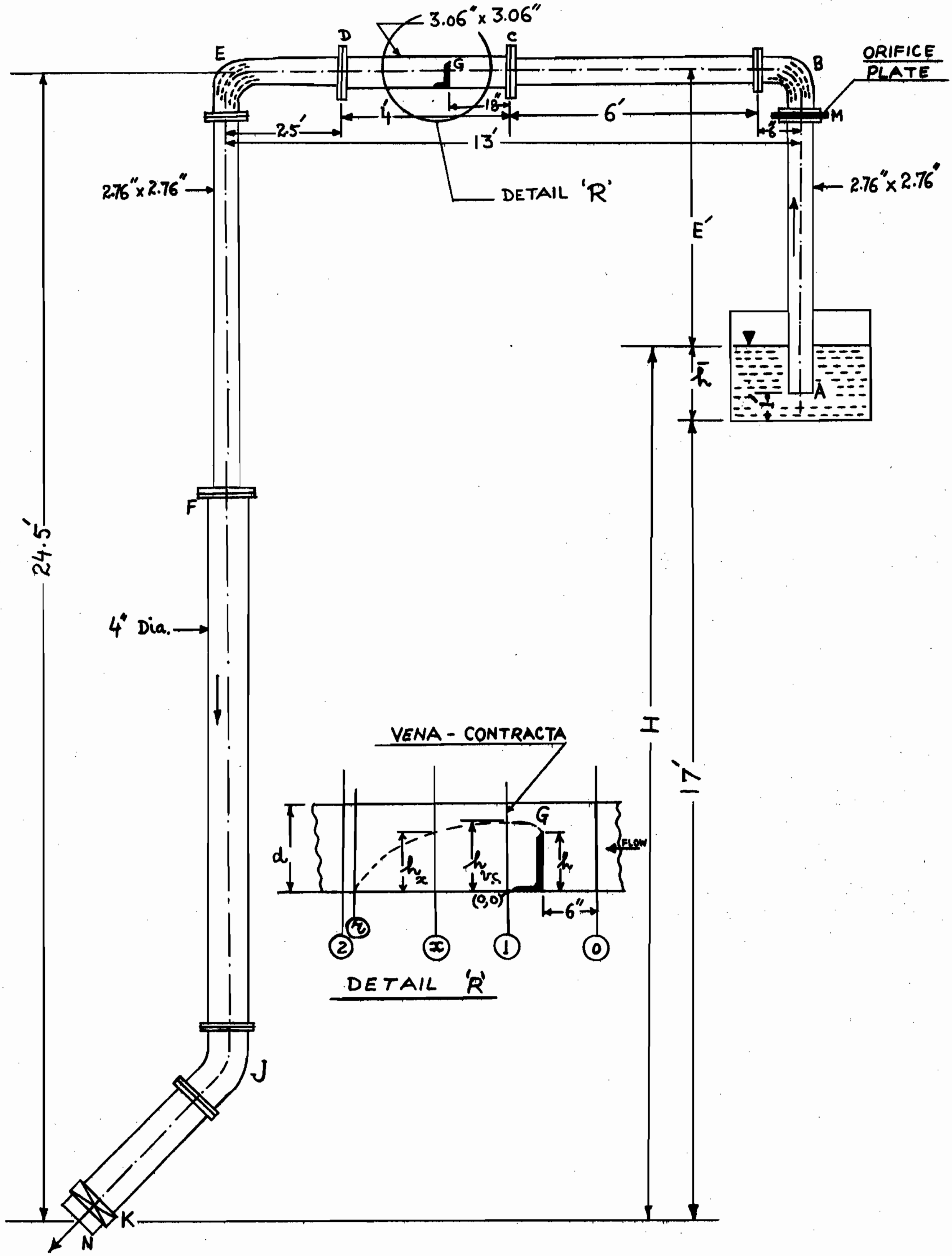

FIGURE 7 A REFERENCE SKETCH

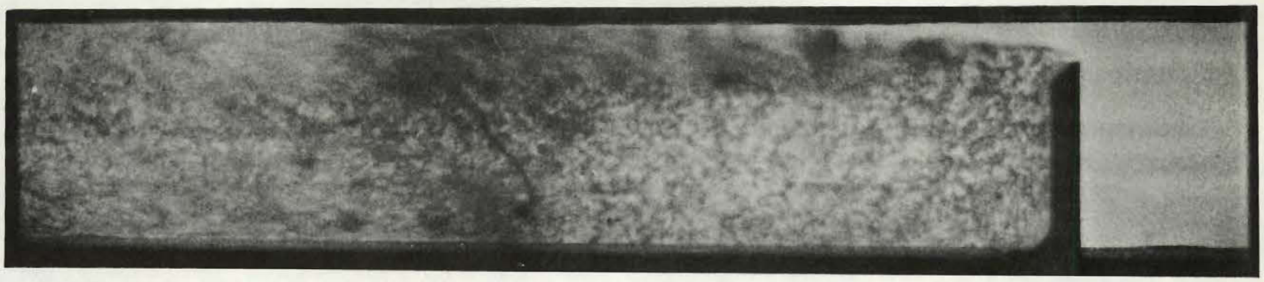

(8.a) $K_1 = 17.4$ $r_2 = 0$

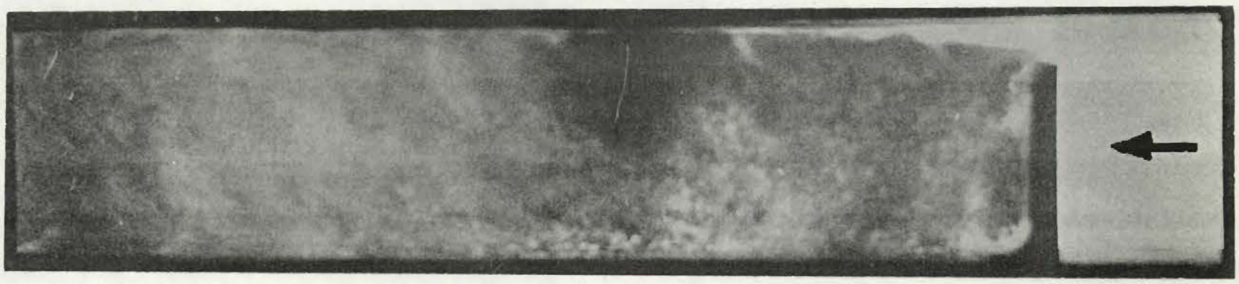

(8.b) $K_1 = 17.4$ $r_2 = 0.078$

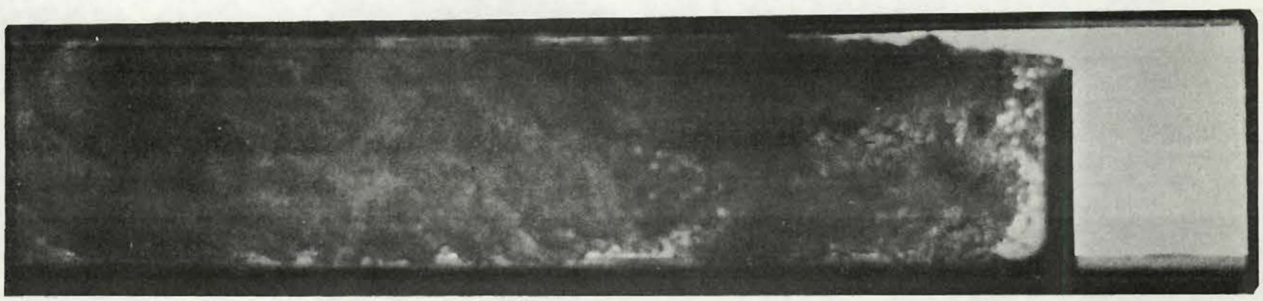

(8.c) $K_1 = 158.7$ $r_2 = 0.166$

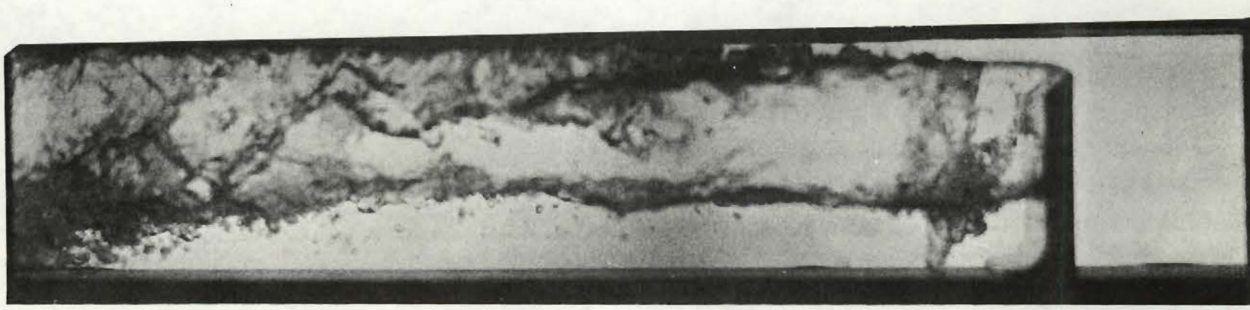

(8.d) $K_1 = 158.7$ $r_2 = 0.305$

Fig. 8 PICTURES OF THE FLOW $\left(\frac{h}{d} = 0.817\right)$

Nominal Gate Opening = 1"

Nominal Orifice Plate Opening = Half

Value of r_2 ($= \frac{Q_{a2}}{Q_w}$) = 0.105

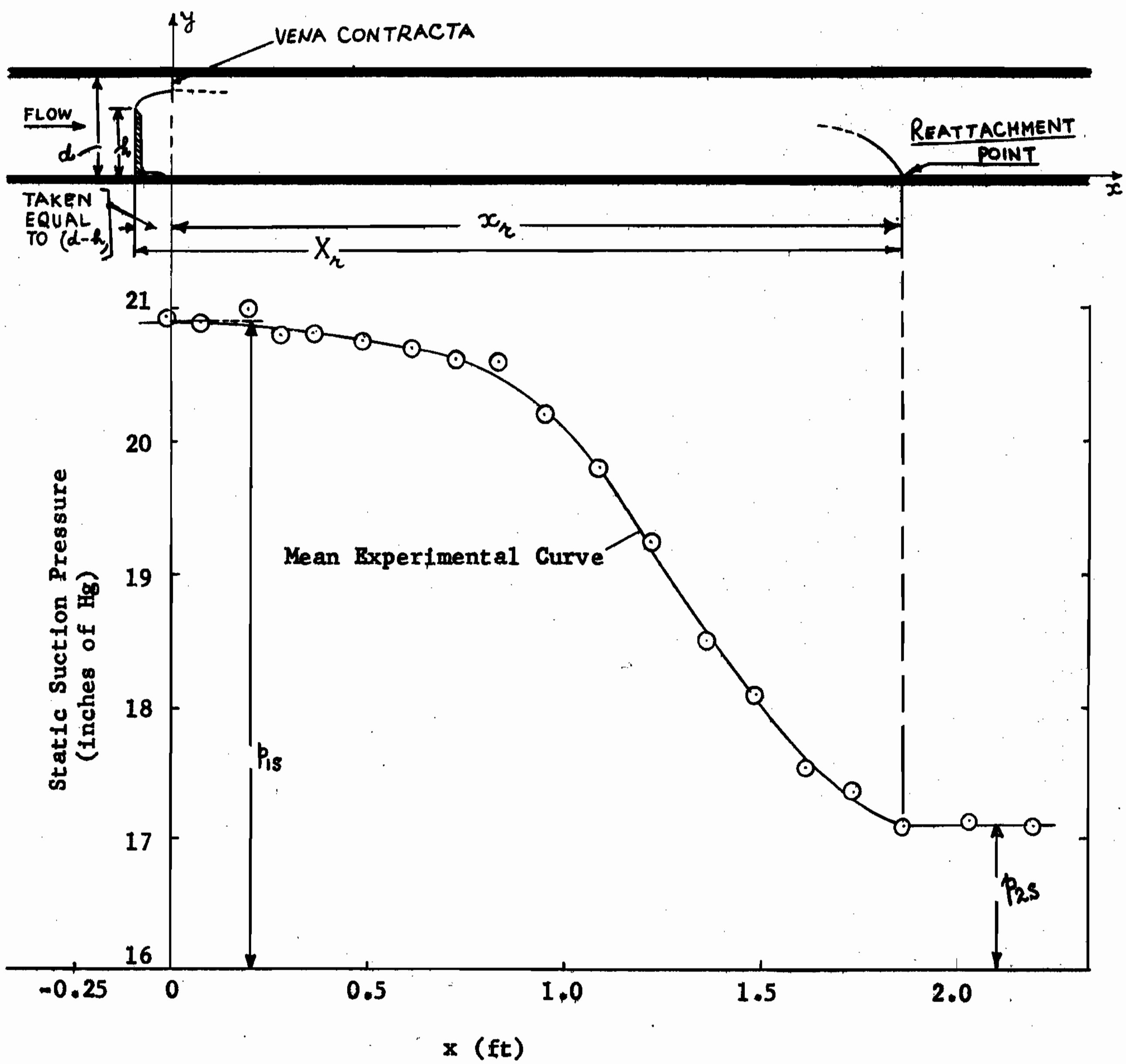

FIGURE 9 A TYPICAL FIGURE SHOWING THE GRAPHICAL METHOD TO FIND p_{1s}, p_{2s}, x_r, AND X_r.

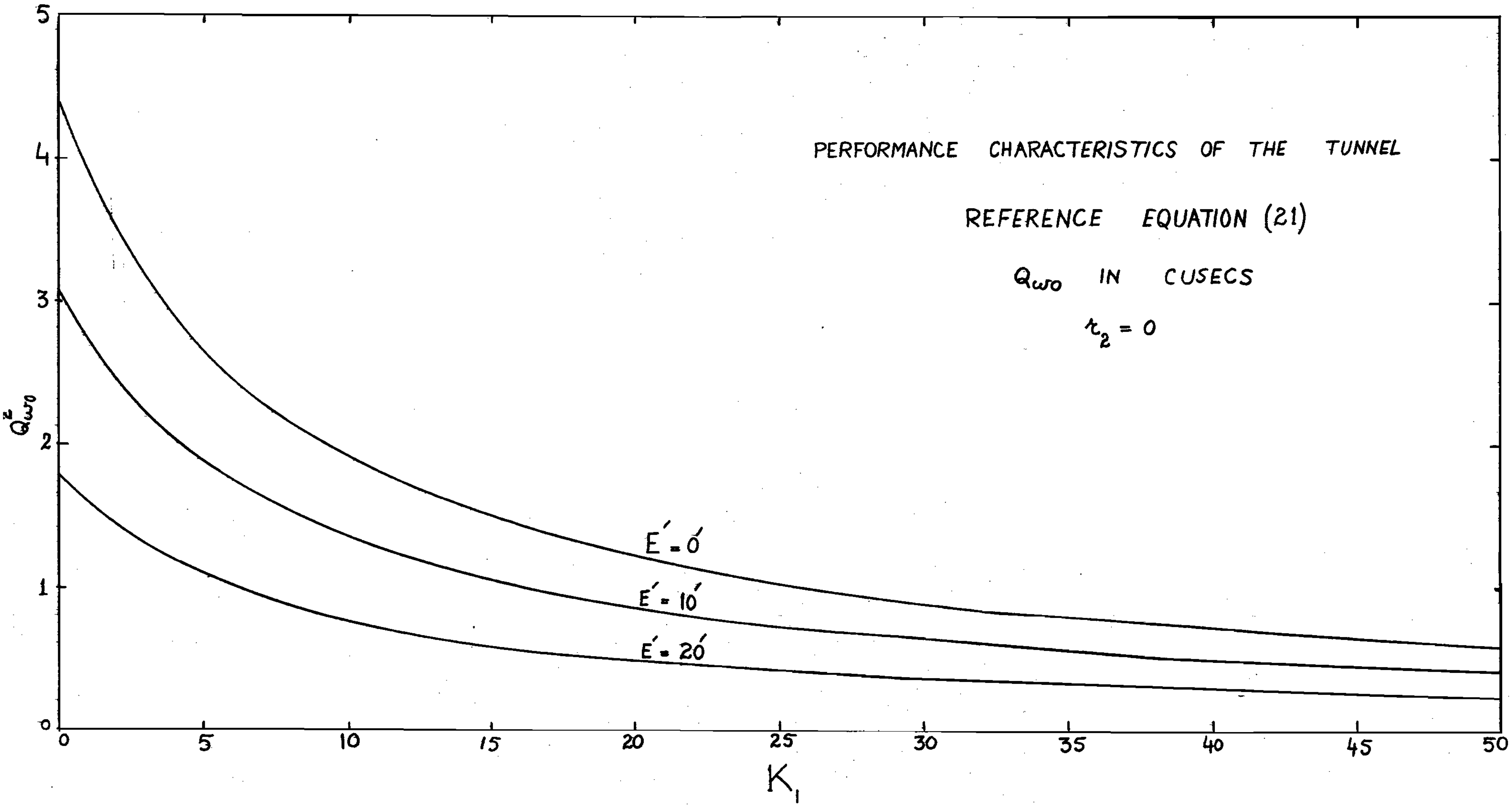
PERFORMANCE CHARACTERISTICS OF THE TUNNEL
REFERENCE EQUATION (21)
Q_{wo} IN CUSECS
$r_2 = 0$
$E' = 0'$
$E' = 10'$
$E' = 20'$
Q^2_{wo}
K_1
0
1
2
3
4
5
0
5
10
15
20
25
30
35
40
45
50

FIG. 10

PERFORMANCE CHARACTERISTICS OF THE TUNNEL

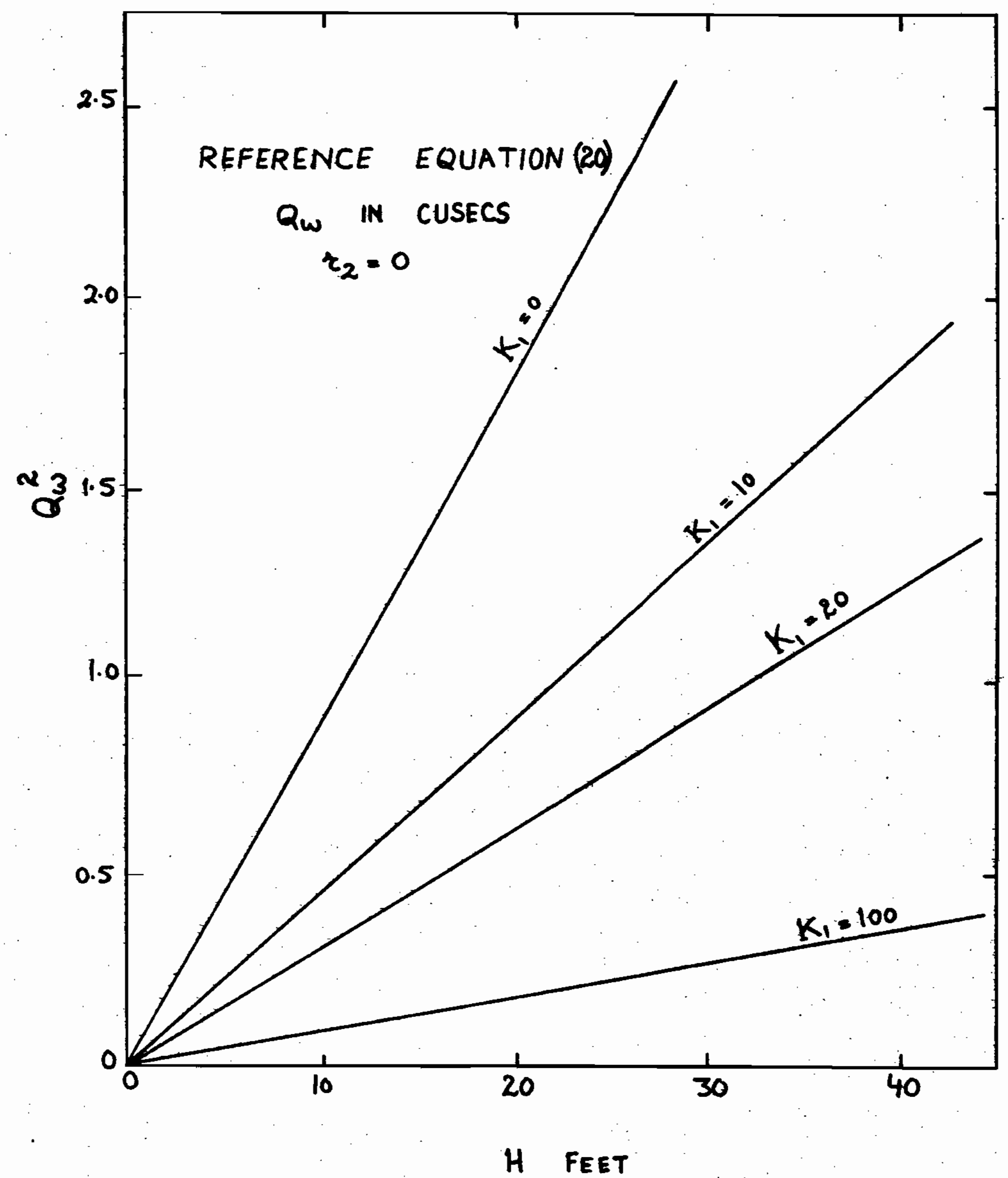

FIG. 11

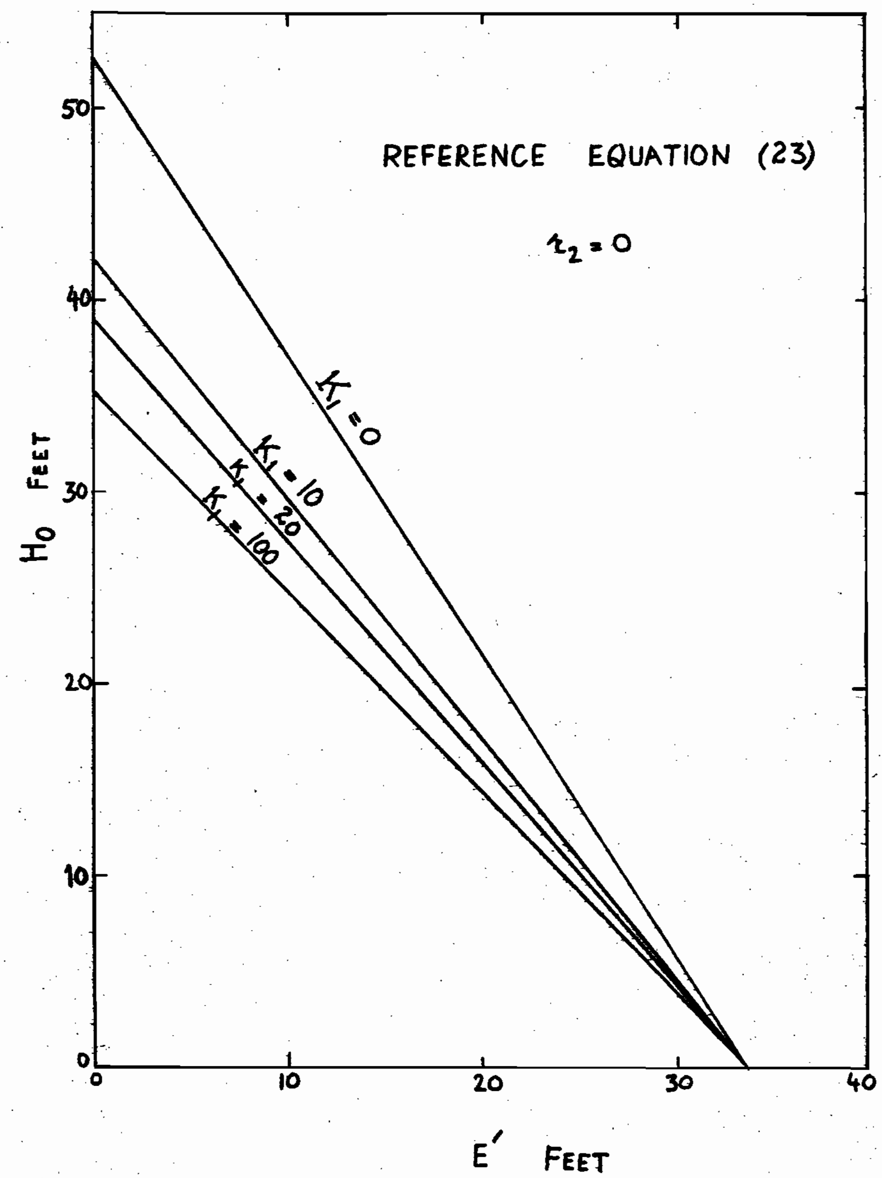

FIG. 12

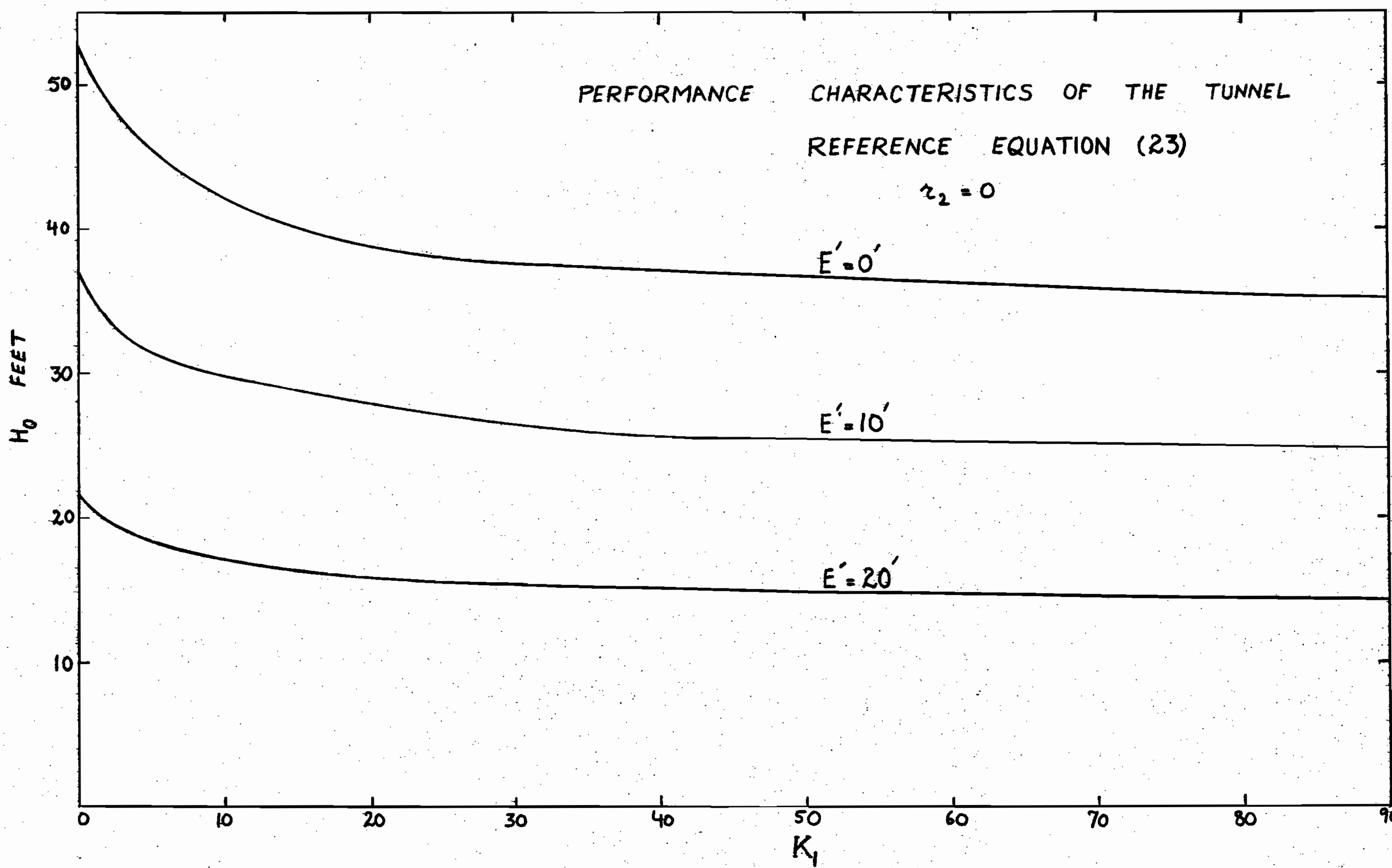
PERFORMANCE CHARACTERISTICS OF THE TUNNEL
REFERENCE EQUATION (23)
$r_2 = 0$
$E' = 0'$
$E' = 10'$
$E' = 20'$
H_0 FEET
50
40
30
20
10
0
10
20
30
40
50
60
70
80
90
K_1

FIG. 13

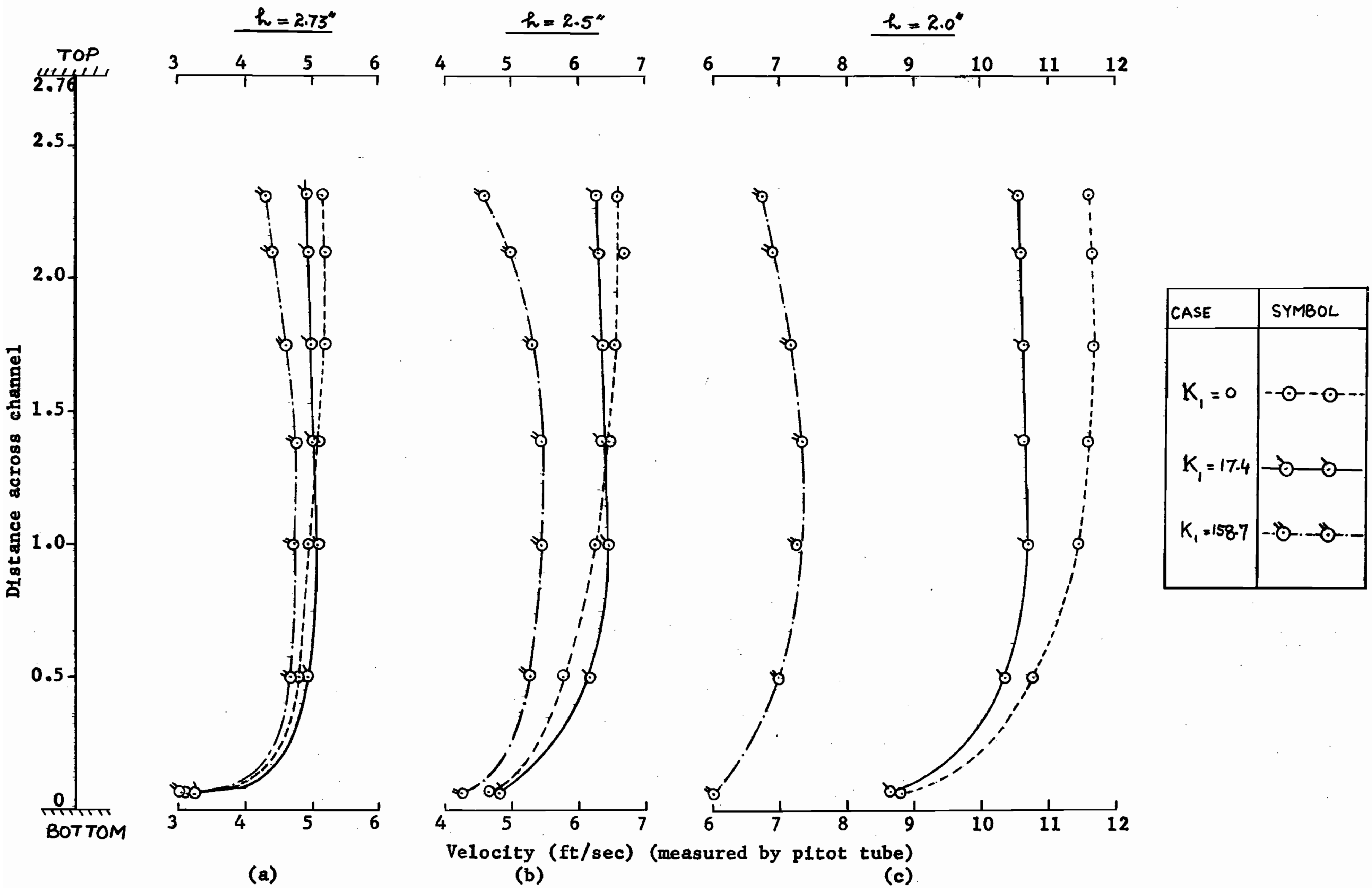

h = 2.73"
h = 2.5"
h = 2.0"
TOP
BOTTOM
2.76
2.5
2.0
1.5
1.0
0.5
0
3
4
5
6
7
8
9
10
11
12
Distance across channel
Velocity (ft/sec) (measured by pitot tube)
(a)
(b)
(c)
CASE
SYMBOL
K1 = 0
K1 = 17.4
K1 = 158.7

FIGURE 14

ARROWS INDICATE POSITION OF REATTACHMENT

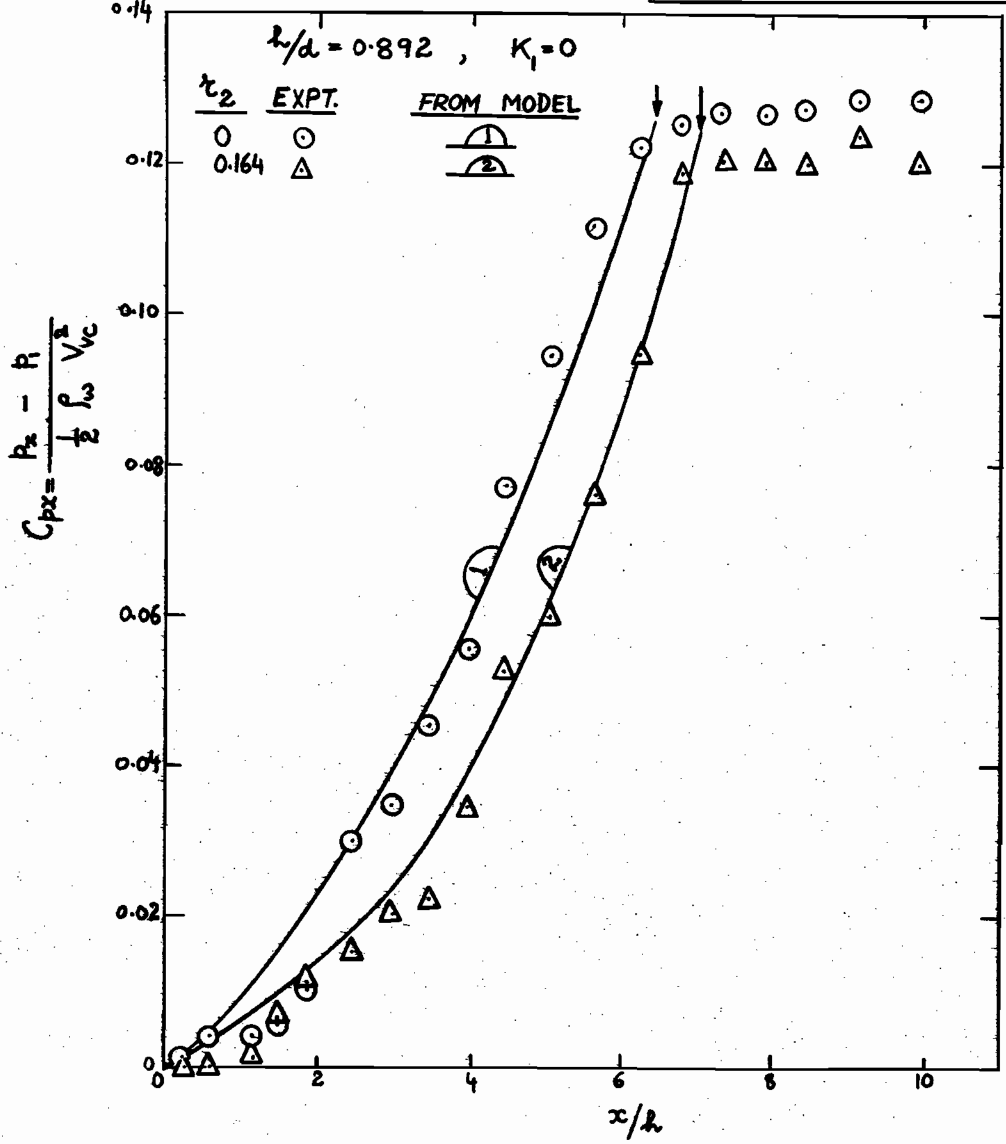

FIG. 15

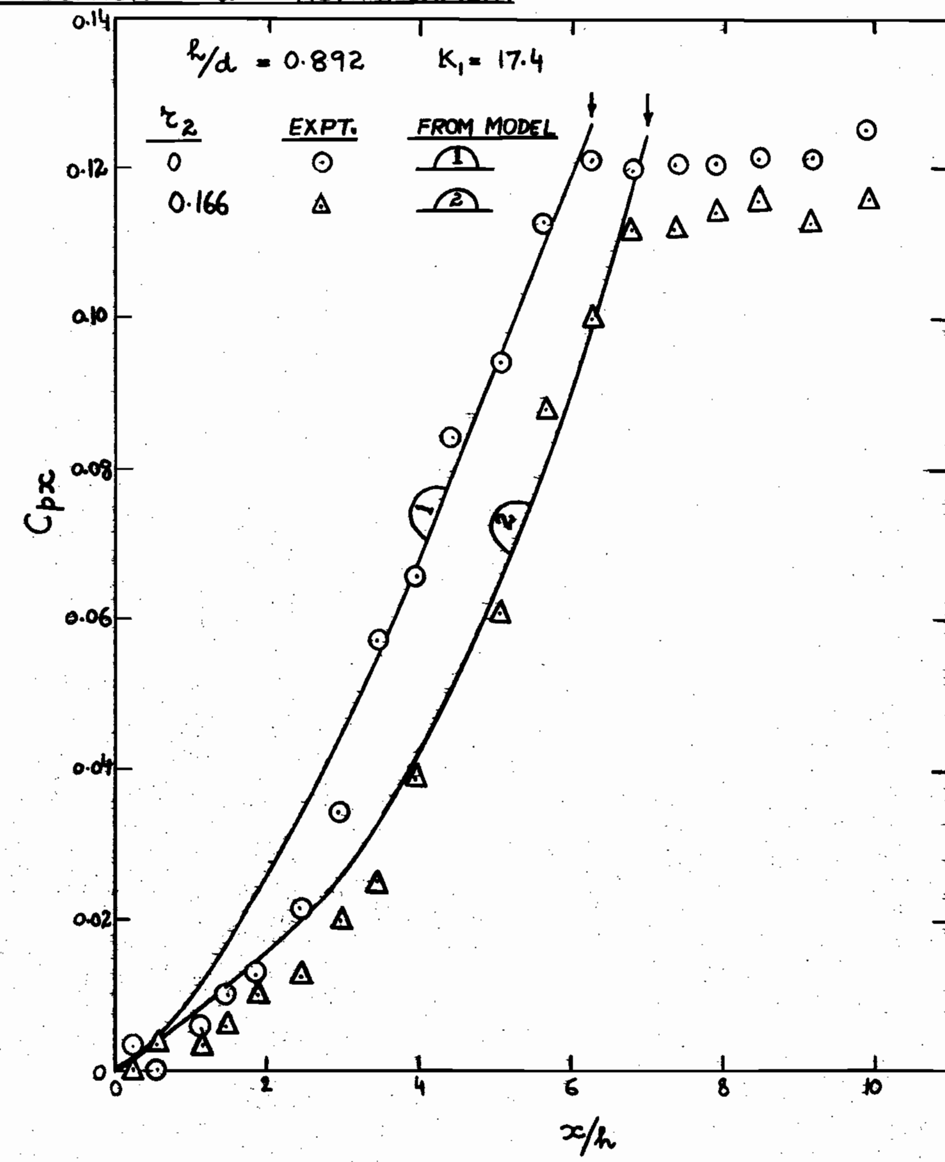

FIG. 16

ARROWS INDICATE POSITION OF REATTACHMENT

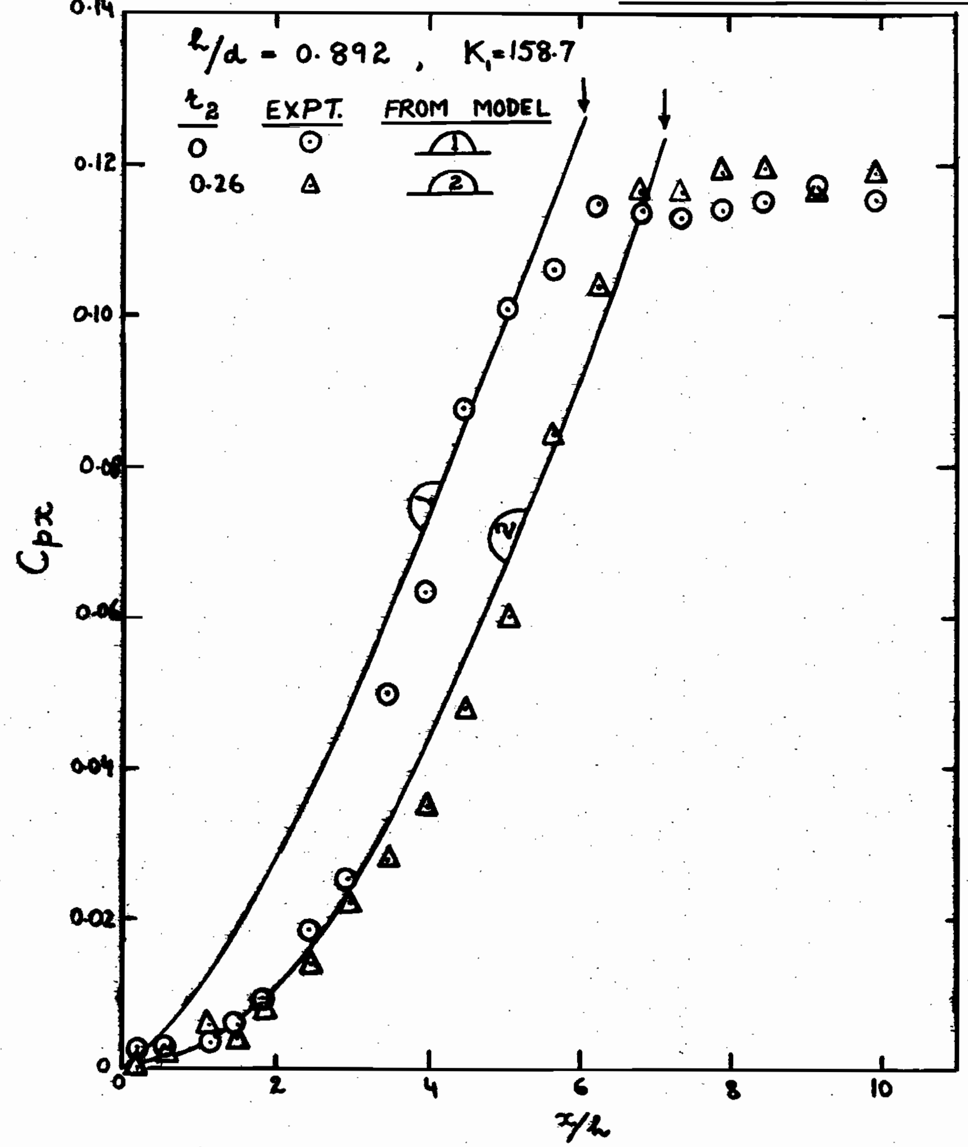

FIG. 17

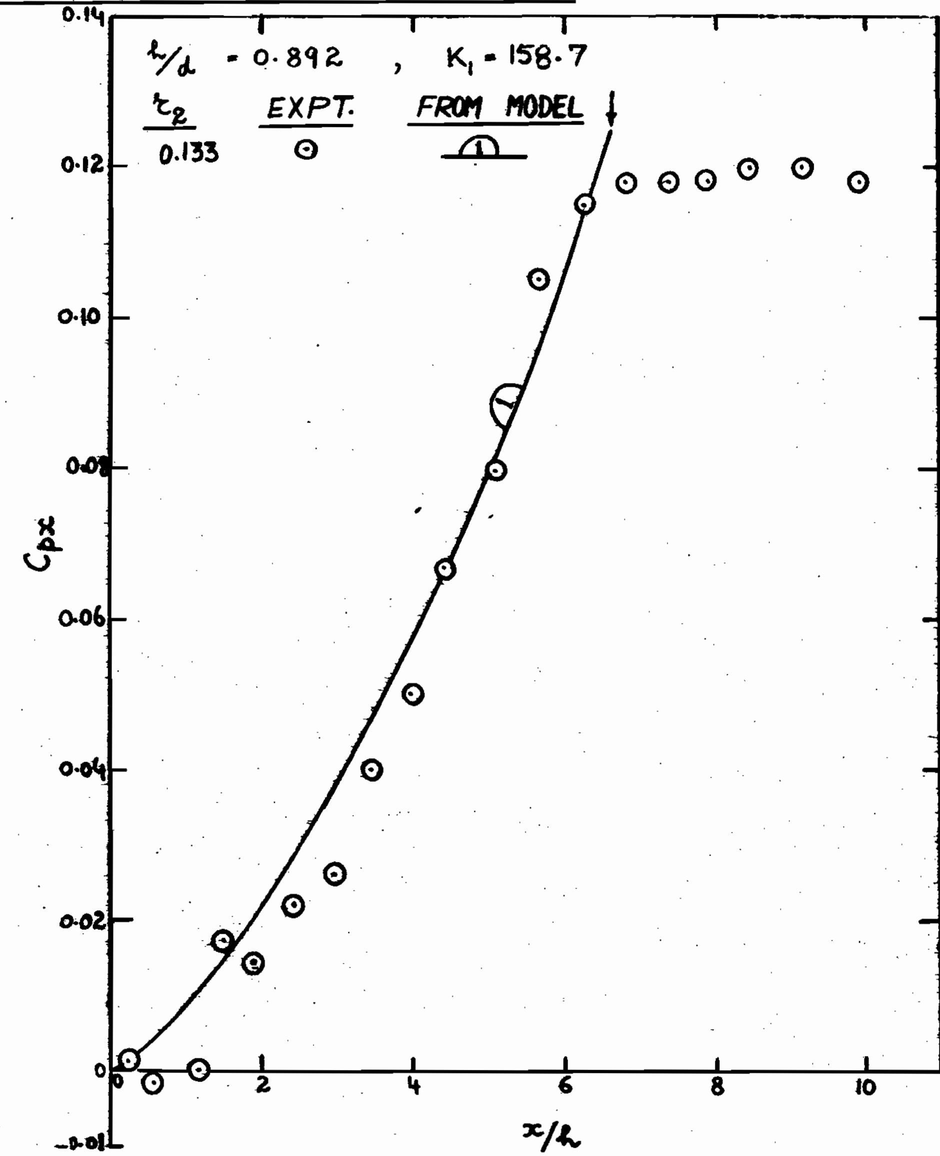

FIG. 18

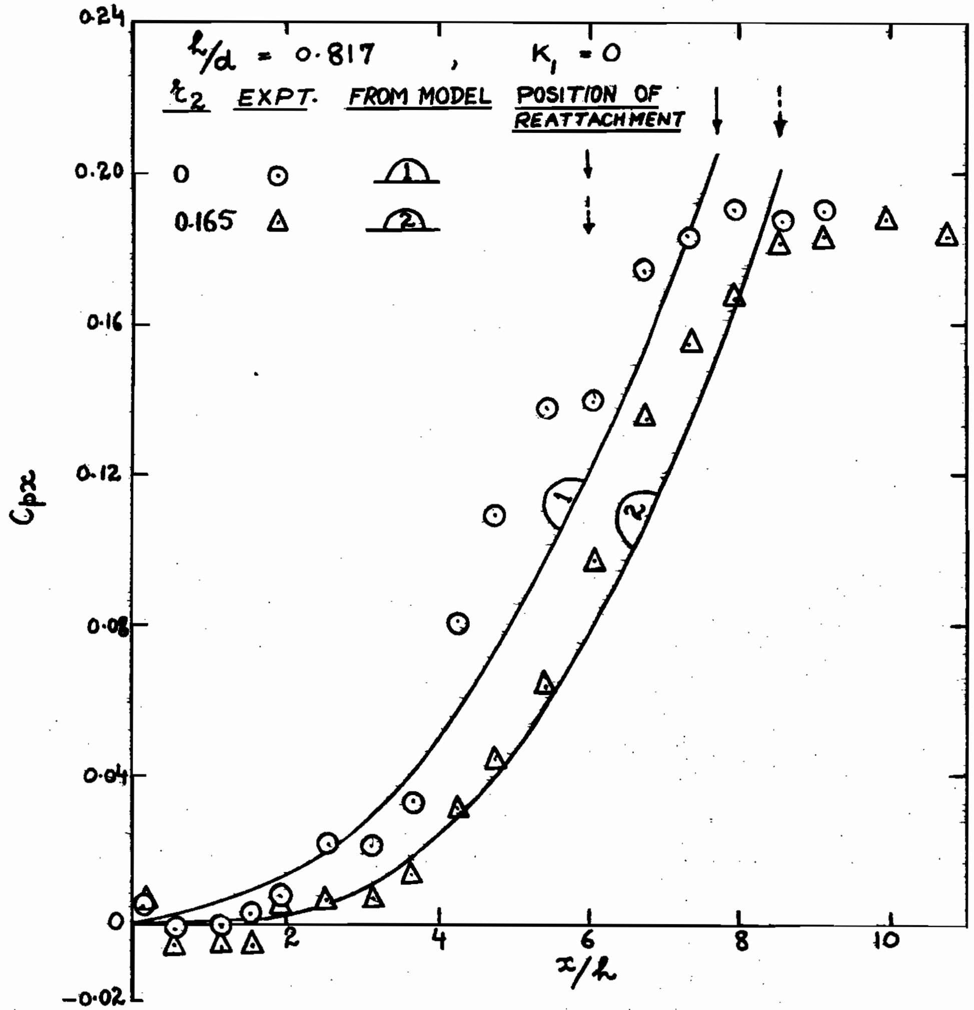

ℓ/d = 0.817 , K_1 = 0
t_2 EXPT. FROM MODEL POSITION OF REATTACHMENT
0
0.165
C_{px}
x/h

FIG. 19

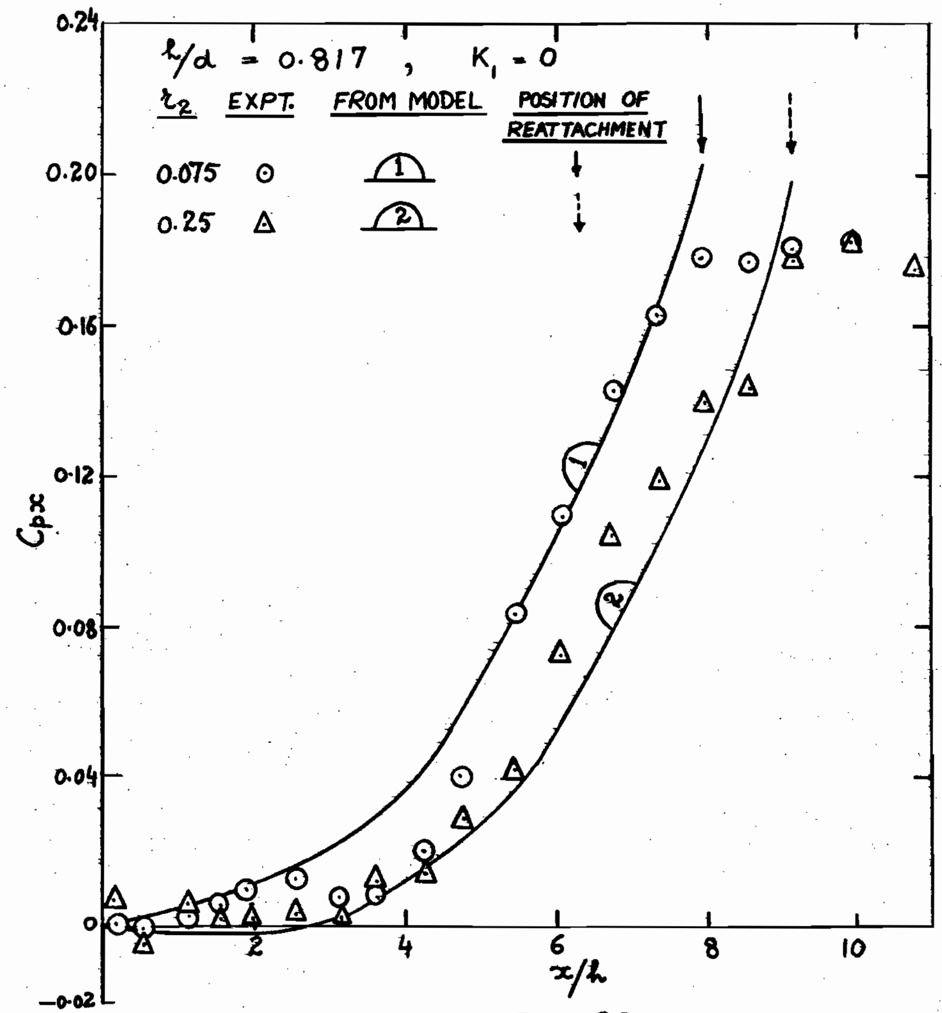

ℓ/d = 0.817 , K_1 = 0
t_2 EXPT. FROM MODEL POSITION OF REATTACHMENT
0.075
0.25
C_{px}
x/h

FIG. 20

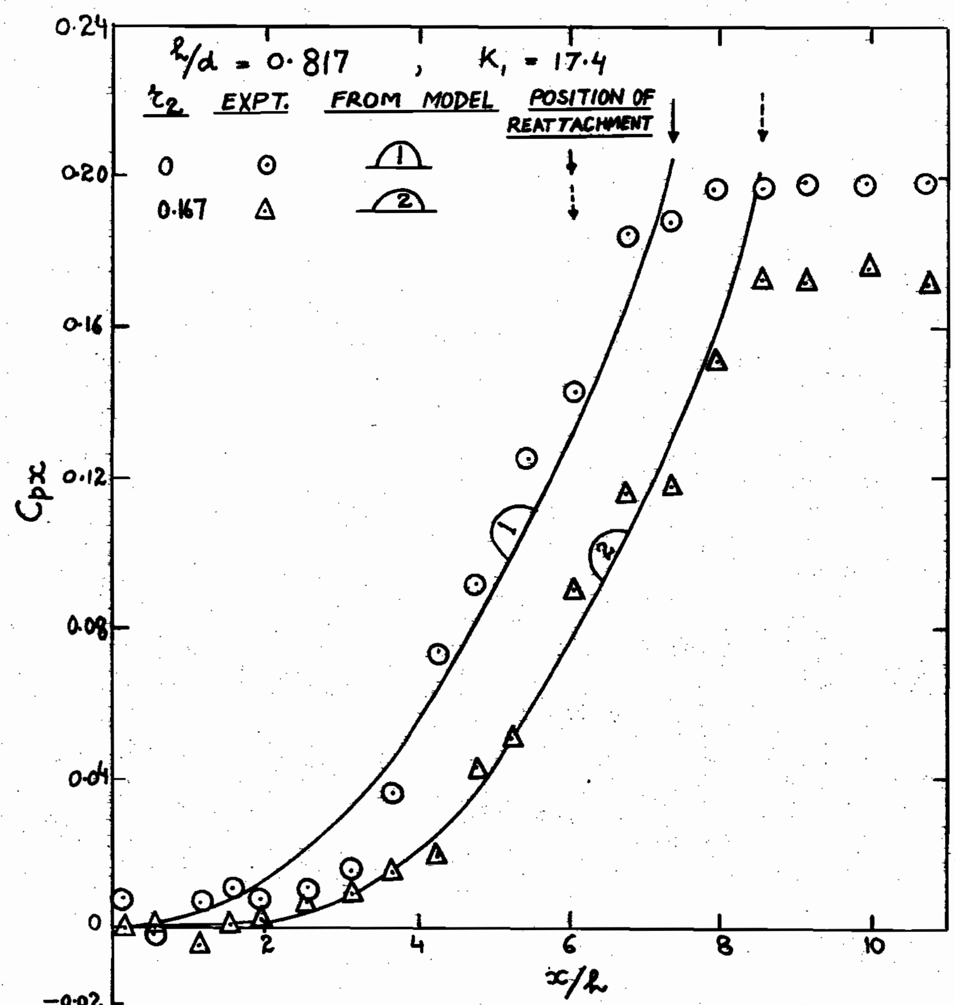

h/d = 0·817 , K1 = 17·4
r2 EXPT. FROM MODEL POSITION OF REATTACHMENT
0
0.167
1
2
0·24
0·20
0·16
0·12
0·08
0·04
0
-0·02
Cpx
2
4
6
8
10
x/h

FIG · 21

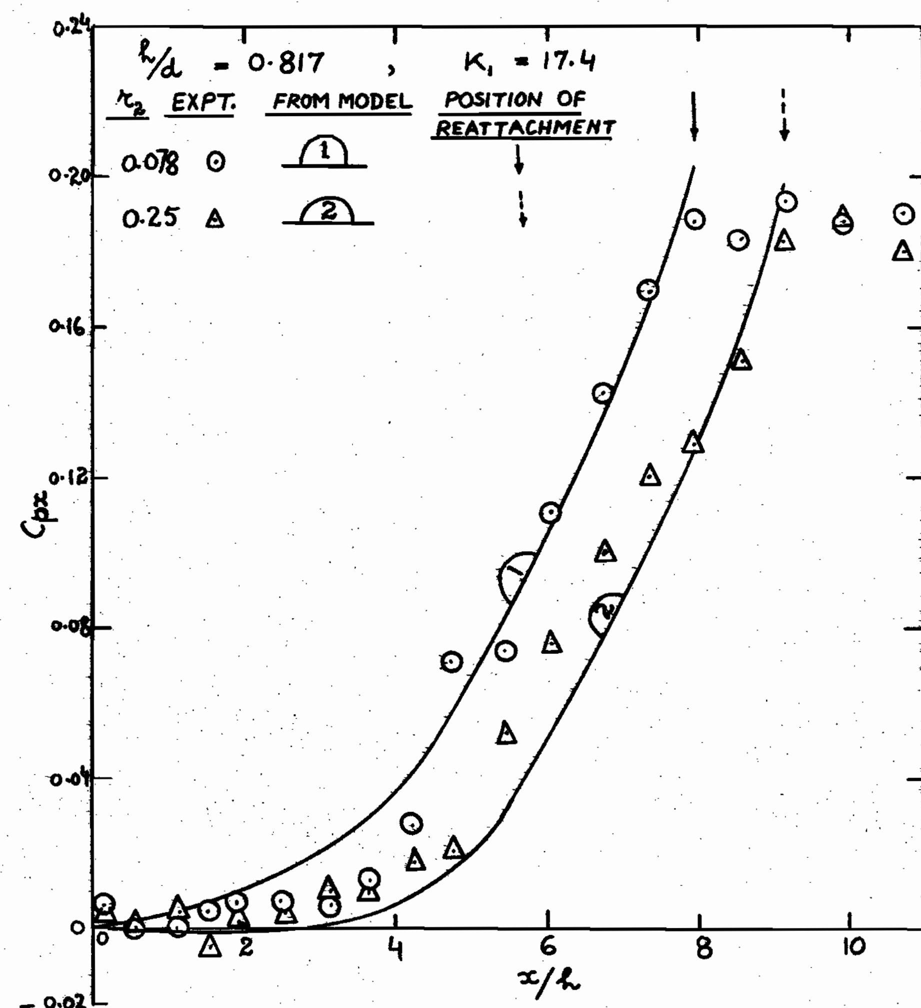

h/d = 0·817 , K1 = 17·4
r2 EXPT. FROM MODEL POSITION OF REATTACHMENT
0.078
0.25
1
2
0·24
0·20
0·16
0·12
0·08
0·04
0
- 0·02
Cpx
0
2
4
6
8
10
x/h

FIG · 22

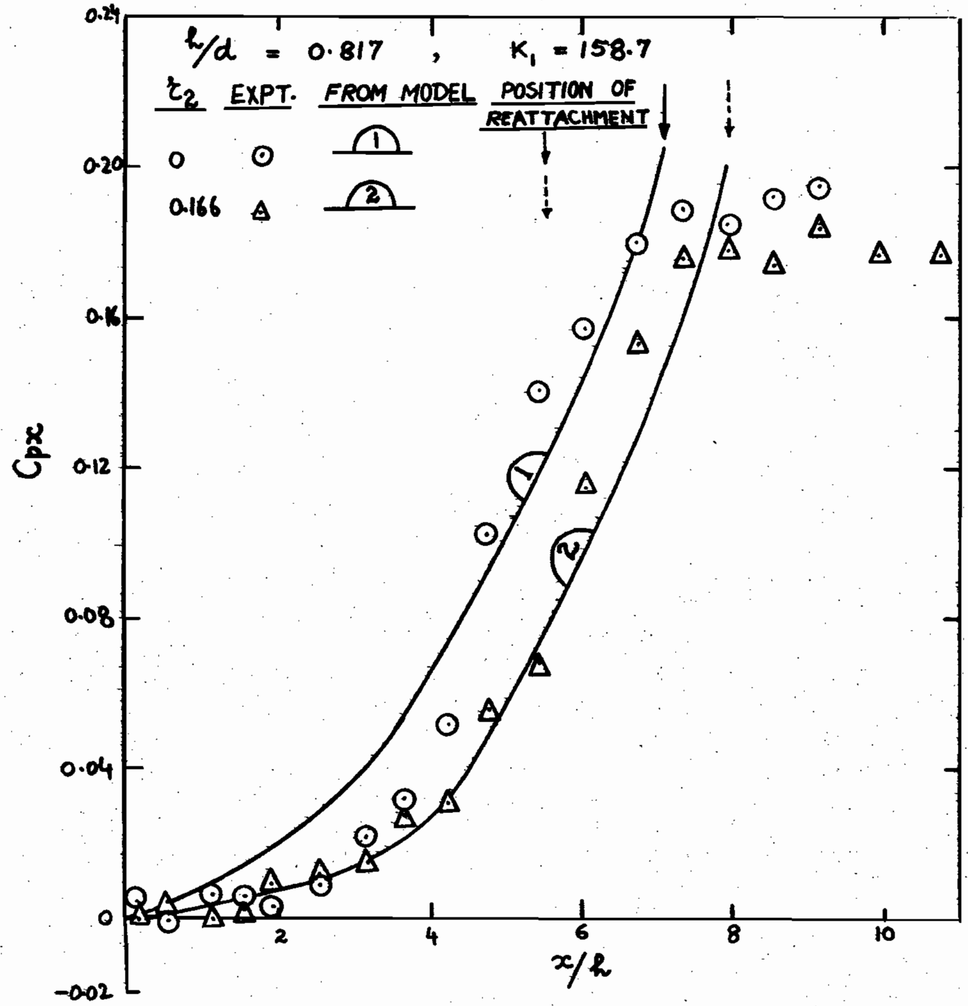
h/d = 0.817 , K1 = 158.7
τ2 EXPT. FROM MODEL POSITION OF REATTACHMENT
0 ⊙ 1
0.166 △ 2
Cpx
x/h

FIG. 23

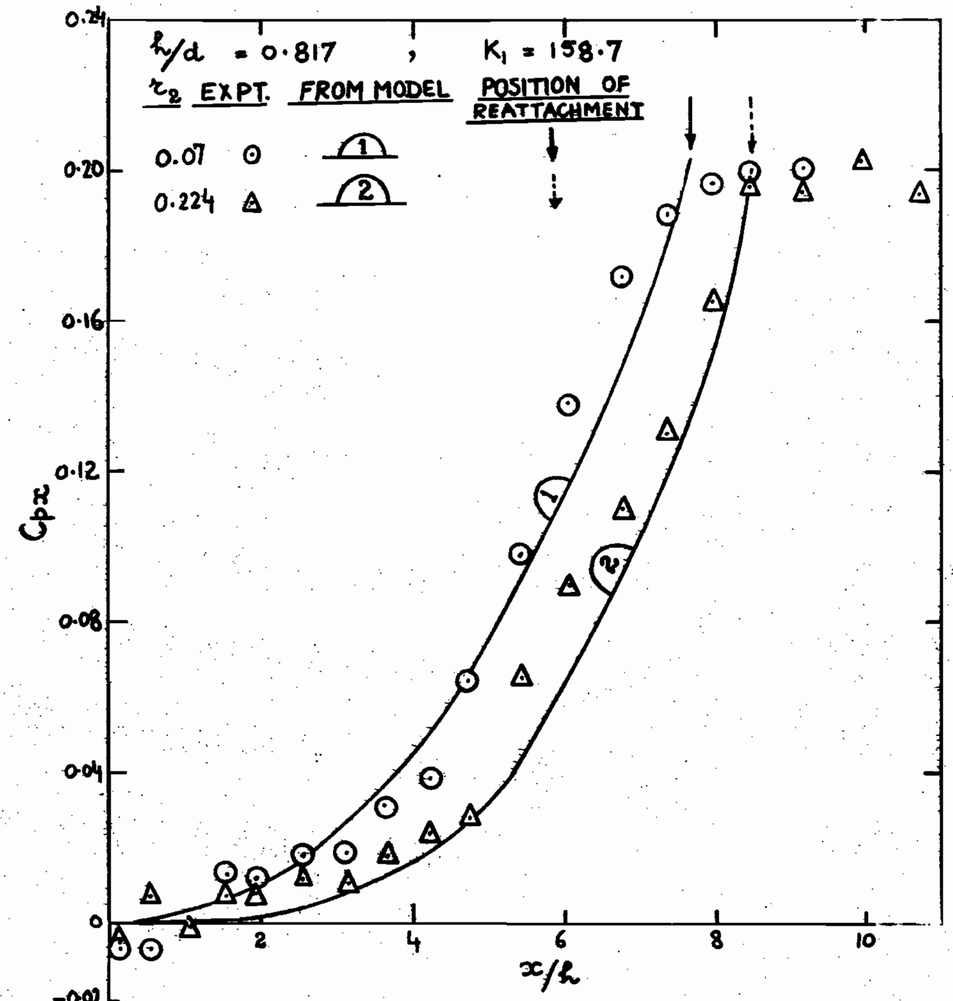
h/d = 0.817 , K1 = 158.7
τ2 EXPT. FROM MODEL POSITION OF REATTACHMENT
0.07 ⊙ 1
0.224 △ 2
Cpx
x/h

FIG. 24

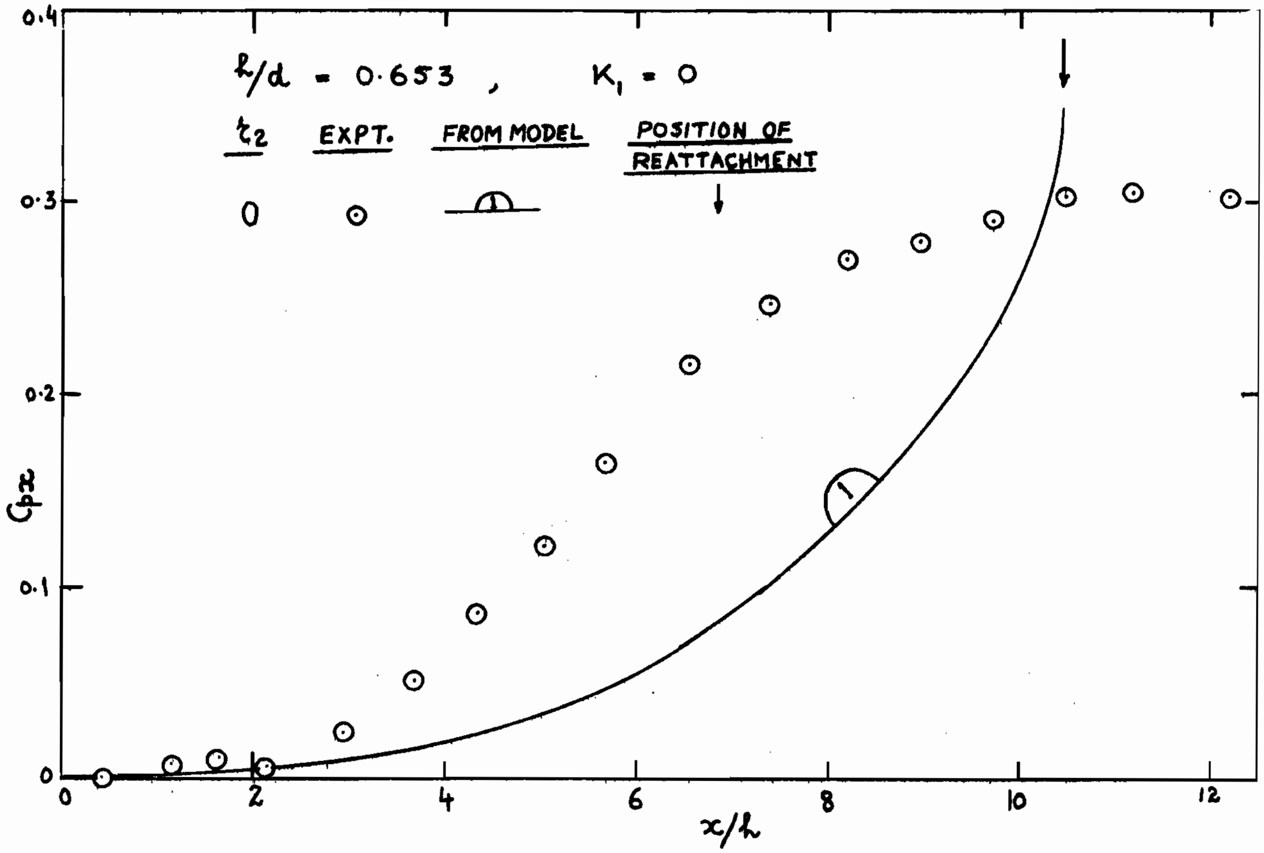

l/d = 0.653 , K1 = 0
t2 EXPT. FROM MODEL POSITION OF REATTACHMENT
0
0.4
0.3
0.2
0.1
0
Cpx
0 2 4 6 8 10 12
x/h

FIG. 25

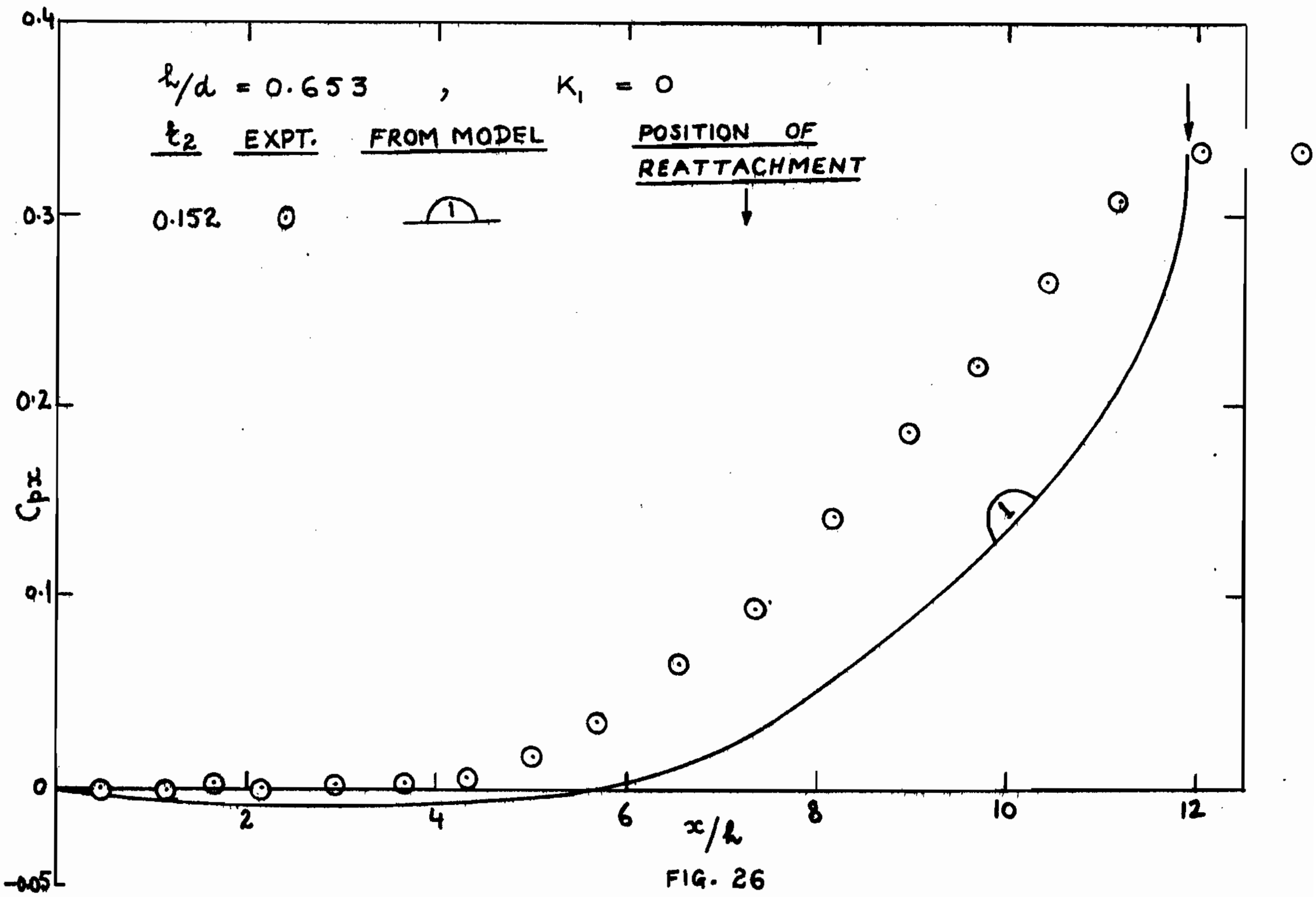

l/d = 0.653 , K1 = 0
t2 EXPT. FROM MODEL POSITION OF REATTACHMENT
0.152
0.4
0.3
0.2
0.1
0
-0.05
Cpx
2 4 6 8 10 12
x/h

FIG. 26

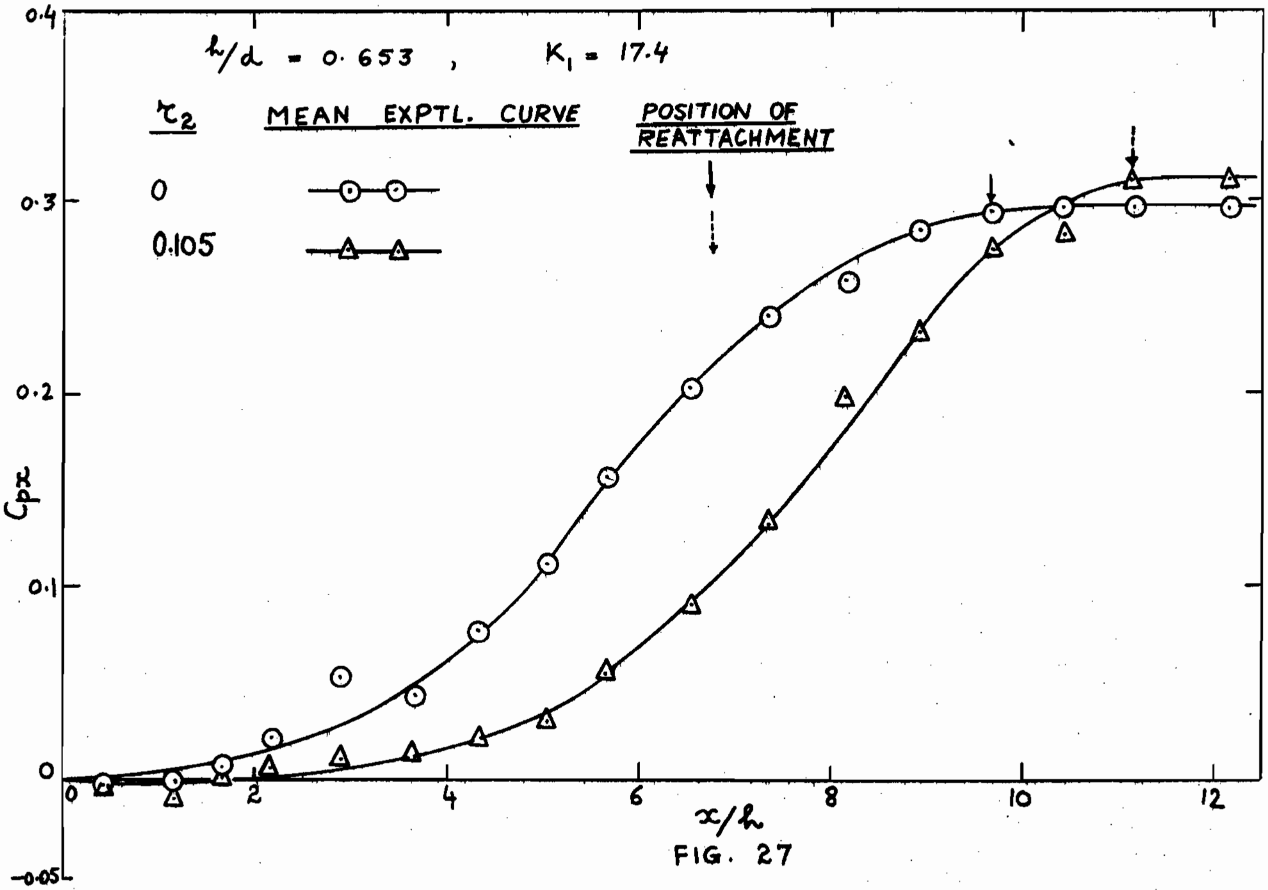

h/d = 0.653 , K1 = 17.4
τ2
MEAN EXPTL. CURVE
POSITION OF REATTACHMENT
0
0.105
Cpx
x/h

FIG. 27

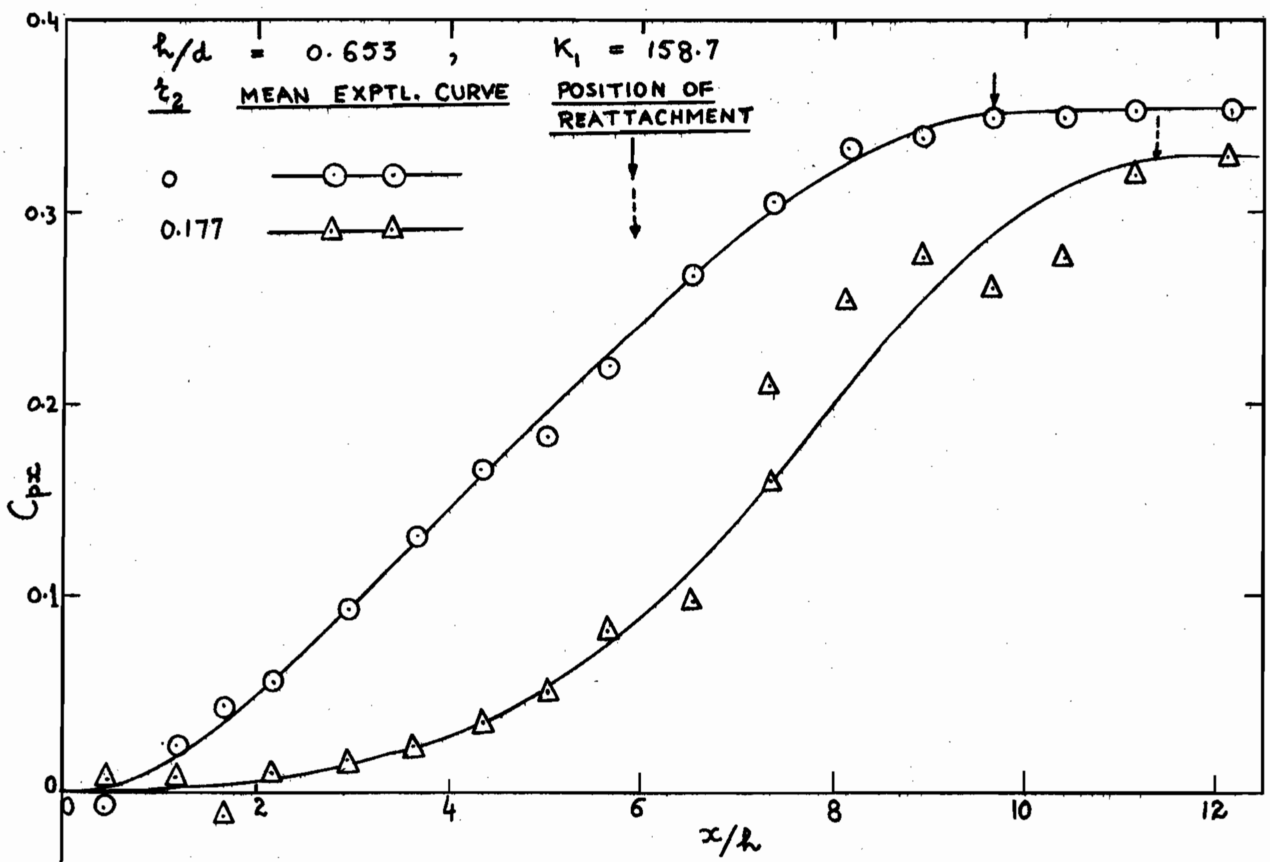

h/d = 0.653 , K1 = 158.7
τ2
MEAN EXPTL. CURVE
POSITION OF REATTACHMENT
0
0.177
Cpx
x/h

FIG. 28

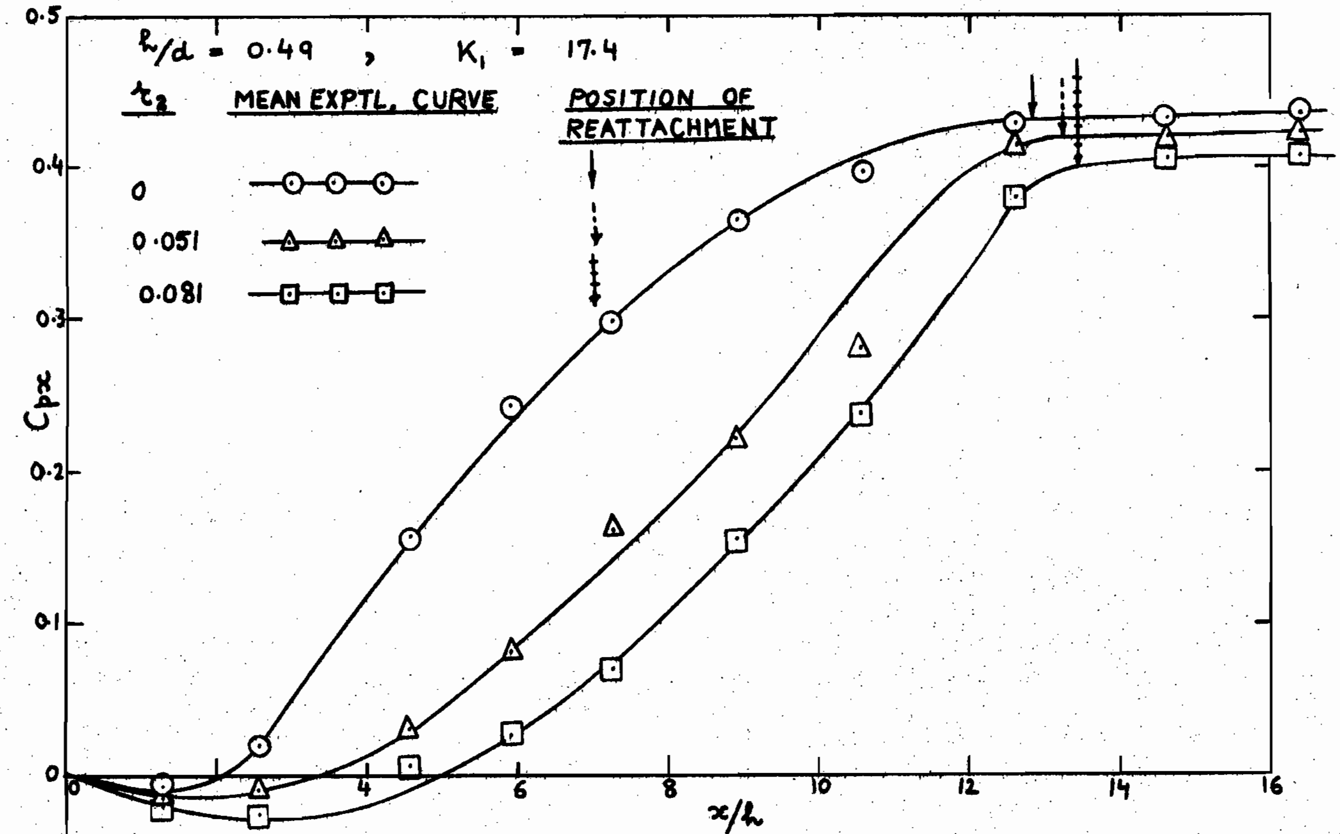
h/d = 0.49 , K1 = 17.4
τ2 MEAN EXPTL. CURVE
POSITION OF REATTACHMENT
0
0.051
0.081
Cpx
x/h
0.5
0.4
0.3
0.2
0.1
0
-0.05
0
4
6
8
10
12
14
16

FIG. 29

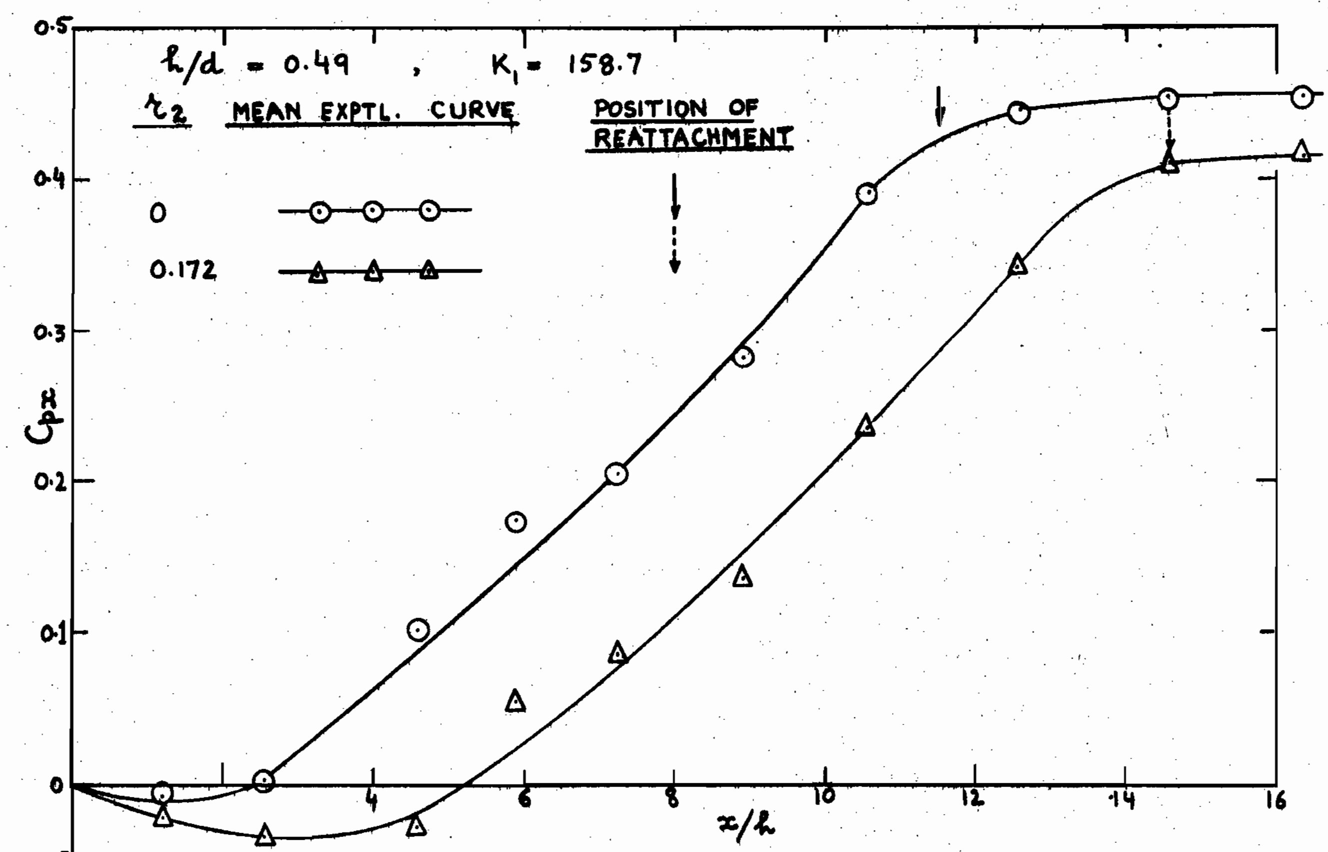
h/d = 0.49 , K1 = 158.7
τ2 MEAN EXPTL. CURVE
POSITION OF REATTACHMENT
0
0.172
Cpx
x/h
0.5
0.4
0.3
0.2
0.1
0
-0.05
4
6
8
10
12
14
16

FIG. 30

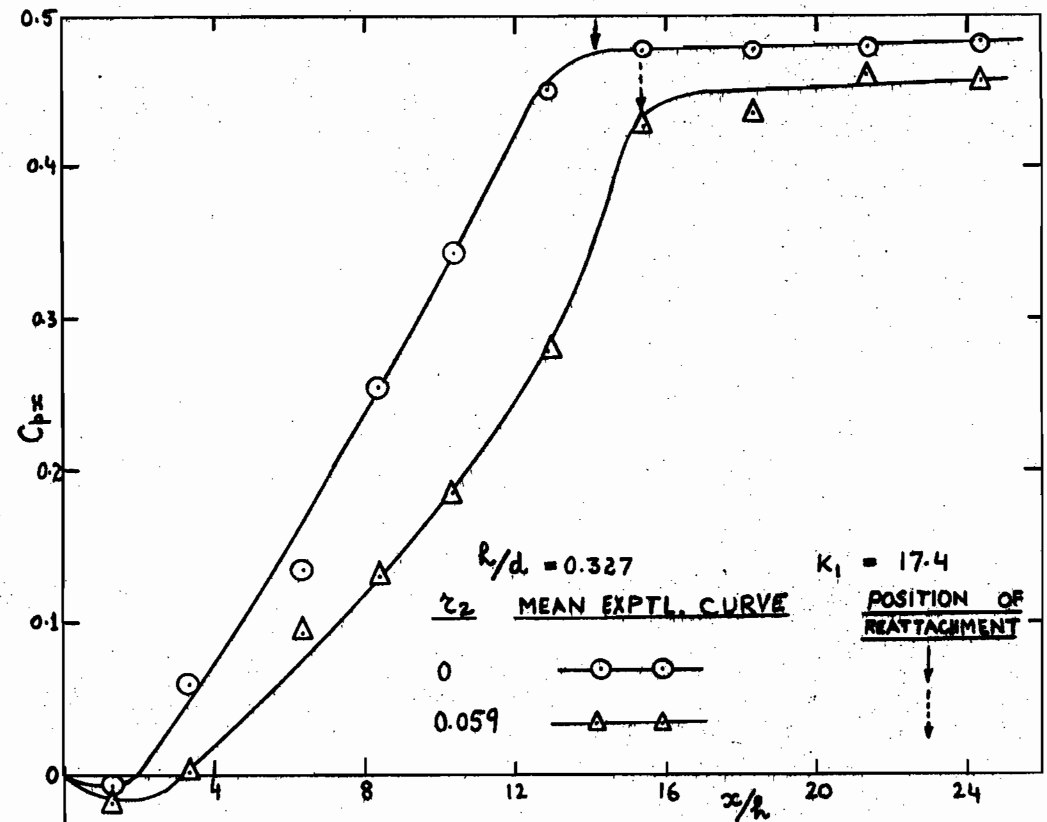

0.5
0.4
0.3
0.2
0.1
0
-0.05
C_{px}
4
8
12
16
20
24
x/h
h/d = 0.327
K_1 = 17.4
τ_2
MEAN EXPTL. CURVE
POSITION OF REATTACHMENT
0
0.059

FIG. 31

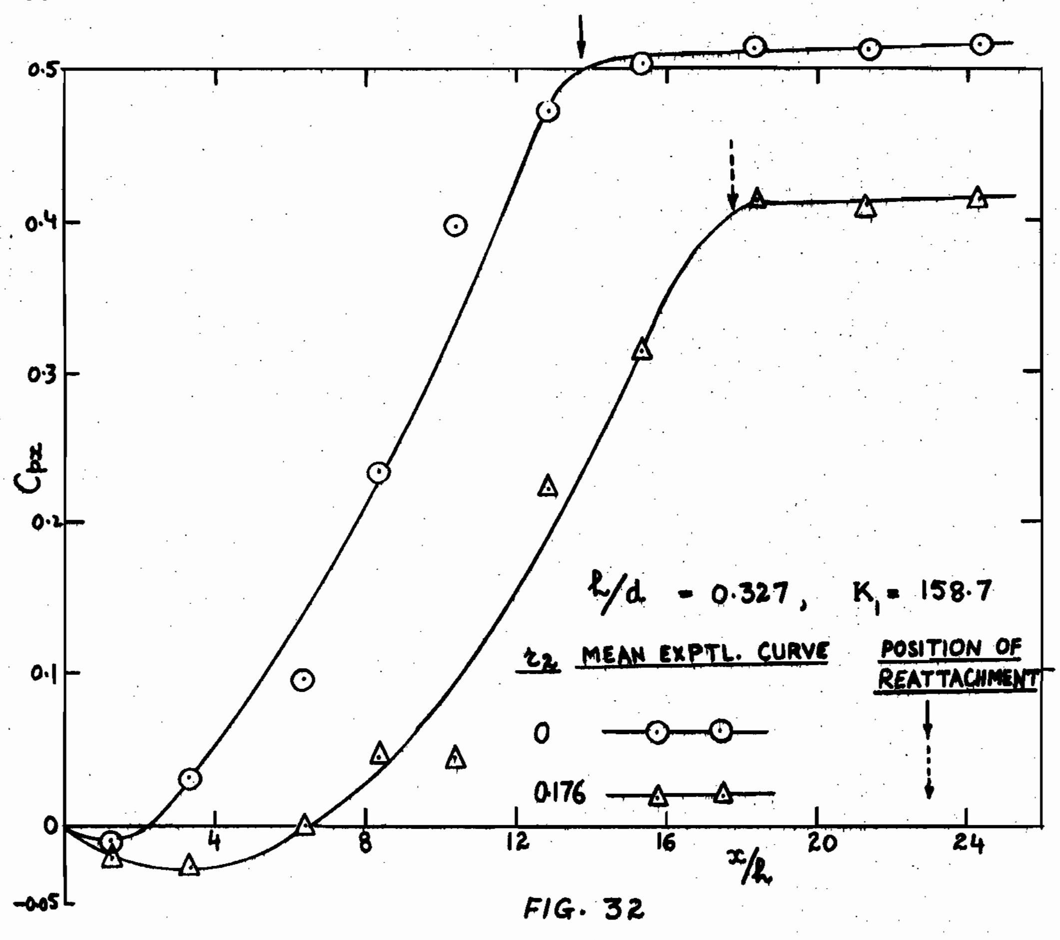

0.5
0.4
0.3
0.2
0.1
0
-0.05
C_{px}
4
8
12
16
20
24
x/h
h/d = 0.327, K_1 = 158.7
τ_2
MEAN EXPTL. CURVE
POSITION OF REATTACHMENT
0
0.176

FIG. 32

EFFECT OF VENTILATION ON OVERALL PRESSURE RECOVERY INDEX

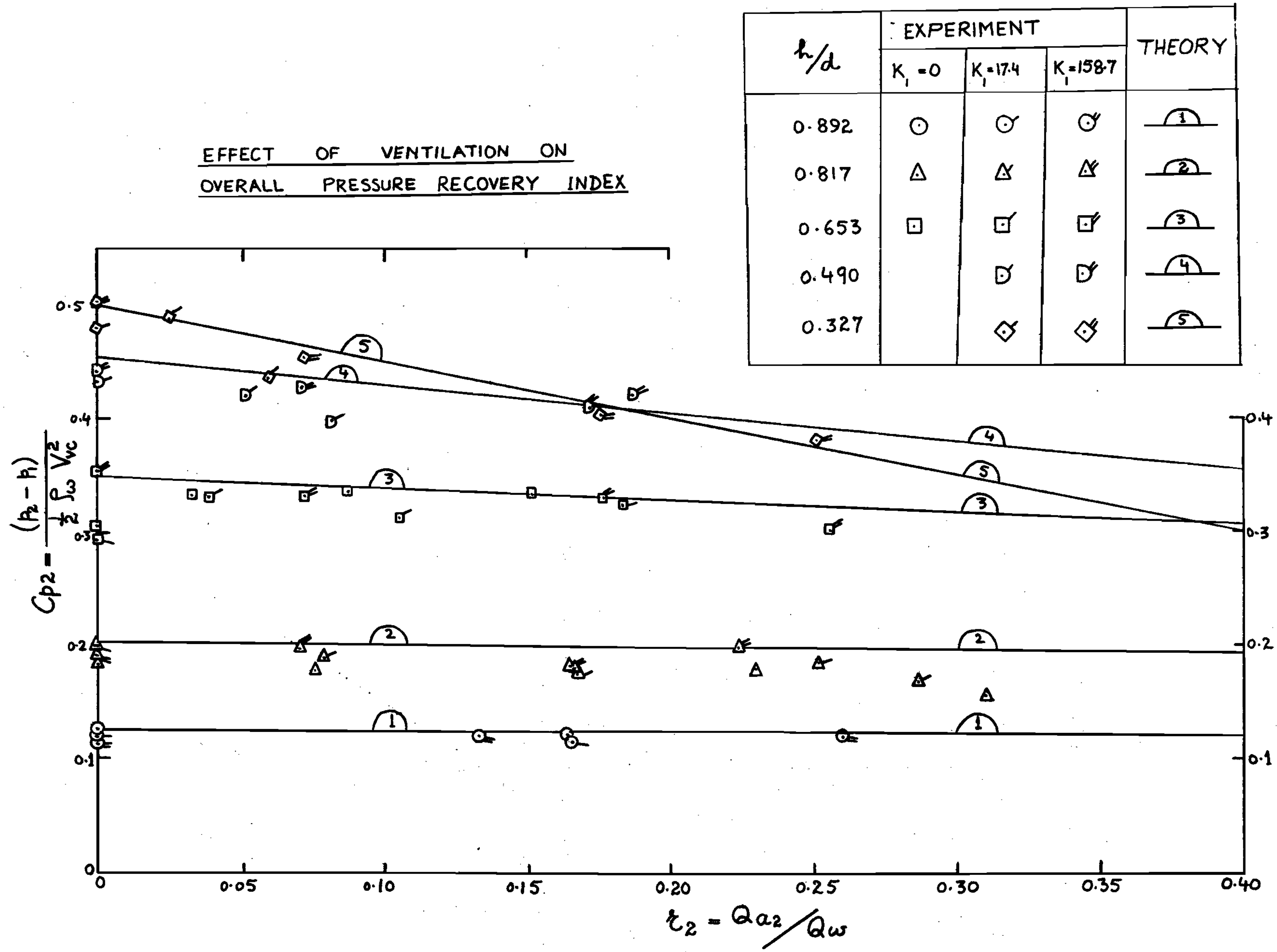

FIG. 33

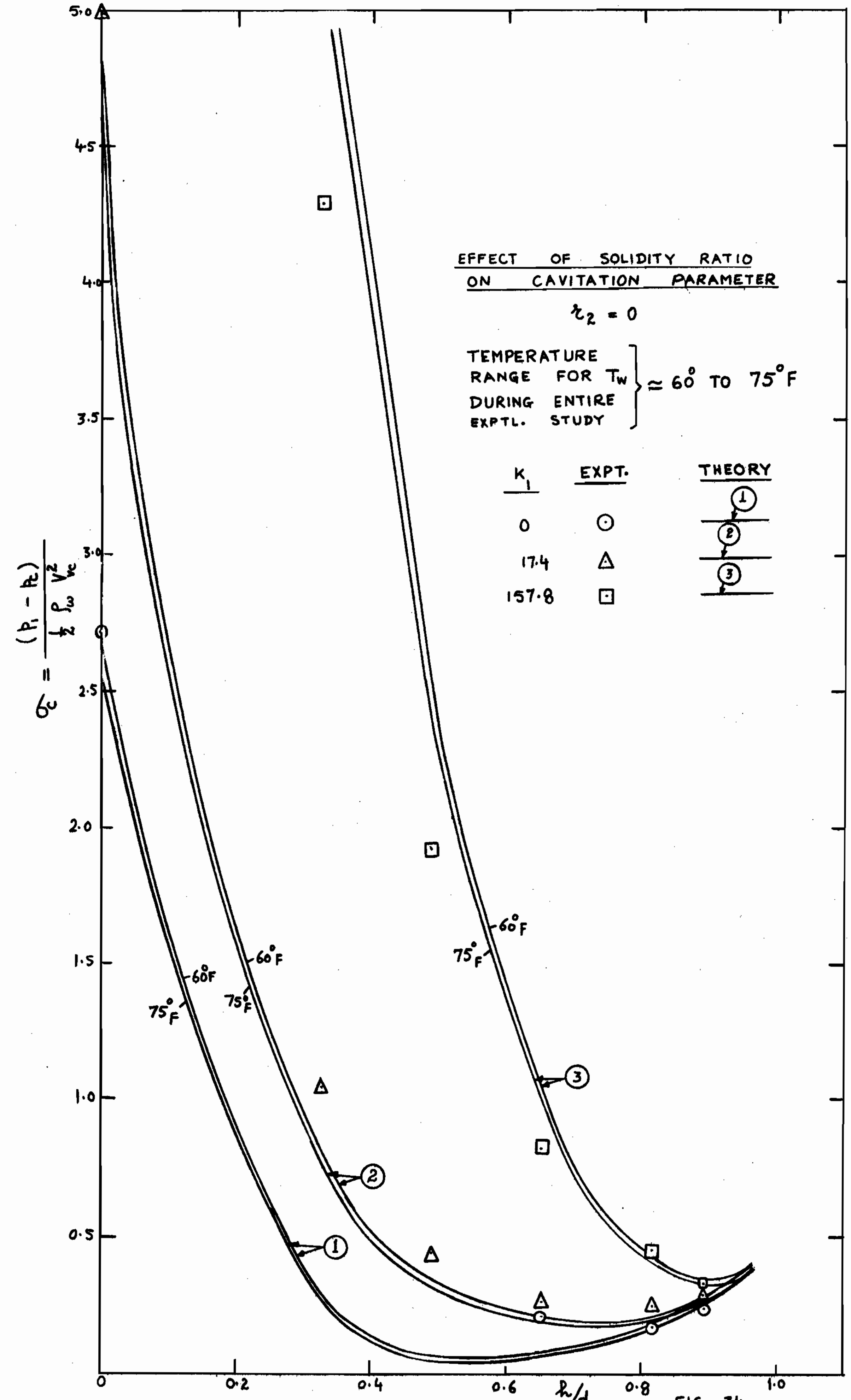

EFFECT OF SOLIDITY RATIO
ON CAVITATION PARAMETER
$r_2 = 0$
TEMPERATURE RANGE FOR T_W DURING ENTIRE EXPTL. STUDY $\simeq 60^\circ$ TO 75°F
K1
EXPT.
THEORY
0
17.4
157.8
1
2
3
60°F
75°F
$\sigma_c = \frac{(p_1 - p_c)}{\frac{1}{2}\rho_3 V_c^2}$
h/d
0
0.2
0.4
0.6
0.8
1.0
0.5
1.0
1.5
2.0
2.5
3.0
3.5
4.0
4.5
5.0

FIG. 34

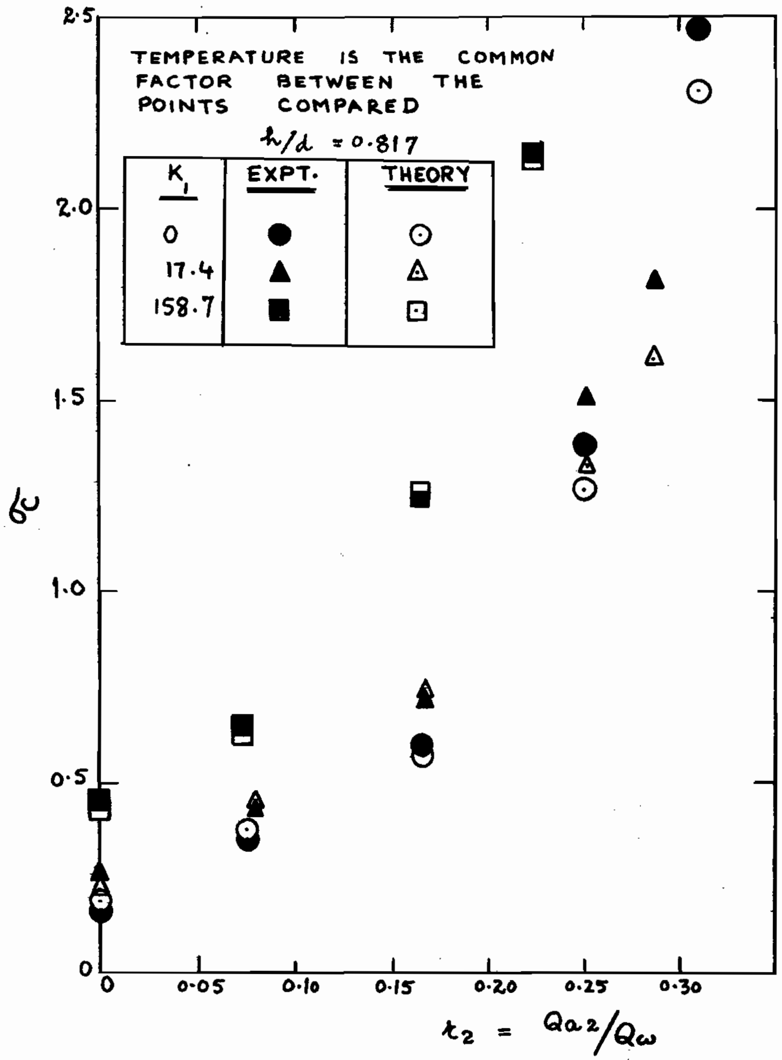

FIG. 35. EFFECT OF VENTILATION ON CAVITATION PARAMETER

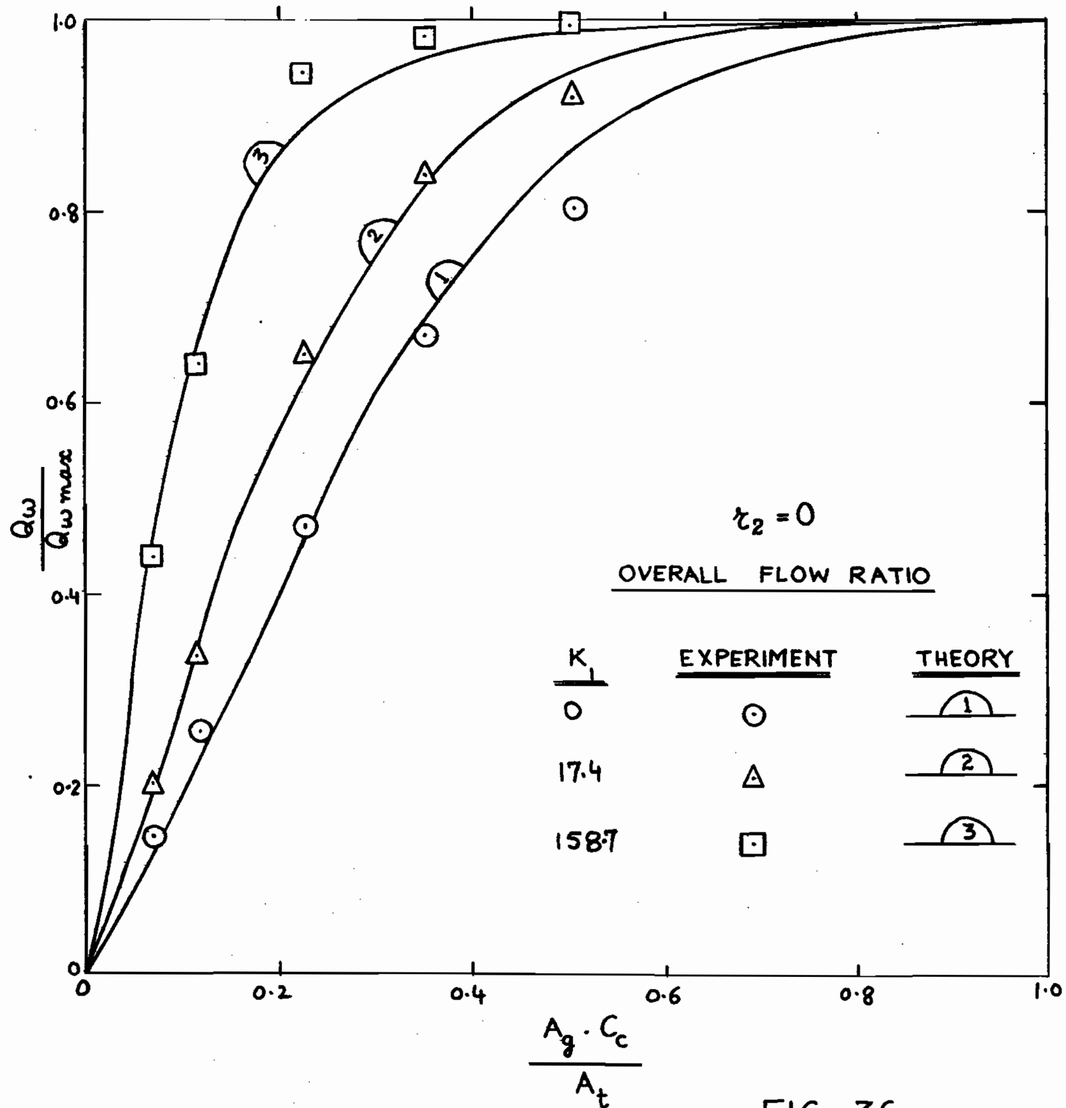

FIG. 36

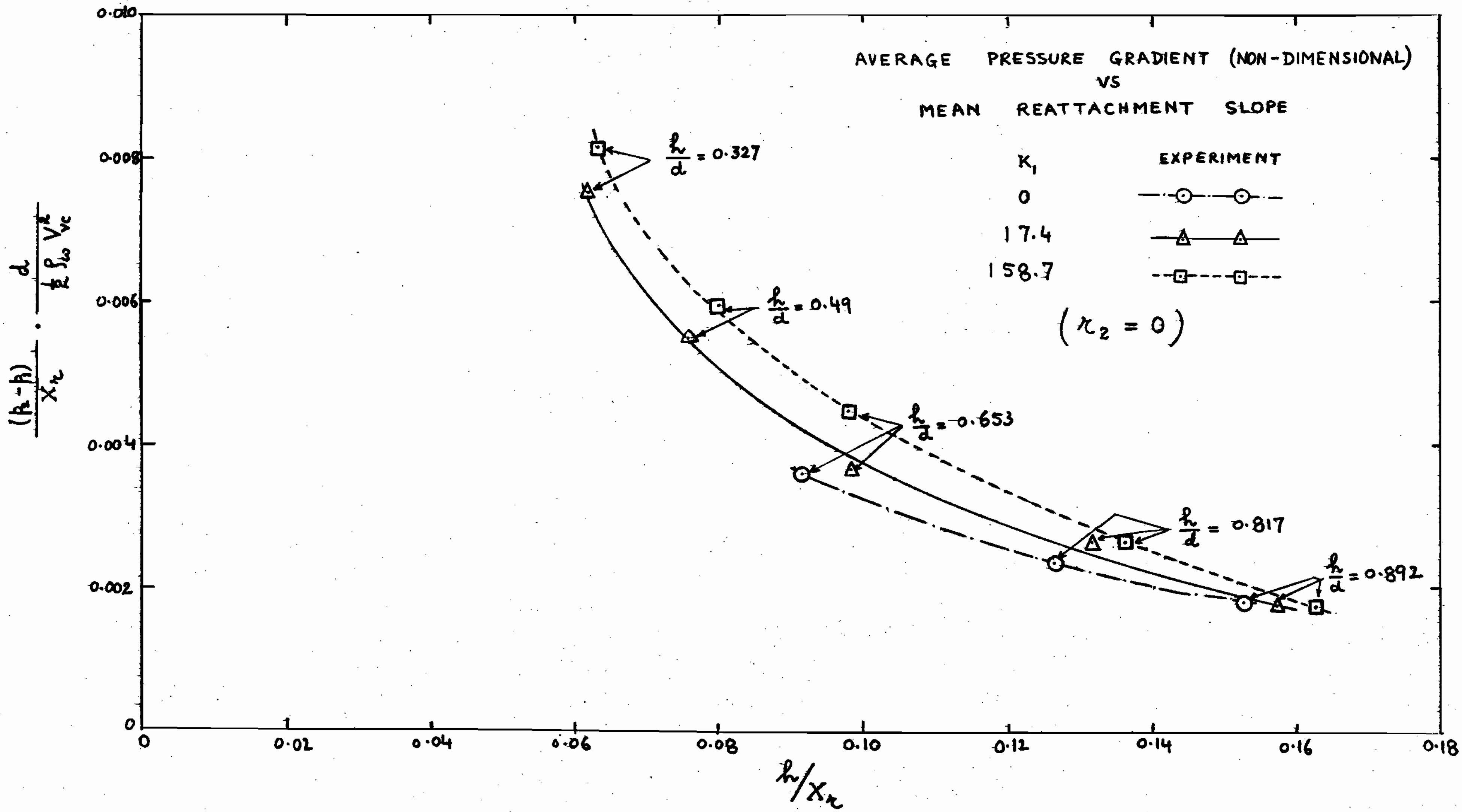

AVERAGE PRESSURE GRADIENT (NON-DIMENSIONAL)
VS
MEAN REATTACHMENT SLOPE
K_1
EXPERIMENT
0
17.4
158.7
$(r_2 = 0)$
$\frac{h}{d} = 0.327$
$\frac{h}{d} = 0.49$
$\frac{h}{d} = 0.653$
$\frac{h}{d} = 0.817$
$\frac{h}{d} = 0.892$
0.010
0.008
0.006
0.004
0.002
0
0.02
0.04
0.06
0.08
0.10
0.12
0.14
0.16
0.18
h/X_r

FIG. 37

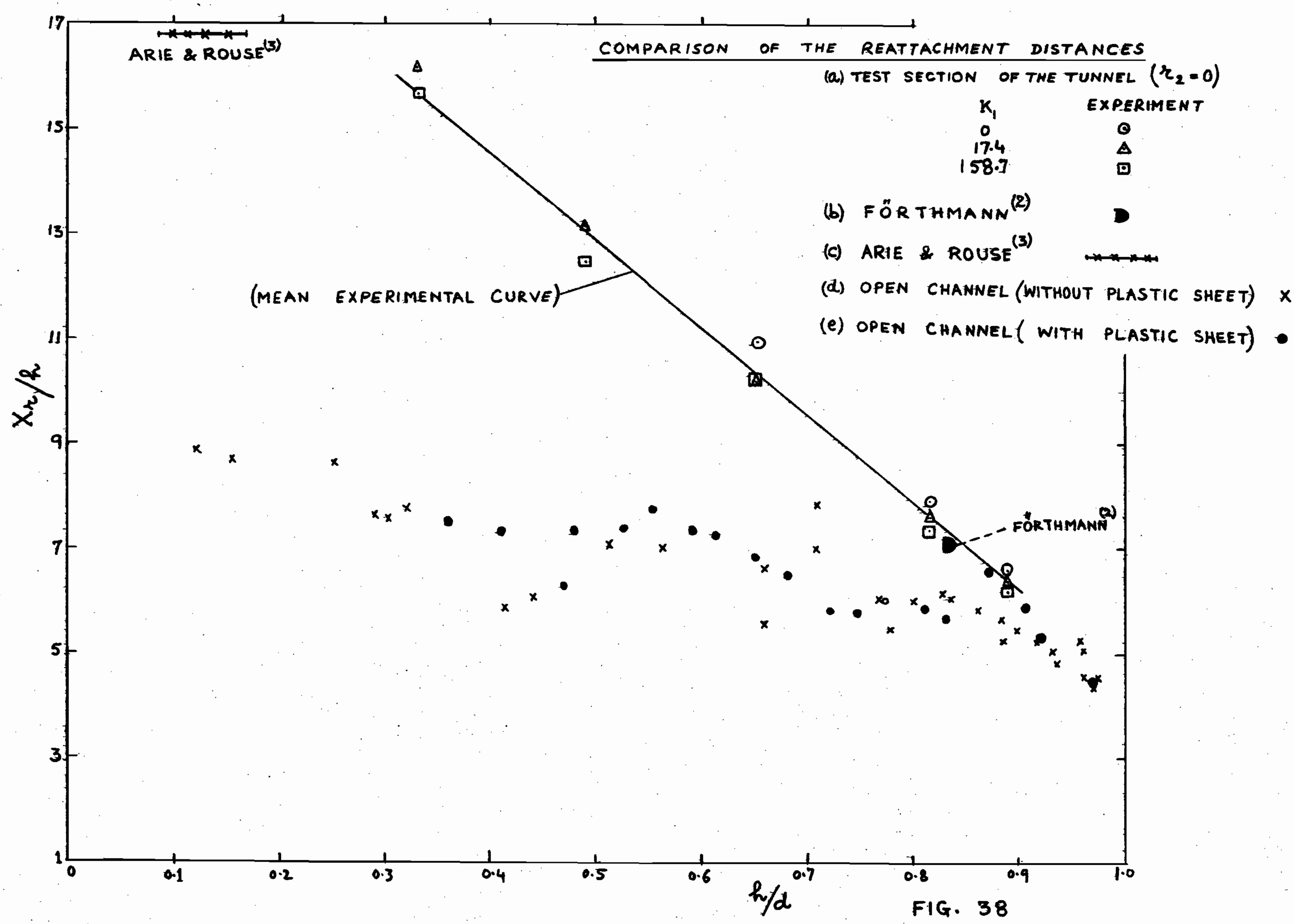

ARIE & ROUSE(3)
COMPARISON OF THE REATTACHMENT DISTANCES
(a) TEST SECTION OF THE TUNNEL ($r_2 = 0$)
K_1
EXPERIMENT
0
17.4
158.7
(b) FÖRTHMANN(2)
(c) ARIE & ROUSE(3)
(d) OPEN CHANNEL (WITHOUT PLASTIC SHEET) x
(e) OPEN CHANNEL (WITH PLASTIC SHEET) •
(MEAN EXPERIMENTAL CURVE)
FÖRTHMANN(2)
X_r/h
h/d
17
15
13
11
9
7
5
3
1
0
0.1
0.2
0.3
0.4
0.5
0.6
0.7
0.8
0.9
1.0

FIG. 38

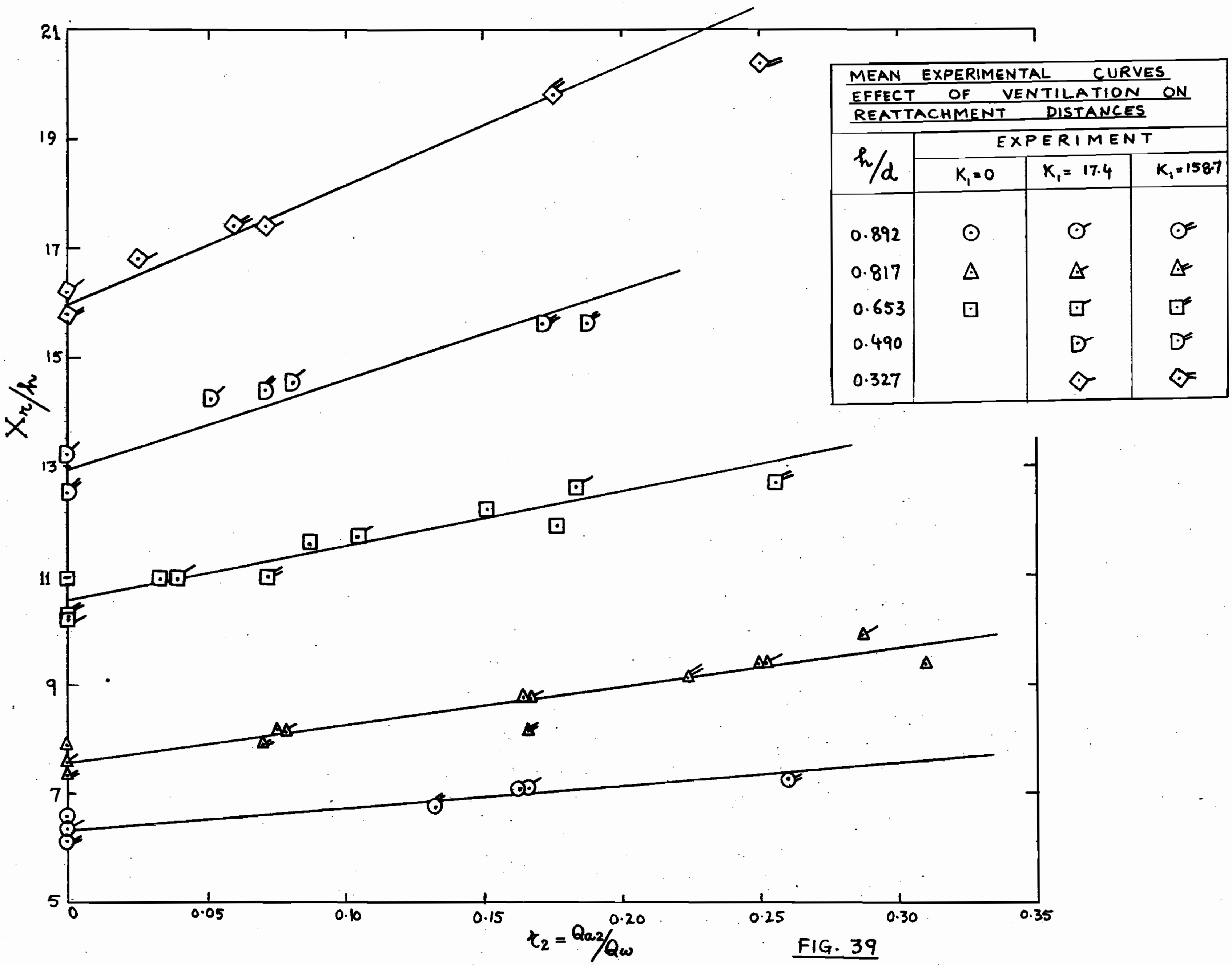

MEAN EXPERIMENTAL CURVES
EFFECT OF VENTILATION ON
REATTACHMENT DISTANCES
EXPERIMENT
h/d
K1 = 0
K1 = 17.4
K1 = 1587
0.892
0.817
0.653
0.490
0.327
21
19
17
15
13
11
9
7
5
Xr/h
0
0.05
0.10
0.15
0.20
0.25
0.30
0.35
τ2 = Qa2/Qw

FIG. 39